

AD-777 241

MODELS OF MULTIPATH PROPAGATION EFFECTS
IN A GROUND-TO-AIR SURVEILLANCE
SYSTEM

T. P. McGarty

Massachusetts Institute of Technology

Prepared for:

Electronic Systems Division
Federal Aviation Administration

25 February 1974

DISTRIBUTED BY:

NTIS

National Technical Information Service
U. S. DEPARTMENT OF COMMERCE
5285 Port Royal Road, Springfield Va. 22151

AD 777 241

TECHNICAL REPORT STANDARD TITLE PAGE

1. Report No. ESD-TR-74-40	2. Government Accession No.	3. Recipient's Catalog No.	
4. Title and Subtitle Models of Multipath Propagation Effects in a Ground-to-Air Surveillance System		5. Report Date 25 February 1974	6. Performing Organization Code
7. Author(s) T. P. McGarty		8. Performing Organization Report No. TN 1974-7	
9. Performing Organization Name and Address Massachusetts Institute of Technology Lincoln Laboratory P. O. Box 73 Lexington, Massachusetts 02173		10. Work Unit No. (TRAIS) 45364 Project No. 034-241-012	11. Contract or Grant No. DOT-FA-72-WAI-261
12. Sponsoring Agency Name and Address Department of Transportation Federal Aviation Administration Systems Research and Development Service Washington, D. C. 20591		13. Type of Report and Period Covered Technical Note	
14. Sponsoring Agency Code			
15. Supplementary Notes The work reported in this document was performed at Lincoln Laboratory, a center for research operated by Massachusetts Institute of Technology under Air Force Contract F19628-73-C-0002.			
16. Abstract Models are developed for the electromagnetic propagation of diffuse and specular multipath for a surface-to-air ATC radar beacon link. The models take into account geometrical, topographical, electrical, and surface characteristics of the multipath propagation environment. The models are used to evaluate signal fading and azimuth estimation performance of a monopulse processor in a ground-based interrogator. The results are applied to assessing the performance of the DABS sensor. Conclusions and recommendations for experimental work are presented. <div style="text-align: right;"> <p>DDC RECEIVED APR 15 1974 RECEIVED D</p> </div> <div style="text-align: center;"> <p>Reproduced by NATIONAL TECHNICAL INFORMATION SERVICE U S Department of Commerce Springfield VA 22151</p> </div>			
17. Key Words Multipath; Diffuse and Specular Channel Characterization Electromagnetic Propagation Antenna Performance		18. Distribution Statement Document is available to the public through the National Technical Information Service, Springfield, Virginia 22151.	
19. Security Classif. (of this report) Unclassified	20. Security Classif. (of this page) Unclassified	21. No. of Pages 158	22. Price \$ 5.00 1.45 MF

Approved for Release
by NSA on 05-08-2014 pursuant to E.O. 13526

TABLE OF CONTENTS

<u>Section</u>		<u>Page</u>
1	INTRODUCTION	1
	1.1 REPORT OUTLINE	2
2	FUNDAMENTAL PHENOMENOLOGY	5
	2.1 SENSOR GEOMETRY	5
	2.2 SIGNAL MODEL	11
3	SPECULAR MULTIPATH	18
	3.1 GEOMETRICAL CONSIDERATIONS	19
	3.2 REFLECTION COEFFICIENT	27
	3.2.1 Fresnel Reflection Coefficient	29
	3.2.2 Diffuse Reflection Coefficient	30
	3.2.3 Diffraction Effects	32
	3.3 EXAMPLES OF RECEIVED SIGNALS	42
	3.4 CONCLUSIONS.	50
4	DIFFUSE MULTIPATH.	63
	4.1 THE SIGNAL MODEL	65
	4.2 THE CHANNEL SPREAD FUNCTION	70
	4.3 PERFORMANCE	102
	4.4 CONCLUSIONS.	110
5	OTHER EFFECTS.	113
	5.1 REFRACTION	113
	5.2 SHADOWING	114
	5.3 SEA SURFACE SCATTERING	117
	5.4 COMPOSITE SCATTERING	120
	5.5 CONCLUSIONS.	120
6	APPLICATIONS	123
	6.1 PERFORMANCE	123
	6.2 LOCALIZATION	124
	6.3 ANTENNA DESIGN	126
	6.4 SIGNAL PROCESSING	130
	6.5 SITING.	130
	6.6 CONCLUSIONS.	130

TABLE OF CONTENTS (Continued)

<u>Section</u>		<u>Page</u>
7	CONCLUSIONS	132
	APPENDIX I.	135
	GLOSSARY OF TERMS.	139
	REFERENCES	145

LIST OF ILLUSTRATIONS

<u>Figure</u>		<u>Page</u>
1	Geometry of Canonical Coordinate System.	7
2	Scattering Plane Geometry	9-10
3	Ray Optics Propagation Geometry	12
4	Diffuse Multipath Reflection	14
5	Definition of Azimuth and Elevation Angles	16
6	Image Antenna Geometry in Scattering Plane Coordinate System.	21
7	Azimuth-Elevation Calculation	24
8	Geometry of Scattering Angle	26
9	Arbitrary Scattering Angle Geometry	28
10	Reflection Coefficient	31
11	Behavior of Diffuse Reflection Coefficient.	33
12	Diffraction From a Rectangular Plane	34
13	Movement of Diffraction Plane and Specular Diffraction.	35

LIST OF ILLUSTRATIONS (Continued)

<u>Figure</u>		<u>Page</u>
14	Wavefront Propagation	37
15	Sketch of Diffraction Pattern	38
16	Geometry of Fresnel Zones	40
17	Charleston, S. C., AN/FPS-27 Site 1, 000 ft Flight Test Results on 253.6-Degree Radial . . .	44
18	Geometry of Reflecting Plane for Cases Discussed	46
19	Beam Power vs Inverse Range; Case I	47
20	Estimated Angle vs Range; Case I	48
21	Multipath Test vs Range; Case I.	49
22	Beam Power in dB vs Range; Case II	51
23	Monopulse Azimuth Estimate; Case II.	52
24	Multipath Detector Output; Case II	53
25	Signal Power vs Range; Case III, No Vertical Aperture.	54
26	Monopulse Azimuth Estimate; Case III, No Vertical Aperture	55
27	Multipath Detector Statistic; Case III, No Vertical Aperture	56
28	Signal Amplitude vs Range; Case III, Vertical Aperture.	57
29	Monopulse Azimuth Estimate; Case III, Vertical Aperture	58
30	Multipath Detector; Case III, Vertical Aperture.	59
31	Diffuse Multipath Geometry	66

LIST OF ILLUSTRATIONS (Continued)

<u>Figure</u>		<u>Page</u>
32	Geometry of Receiving Aperture	68
33	Geometry of Direct Path	72
34	Time Variation of Area.	74
35	Area, $S(t)$, vs time ($z_1 = 10\text{m}$, $z_2 = 3\text{ km}$, $R = 15\text{ km}$)	77
36	Differential Area vs Time ($S(t + T) - S(t)$; $T = 1\text{ }\mu\text{sec}$; $z_1 = 10\text{ m}$, $z_2 = 3\text{ km}$, $R = 15\text{ km}$) .	79
37	Differential Area vs Time ($S(t = T) - S(t)$; $T = 1.6\text{ }\mu\text{sec}$; $z_1 = 10\text{ m}$, $z_2 = 3\text{ km}$, $R = 15\text{ km}$)	80
38	Scattering Geometry.	81
39	Scattering Cross-Section vs Azimuth ($\phi_i = \phi_s = 88^\circ$, $s = 1/2$)	86
40	Scattering Cross-Section vs Azimuth ($\phi_i = \phi_s = 88^\circ$, $s = 1/2^6$)	87
41	Scattering Cross-Section vs Azimuth ($\phi_i = \phi_s = 88^\circ$, $s = 2$)	88
42	Scattering Cross-Section vs Azimuth ($\phi_i = \phi_s = 88^\circ$, $s = 2^6$)	89
43	Spread Function Geometry	91
44	Scattering Geometry.	93
45	Contour Plot of Scattering Cross-Section ($R = 10\text{ km}$, $z_2 = 1\text{ km}$, $s = 0.5$)	96
46	Contour Plot of Scattering Cross-Section ($R = 50\text{ km}$, $z_2 = 1\text{ km}$, $s = 0.5$)	97
47	Contour Plot of Scattering Cross-Section ($R = 50\text{ km}$, $z_2 = 1\text{ km}$, $s = 2.0$)	98
48	Contour Plot of Scattering Cross-section ($R = 50\text{ km}$, $z_2 = 1\text{ km}$, $s = 4.0$)	99

LIST OF ILLUSTRATIONS (Continued)

<u>Figure</u>		<u>Page</u>
49	Plot of Channel Spread Function vs Azimuth for Two Correlation Lengths.	101
50	Plot of Multipath Energy to Signal vs Range .	103
51	Standard Deviation of Angle Estimate	108
52	Plot of Aircraft Altitude vs Maximum Range to Horizon.	115
53	Model of Ocean Waves	118
54	Real Part of Fourier Transform	127
55	Imaginary Part of Fourier Transform	128
56	Power Spectrum	129

SECTION ONE
INTRODUCTION

As a signal is transmitted from one point to another above a surface with electrical properties differing from that of the propagation medium, reflected signals may be generated. These signals then appear, along with the signal travelling over the direct path, at the receiver. These additional signals directly affect the communication and direction finding capabilities of a surveillance link operating in this environment. These signals are commonly called multipath and it is the purpose of this report to describe models of such phenomena that are useful for ascertaining the efficacy of such a link for surveillance.

Specifically, the models developed are to be used to evaluate multipath effects on the DABS (Discrete Address Beacon System) performance. For this system, a downlink receiver (sensor) is on the surface and the transmitter is located in an aircraft. Clearly, due to reciprocity, the role of the transmitter and receiver can be interchanged but, in this report, we shall use the stated nomenclature. The link being discussed is one where the receiver is close to the ground (5-50 m high) while the transmitter is at a higher altitudes (500-15,000 m) and the range is large (10-100 km). This is in contrast to ground-to-ground or air-to-air links as found in mobile radio or satellite communications respectively.

What we shall do in this report is consider those effects which are relevant to the ground-to-air environment and develop models which are

appropriate. Our interest will not be in the microstructure of diffraction effects due to specific structures but will be towards developing models that can be easily used to evaluate the multipath effects on system performance. Namely, we shall be interested in the general macrostructure of the multipath environment.

The two main functions of this report are:

1. Model Description: In this area, we evaluate the topographical, geometrical, electrical, and system parameters and how they affect the RF signal at the receiving antenna. Specifically, specular and diffuse multipath are discussed in detail in terms of the above parameters.
2. System Performance: Once the multipath model has been developed, the effects of the multipath signal on the SNR (signal-to-noise ratio) and direction finding capabilities of a monopulse antenna with a 2° beamwidth and vertical sector beam are ascertained.

1.1 REPORT OUTLINE

In Section 2, we discuss first the geometry of the aircraft and the sensor by introducing a canonical coordinate system. The large scale topographic features such as hills, buildings, etc. are then defined in terms of this coordinate system. We then proceed to discuss the difference between specular and diffuse multipath and the surface conditions that give rise to each of them. A model of the RF envelope of the receiving antenna output is presented. This equation is the basis for the multipath model development.

Section 3 discusses the nature and effects of specular multipath on the received signal. Using the geometrical models developed in Section 2, a geometrical optics analysis of specular reflections is developed. The path length, angle of incidence, azimuth, and elevation of the received specular multipath signal are determined. Since specular multipath arises from large scale surface areas, the reflection coefficient is studied in detail. The effects of electrical properties at the reflecting surface, finite aperture diffraction and losses due to diffuse multipath are considered. The section concludes with a discussion of the use of the models in the analysis of signal fading and monopulse azimuth estimation. These issues are related to the performance of DABS.

The model for diffuse multipath is developed in Section 4. In contrast to specular multipath, which is a highly deterministic phenomenon, diffuse multipath is random in nature. To account for this, a model is developed for the second order statistical properties of the multipath field. A function called the channel spread function is introduced. The spread function is then evaluated in terms of the surface properties using the Kodis-Barrick scattering cross-section model. Section 4 concludes with a discussion and evaluation of the effects of diffuse multipath on azimuth estimation performance. It is shown that there is a negligible effect in the DABS case.

Section 5 discusses other effects that, although not included in the models, may in time be important. These effects include refraction, line-of-sight limitations, shadowing, sea-surface scattering, and composite scattering.

The last major technical section is Section 6. Here we discuss the various applications to which the models may be put to use. Specifically,

we mention link and azimuth estimation performance and localization techniques. Also discussed are antenna design, signal processing, and siting.

The conclusions of the report are detailed in Section 7. Basically, we show that DABS should function acceptably based on the multipath model developed in this report. We also comment on the other uses of the model and briefly on its shortcomings.

SECTION TWO

FUNDAMENTAL PHENOMENOLOGY

In order to fully understand the effect of multipath on the energy received at an antenna aperture, it is first necessary to describe the total environment in which the signal transmission is taking place. This environment includes the reflection geometries involved between transmitter and receiver, the nature of the waveform transmitted and the effects of the receiver antenna on the received signal energy. In this section we shall treat each of these issues separately and on a level which will provide the reader with a qualitative as well as quantitative understanding of the problems involved.

2.1 SENSOR GEOMETRY

The basic geometry of the aircraft and DABS ground receiver is quite simple. In order to avoid certain analytical problems we shall first assume that we have a flat earth. Let us then choose a point O on the earth plane and at this point construct a set of three orthogonal axes, one being normal to the plane. This will be defined as the canonical coordinate system and will be used throughout the report. The interrogator antenna DABS sensor is located at an altitude z_1 above the origin. This point represents the phase or geometrical center of the antenna. It is that point to which all phase delays are referenced. The earth plane is designated the x, y plane and in this context, the antenna coordinates are $(0, 0, z_1)$. The aircraft is at an altitude

z_2 above the plane and at position x_2 and y_2 on the plane. Thus, the aircraft's position is (x_2, y_2, z_2) . The range from the antenna is given by R_T where

$$R_T = [(z_2 - z_1)^2 + x_2^2 + y_2^2]^{1/2} \quad (2.1)$$

This geometry is shown in Fig. 1. Another important constant is the ground range R where

$$R = [x_2^2 + y_2^2]^{1/2} .$$

Actually, the earth's surface is not a flat plane but contains hills and other large obstructions such as buildings and bridges. These may be considered large scale surface perturbations, being the size of many wavelengths of the transmitted radiation. There are also small scale obstructions such as small rocks, trees, grass, water, roadway surfaces, etc. which are in size less than several wavelengths. It is necessary to consider both of these classes of obstructions in any model. In many cases, the large scale obstructions are limited in number and are easily defined and characterized. For example, a large hill can be easily identified from a topographic map. However, the small scale obstructions are quite numerous and detailed in their shape as compared to a long smooth hill. Thus, the large scale obstructions are often amenable to a deterministic analysis whereas random analyses are necessary for the understanding of the small scale effects. Thus, we shall leave discussion of the latter to Section 4 and consider the former here.

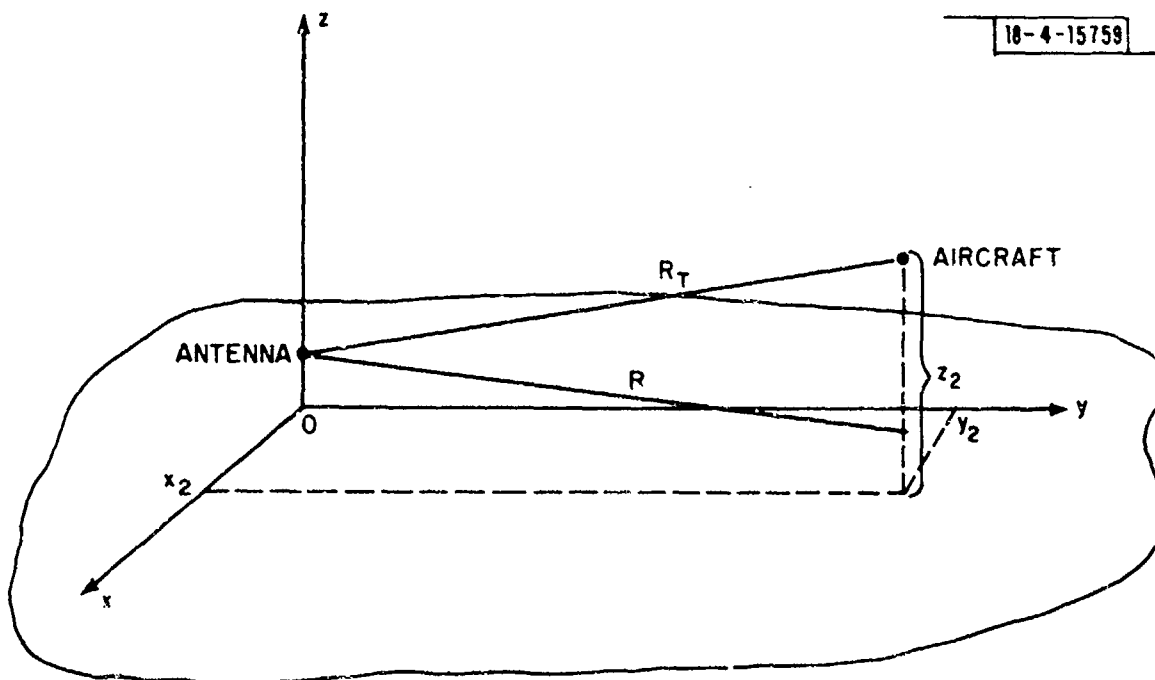
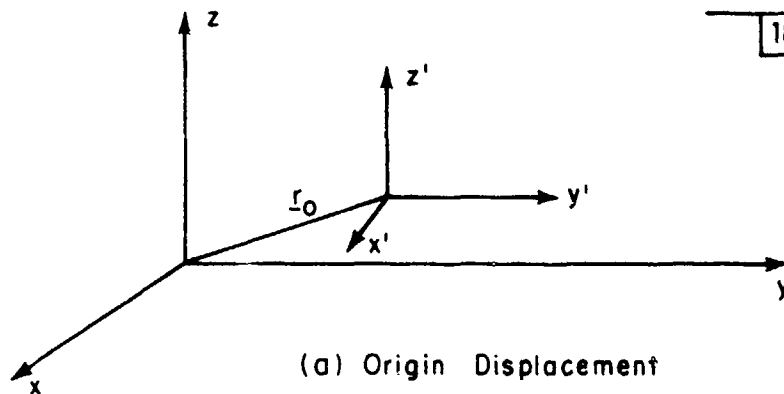


Fig. 1. Geometry of canonical coordinate system.

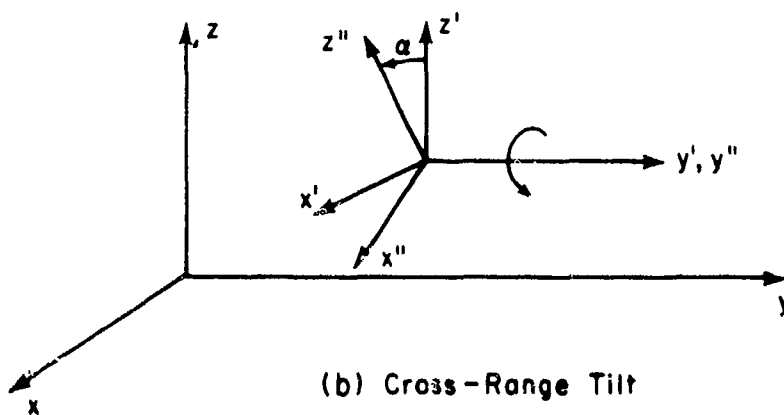
We shall assume that any large scale obstructions can be represented as a suitably sized section of a plane that has been positioned to coincide with the actual obstruction. For example, if there is a large building parallel to the y axis in Fig. 1, then it can be represented by a plane of equivalent size and electrical properties located at the same position. These equivalent planes will be defined relative to the canonical coordinate system.

A model of the scattering surface is constructed in the fashion shown in Fig. 2. From the canonical system we displace another orthogonal coordinate system (x', y', z') by a vector \underline{r}_0 (Fig. 2(a)). Then this system is rotated about the y' axis by an angle α (see Fig. 2(b)) called the cross-range tilt. It is called cross-range because the y -axis is usually associated with the horizontal range and multipath reflections from such a tilted surface will cause monopulse azimuth errors in the cross-range direction. The resulting coordinate system x'', y'', z'' (Fig. 2(b)) is then rotated about x'' to an angle β (see Fig. 2(c)) yielding a final coordinate system x''', y''', z''' . β is called the range tilt angle. Finally, in this coordinate system on the x''', y''' plane, we define a surface S (see Fig. 2(d)) as the scattering surface. In this fashion we can construct a set of contiguous surfaces which represent the large scale surface topography and present a one-to-one mapping of the large scale surface topography. In the next section we shall particularize this further in the study of specular reflections. We shall also see in Section 4 that surface roughness, namely small scale surface irregularities, can be included directly by superposition.

18-4-15760



(a) Origin Displacement



(b) Cross-Range Tilt

Fig. 2. Scattering plane geometry.

18-4-16213

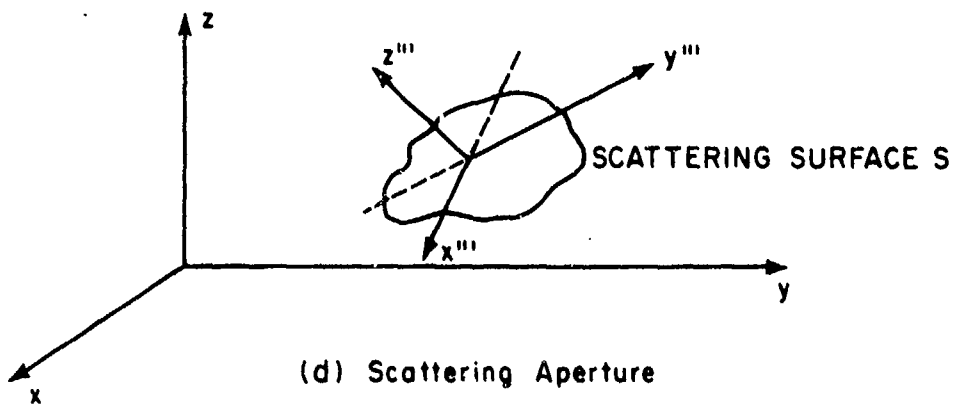
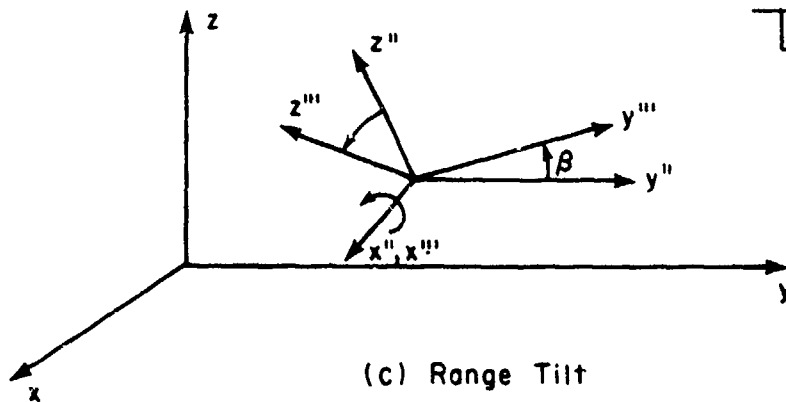


Fig. 2. Scattering plane geometry (Continued).

2.2 SIGNAL MODEL

Now, with the description of the geometry of the environment, it is possible to discuss the nature of the signal propagation. We shall concentrate on the signal transmitted by the aircraft and received by the sensor antenna, which we term the downlink signal. For large scale irregularities, such as hills, we can use the simplifying analytical techniques of ray theory to determine the propagation of the electromagnetic energy from the transmitter to receiver. For example, in Fig. 3, we depict the aircraft at T and the receiver at R. We assume that the x, y plane is the surface of the flat earth model and that S is a separate large scale scattering surface. The points P and G are the reflection points on these two surfaces. Path ① is called the direct propagation path and represents the free space propagation from T to R. Path ②, TGR, is the ground propagation path with reflection point G. The reflection point is determined directly from the image antenna at R'. Path ③, TPR, is what we shall call a multipath signal return. It is a signal return that results from other than flat earth reflections. It is this type of return that proves to be most detrimental to direction finding (DF) accuracy.

The signal returns in Fig. 3, are clear, well defined signals which appear at the receiver as signals coming from directions other than the direct propagation path. Such strong well defined returns are called specular multipath and result from large reflecting surfaces such as buildings and hills. A second kind of multipath signal, called diffuse multipath, occurs due to the small scale surface irregularities. Obstructions such as trees, windows, rocks, and other "small" obstructions cause multipath returns to appear to

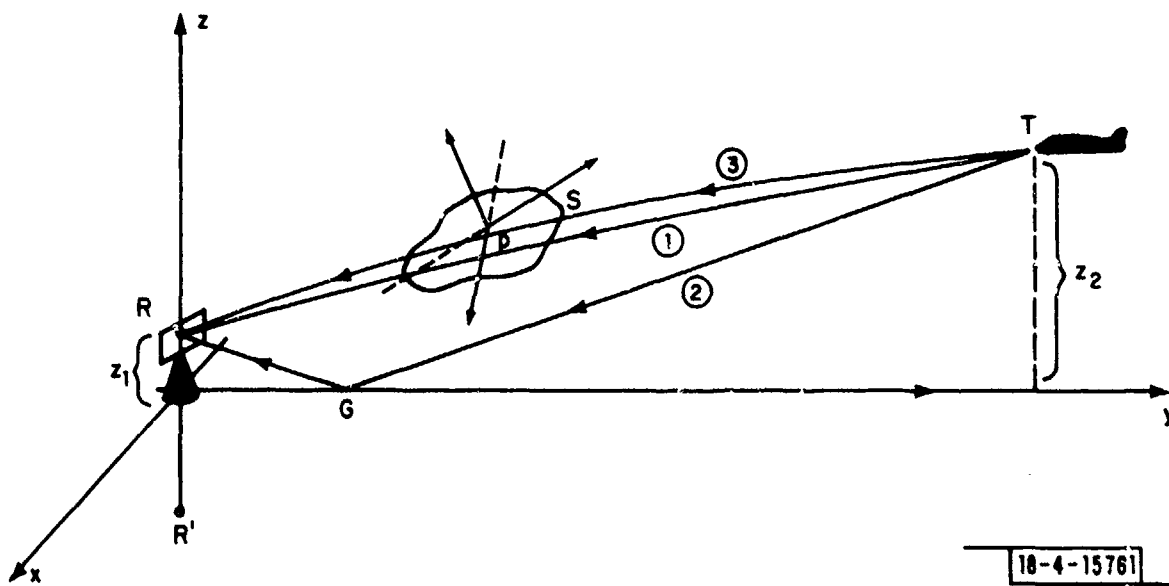


Fig. 3. Ray optics propagation geometry.

come from a spectrum of directions instead of a single well defined direction. An example of such a phenomenon is shown in Fig. 4 where we depict many small reflectors. Diffuse multipath is a random phenomenon as a result of large number of objects giving rise to it. As such, an analysis of its effect must be phrased in terms of these random orientations. Furthermore, the analysis of diffuse multipath effects requires the inclusion of diffraction phenomena and cannot be performed using classical ray optics techniques.

To observe the effects that these different phenomena have on the received signal, a model for such a signal must be developed. In general, the signal will be narrowband, centered about a carrier frequency ω_c . We assume that the transmitter emits a spherical wave from an omnidirectional antenna (variations from which will be considered later) having a time variation of the form,

$$\tilde{s}(t) = \sqrt{2} \operatorname{Re}[s(t) \exp(j\omega_c t)] \quad (2.3)$$

The term $\tilde{s}(t)$ is the complex envelope of the signal and has the form

$$\tilde{s}(t) = \sqrt{E_s} \tilde{f}(t) \quad (2.4)$$

where E_s is the signal energy and $\tilde{f}(t)$ is a normalized version of the temporal variation. Namely,

$$\int_{-\infty}^{\infty} \tilde{f}(t) \tilde{f}^*(t) dt = 1 \quad (2.5)$$

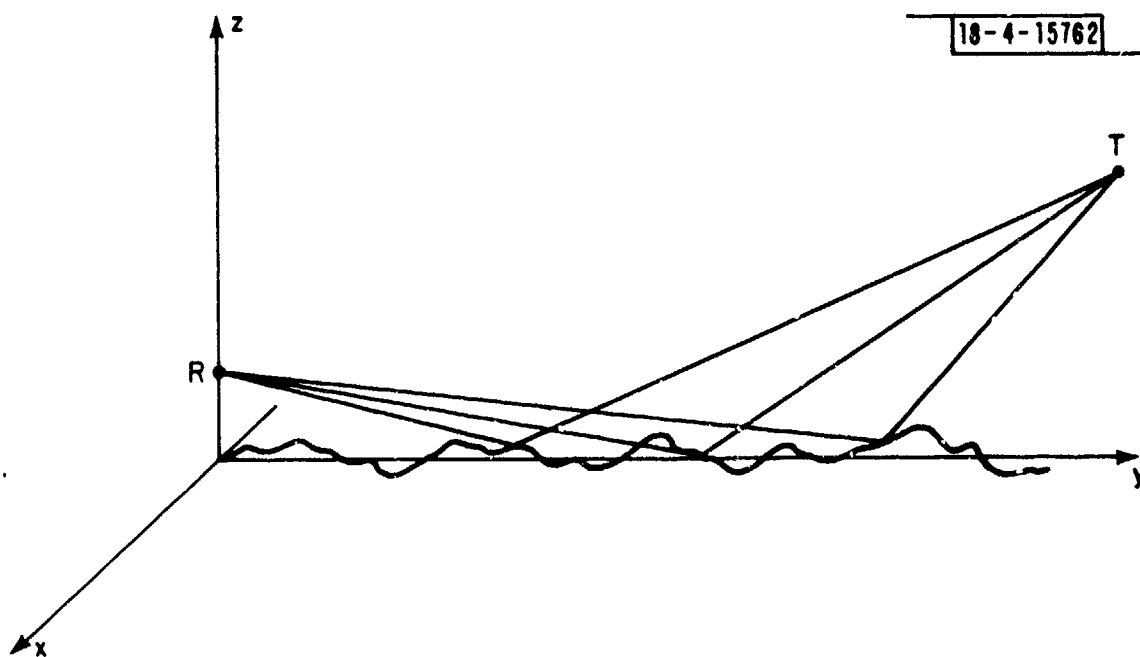


Fig. 4. Diffuse multipath reflection.

The signal $\tilde{f}(t)$ is the complex envelope of the time variation and can take on any arbitrary form depending on the signal format required. The signal $\tilde{f}(t)$ corresponds to the video output (e.g., baseband signal, see Van Trees).

We now want to consider the complex envelope of the RF signal at the output of the antenna. This signal will be affected by the transmitter, the transmission channel, and the antenna. To understand the antenna effects we must first define the incident characteristics of a plane wave, via its ray, upon the antenna.

In Fig. 5 we have drawn an array in the canonical coordinate system and have defined a normal vector \underline{n} relative to the aperture. An incident plane wave is described by a wave vector \underline{k} . The elevation angle of arrival of the plane wave, ϕ , is the angle between the wave vector and the plane formed by the vector \underline{n} and the x axis. The azimuth θ is defined by the angle made in the \underline{n} , x plane as shown. The antenna attenuates the amplitude of a signal coming from direction ϕ , θ by a factor $G(\theta, \phi)$ which is called the antenna gain in that direction. Thus, the envelope of the RF signal for one particular path can be given by

$$\sqrt{E_s A} G(\theta, \phi) \frac{\rho}{R} \tilde{f}(t - R/c) e^{j\psi} \quad (2.6)$$

where R is the path length, ψ the path phase, A the area of the antenna, ρ the channel transmission factor and c is the propagation velocity.

A general model for the RF envelope can now be proposed. If there is a free space signal and N specular multipath signals incident on the antenna,

18-4-15763

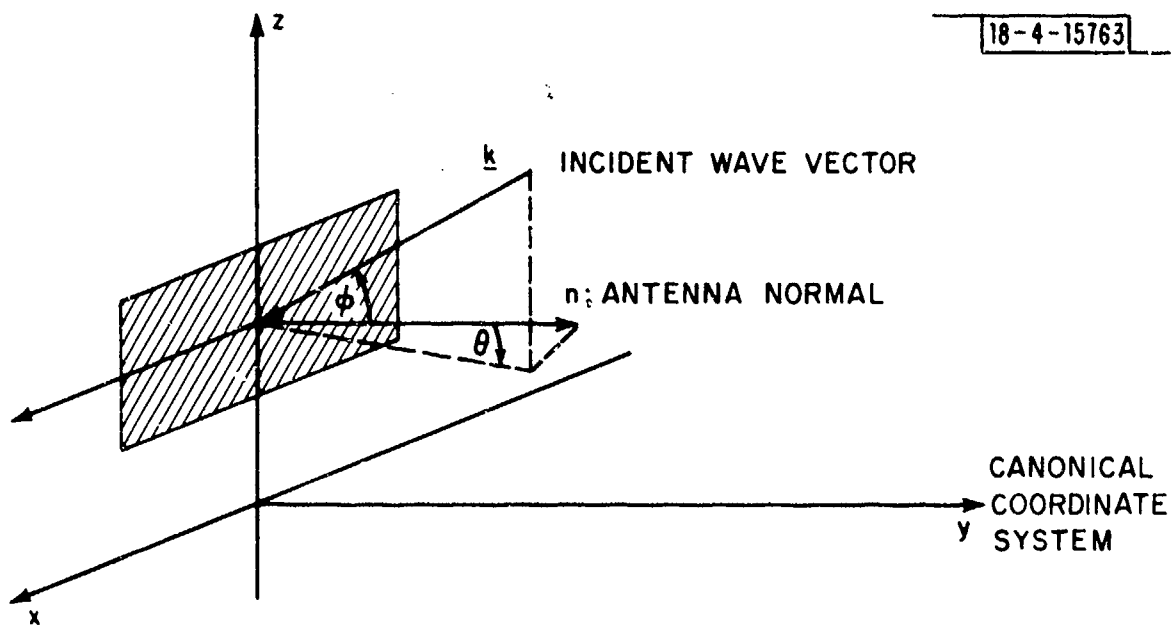


Fig. 5. Definition of azimuth and elevation angles.

plus diffuse multipath and noise, then the received signal is given by;

$$\begin{aligned} \bar{r}(t) = & \sqrt{E_s A} \sum_{i=0}^N G(\theta_i, \phi_i) \frac{\rho_i}{R_i} \tilde{f}(t - R_i/c) \exp(j\psi_i) \\ & + \iint G(\theta, \phi) \tilde{b}(\theta, \phi, t) d\theta d\phi + \tilde{n}(t) \quad . \quad (2.7) \end{aligned}$$

Here θ_i, ϕ_i are the azimuth and elevation of the i th specular signal and ρ_i, R_i and ψ_i are the transmission gain, range and phase respectively. The $i=0$ terms correspond to the free space path. The term $\tilde{b}(\theta, \phi, t)$ represents the effects of diffuse multipath to be discussed in Section 4. The noise $\tilde{n}(t)$ represents all noise not attributable to signal transmission observed at the RF output.

One of the purposes of this report is to describe how one can evaluate all of the terms that appear in this expression and show how they relate to the actual terrain topography. For example, the quantity ρ will depend on reflection coefficients, diffraction effects, diffuse reflection effects, as well as the vagaries of the transmitting antenna. The term $\tilde{b}(\theta, \phi, t)$ is a random process imbedded in a random field. The evaluation of its statistics is quite involved and will require some detailed knowledge of the surface topography.

SECTION THREE

SPECULAR MULTIPATH

The dominant multipath effect in terms of direction finding and communications in the DABS environment is specular multipath. As we shall see in the next section, diffuse multipath plays a second order role which, though marginally important, does not limit the performance of the DABS system. Specular multipath is felt in terms of signal fading and azimuth estimation errors. It can be analyzed deterministically for each specific geometry or probabilistically for an ensemble of such geometries. It has been found that a deterministic analysis provides greater insight into how it can affect system performance. In this section we shall concentrate on a deterministic analysis and briefly comment on proposed random models.

As introduced in the last section, the direct free space signal plus the specular signal received at the RF output of the antenna is given by

$$\sqrt{E_s A} \sum_{i=0}^N G(\theta_i, \phi_i) \frac{\rho_i}{R_i} \tilde{f}\left(t - \frac{R_i}{c}\right) \exp[j\psi_i] \quad (3.1)$$

where $i=0$ corresponds to the direct path ray. The problem is to deterministically evaluate θ_i , ϕ_i , ρ_i , R_i and ψ_i for each of the rays. This is to be done knowing the number of scatterers, the surface geometry, the antenna pattern, the aircraft position and the electrical properties of the surface.

3.1 GEOMETRICAL CONSIDERATIONS

To evaluate these quantities, we must first further quantify the geometry. Let us assume that the receiving antenna is an array and the phase (geometrical) center of the array is at some vector \underline{r}_1 where

$$\underline{r}_1 = \begin{bmatrix} x_1 \\ y_1 \\ z_1 \end{bmatrix} \quad (3.2)$$

which is a generalization of the definition of Section Two. Likewise, assume the aircraft is at \underline{r}_2 where

$$\underline{r}_2 = \begin{bmatrix} x_2 \\ y_2 \\ z_2 \end{bmatrix} \quad (3.3)$$

Both of these vectors are defined relative to the canonical coordinate system developed in the last section. Now we will define the i th scattering plane ($i \geq 2$) as the septuple P_i of surface area S_i , with tilts α_i, β_i ($i \geq 2$) where;

$$P_i = \left\{ \underline{r}_{0_i}, \alpha_i, \beta_i, S_i, \epsilon_i, \sigma_i, \sigma_{s_i} \right\} \quad (3.4)$$

Here, \underline{r}_{0_i} is the offset vector of the i th scattering plane (see Fig. 2), ϵ_i and σ_i are the dielectric constant and conductivity of the plane. σ_{s_i} is the surface roughness coefficient as obtained for diffuse multipath effects. This septuple completely defines the scattering plane and will provide all the information

necessary for our model of the channel. Given the antenna gain, the received signal is completely defined.

We shall proceed by first determining R_i , the range between the transmitter on the aircraft and the receiver via the i th multipath source. We shall briefly outline this derivation and present the result. When using a ray optics approach the point of reflection from the i th surface is determined by extending the ray from the source to the image antenna. The image antenna is defined as being that point relative to the scattering plane (x''', y''' plane) which is equidistant from the opposite side of the plane as the receiver and lying on the normal created by the receiver and the scattering plane. For example, in Fig. 6 we have depicted an antenna at R in the y, z plane and a transmitter at T also in the y, z plane. The image antenna, since the x, y plane is the scattering plane, is at the point R'. The line RO is normal to the x, y plane. The length of the path is $\overline{TS} + \overline{SR}$ or equivalently \overline{TR}' . The vector \underline{r}'_i is the vector from the origin to the image antenna. What should be noted in this figure is that since the x, y plane is the scattering plane and the image antenna lies along the normal RO at the same distance from the x, y plane as \underline{r}_i , then \underline{r}'_i has the same x, y coordinates as \underline{r}_i and a z coordinate that is the negative of \underline{r}_i . This then suggests how the image antenna for the i th scattering plane can be obtained. Namely, translate and rotate the coordinate system, relative to the canonical system, using \underline{r}_{0_i} , α_i and β_i and employ the algorithm suggested above. Then retranslate and rotate back to the canonical coordinate system. Doing this we find that the position of the image antenna in the canonical coordinate system is given by \underline{r}'_i where

$$\underline{r}_i = \mathcal{R}_i(\underline{r}_1 - \underline{r}_{0_i}) + \underline{r}_{0_i} \quad (3.5)$$

where \mathcal{R}_i is the matrix which performs the above mentioned operations. The entries of \mathcal{R}_i are;

$$\mathcal{R}_i = \begin{bmatrix} \cos^2 \alpha_i - \sin^2 \alpha_i \cos 2\beta_i & \vdots & \sin \alpha_i \sin 2\beta_i & \vdots & \sin 2\alpha_i \cos^2 \beta_i \\ \sin \alpha_i \sin 2\beta_i & \vdots & \cos 2\beta_i & \vdots & \cos \alpha_i \sin 2\beta_i \\ -\sin 2\alpha_i \cos^2 \beta_i & \vdots & \cos \alpha_i \sin 2\beta_i & \vdots & \sin^2 \alpha_i - \cos^2 \alpha_i \cos 2\beta_i \end{bmatrix} \quad (3.6)$$

Thus R_i , the path length, via the i th multipath reflector, is determined by

$$R_i = [(\underline{r}_2 - \underline{r}_{1_i})^T (\underline{r}_2 - \underline{r}_{1_i})]^{1/2} \quad (3.7)$$

This is the value of R_i used in (2.7). Now ψ_i represents the phase of the i th path. If we arbitrarily define ψ_0 then

$$\psi_i = \psi_0 + 2\pi \frac{(R_i - R_0)}{\lambda_0} + \psi_{F_i} \quad (3.8)$$

where λ_0 is the free space wavelength and R_0 is

$$R_0 = [(\underline{r}_2 - \underline{r}_1)^T (\underline{r}_2 - \underline{r}_1)]^{1/2} \quad (3.9)$$

The term ψ_{R_i} is the phase of the i th reflection process which we shall define shortly (see 3.2.1).

In a similar fashion, we can use this formalism to evaluate the azimuth and elevation (θ_i, ϕ_i) of the i th multipath source. Consider the geometry in Fig. 7(a). The xy plane is the reflection plane which contains a point of reflection, S . Note that at the point S the ray changes direction and is reflected to the antenna. The azimuth and elevation are then defined relative to the vector that represents the scattered wave. Let us call that vector \underline{r}_{-s_i} . Now \underline{r}_{-s_i} relative to an arbitrary shift of coordinates is equal to the vector \underline{s}_i , the incident vector, except that the z coordinate has its sign changed. From the geometry, \underline{s}_i is given by

$$\underline{s}_i = \underline{r}_2 - \underline{r}'_{1_i} \quad (3.10)$$

We can normalize \underline{s}_i so that it has unit length. This is defined as the vector \underline{r}_i where;

$$\underline{r}_i = \frac{\underline{r}_2 - \underline{r}'_{1_i}}{|\underline{r}_2 - \underline{r}'_{1_i}|} \quad (3.11)$$

Consider Fig. 7(b). Here we depict \underline{r}_{-s_i} , the scattered version of \underline{s}_i . The elevation of the multipath relative to the array is defined as $-\phi'_i$, as shown, and the azimuth is $-\theta'_i$ as shown. Thus ϕ'_i and θ'_i are easily obtained by knowing the components of \underline{r}_{-s_i} which are directly obtained from \underline{s}_i as described.

This technique can then be extended to any arbitrarily rotated plane following the reasoning developed before. Namely, \underline{r}_{-s_i} can be shown to be;

$$\underline{r}_{s_i} = \mathcal{R}_i \underline{r}_i \quad (3.12)$$

so that the azimuth is given by

$$\theta_i = \tan^{-1} \left[\frac{r_{s_{i1}}}{r_{s_{i2}}} \right] \quad (3.13)$$

and the elevation;

$$\phi_i = \tan^{-1} \left[\frac{r_{s_{i3}}}{\left[r_{s_{i1}}^2 + r_{s_{i2}}^2 \right]^{1/2}} \right] \quad (3.14)$$

where

$$\underline{r}_{s_i} = \begin{bmatrix} r_{s_{i1}} \\ r_{s_{i2}} \\ r_{s_{i3}} \end{bmatrix} \quad (3.15)$$

Thus, given the parameters, we can obtain θ_i , ϕ_i and then knowing the form of the antenna gain $G(\theta_i, \phi_i)$ we obtained the antenna dependent portion of the i th return.

Another term that is of interest is the angle made between the scattering plane and the incident ray. As we shall see, this is important in evaluating the Fresnel reflection coefficient of the scattering surface. In the case where the scattering plane is the x, y plane then as shown in Fig. 8 this angle is given by the angle ξ . The angle TSR, equals $\pi - 2\xi$. Now consider the

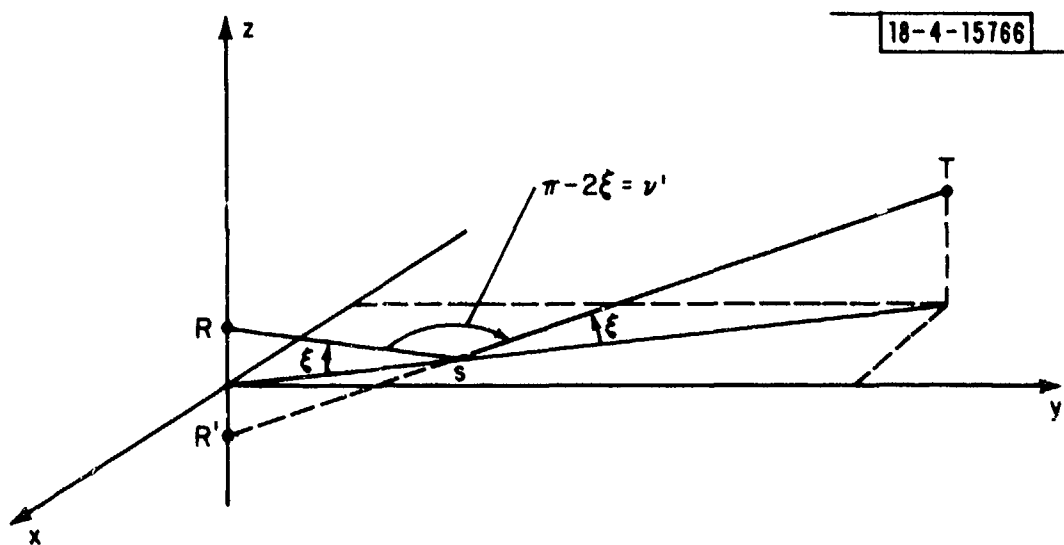


Fig. 8. Geometry of scattering angle.

general case. Let \underline{v}_3 be a vector from the origin to the receiver at R and let \underline{v}_1 be a vector to the image receiver at R'. Then the vector $\underline{v}_3 - \underline{v}_1 = \underline{v}_4$ is normal to the plane of scattering. For example, in Fig. 9 it is normal to the x, y plane. Now let \underline{v}_2 be a vector to the transmitter. Let \underline{v}_5 be the vector from the transmitter to image antenna. Now this vector is in the direction of the ray incident on the scattering plane for which \underline{v}_4 is a normal vector. Let γ be the angle between \underline{v}_4 and \underline{v}_5 . This angle can be obtained from the relationship.

$$\frac{\underline{v}_4^T \underline{v}_5}{|\underline{v}_4^T \underline{v}_5|} = \cos \gamma \quad . \quad (3.16)$$

Then by this simple geometrical argument ξ equals $((\pi/2) - \gamma)$ (see Fig. 9).

3.2 REFLECTION COEFFICIENT

The last factor required for (3.1) is an evaluation of the reflection coefficient, ρ_i . This coefficient depends upon the electrical properties of the surface, the size of the surface, and the small scale surface perturbations. The electrical properties are used to evaluate the Fresnel reflection coefficient, which has both an amplitude and phase. The size of the scattering surface defines an aperture and the surface roughness determines the diffractive effects that may arise. This is a very complex issue and must be dealt with in detail. Finally, diffuse scattering behavior of the large scale surface may tend to disperse the incident energy.

18-4-15767

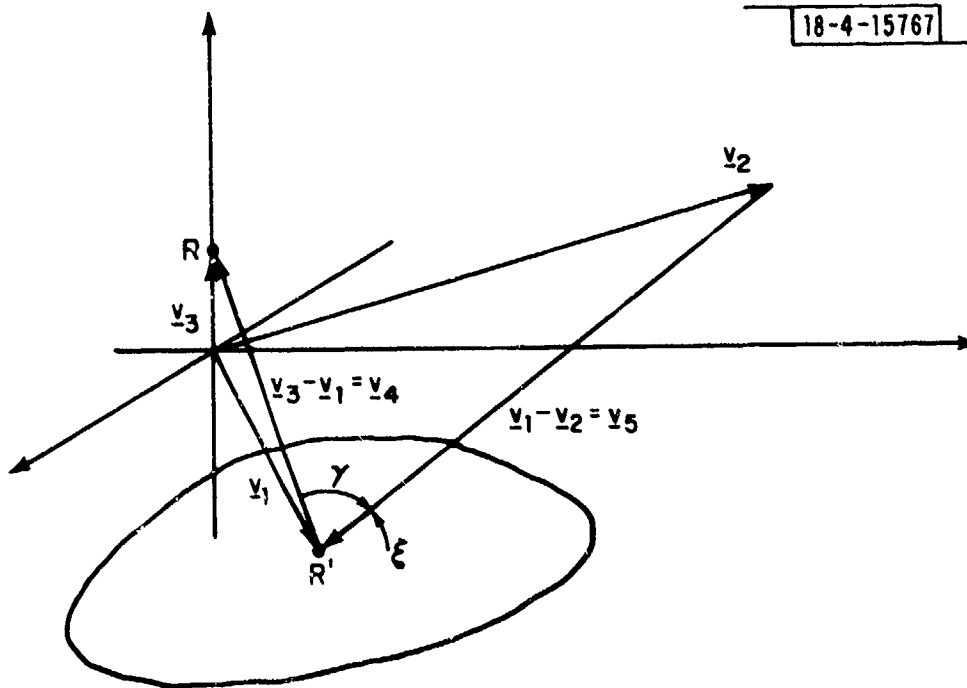


Fig. 9. Arbitrary scattering angle geometry.

Considering the above three effects the reflection coefficient, ρ_i , can be written as;

$$\rho_i = \eta_{A_i} \eta_{D_i} \eta_{F_i} \quad (3.17)$$

where η_{A_i} is the coefficient accounting for the finite aperture effect, η_{D_i} the diffuse reflection coefficient and η_{F_i} the Fresnel reflection coefficient due to the electrical properties of the surface.

3.2.1 Fresnel Reflection Coefficient

The Fresnel reflection coefficient η_{F_i} and the phase ψ_{F_i} , (3.8), can be obtained by an analysis of the reflection of electromagnetic waves from smooth surfaces with known electrical properties. The properties of the reflector also depend upon the polarization of the incident plane wave. To simplify the analysis we shall assume a single polarization, vertical, and avoid until Section 5 any of the problems associated with depolarizing surfaces.

The complete reflection coefficient is a complex quantity $\tilde{\eta}_{F_i}$ with

$$\tilde{\eta}_{F_i} = \eta_{F_i} \exp(j\psi_{F_i}) \quad (3.18)$$

It is shown in Jordan and Balmain (p. 631) that for vertical polarization

$$\tilde{\eta}_{F_i} = \frac{(\epsilon_x - jx) \sin\xi - \sqrt{(\epsilon_x - jx) - \cos^2\xi}}{(\epsilon_x - jx) \sin\xi + \sqrt{(\epsilon_x - jx) - \cos^2\xi}} \quad (3.19)$$

where j equals $\sqrt{-1}$ and ξ is the angle of incidence given by $(\pi/2) - \gamma$, where γ is defined in (3.16). x is

$$x = \sigma / \omega \epsilon_v \quad (3.20)$$

where σ is the reflector's conductivity, ω the angular frequency of the incident radiation and ϵ_v the dielectric constant of the propagation medium. Also

$$\epsilon_r = \epsilon / \epsilon_v \quad (3.21)$$

where ϵ is the dielectric constant of the scattering surface.

Thus for different electrical surface constants, ϵ and σ , values of η_{F_i} and ψ_{F_i} can be obtained as a function of the incident angle ξ . Usually ξ is quite small, which means that η_{F_i} is close to unity and ψ_{F_i} close to π . However, for different surfaces, the behavior of these terms as a function of ξ varies significantly. In Fig. 10 we have shown the magnitude and phase for a typical surface. It can be seen from Fig. 10 that a significant change in η_{F_i} occurs as ξ increases. Also the dip at the Brewster angle may vary from a significant drop to only a 3 dB drop in amplitude depending upon the surface characteristics.

3.2.2 Diffuse Reflection Coefficient

When the surface of the scatterer is rough, energy from the incident ray is scattered away from the specular scattering direction (and thus is lost from the received signal). To account for this effect, we introduce the diffuse

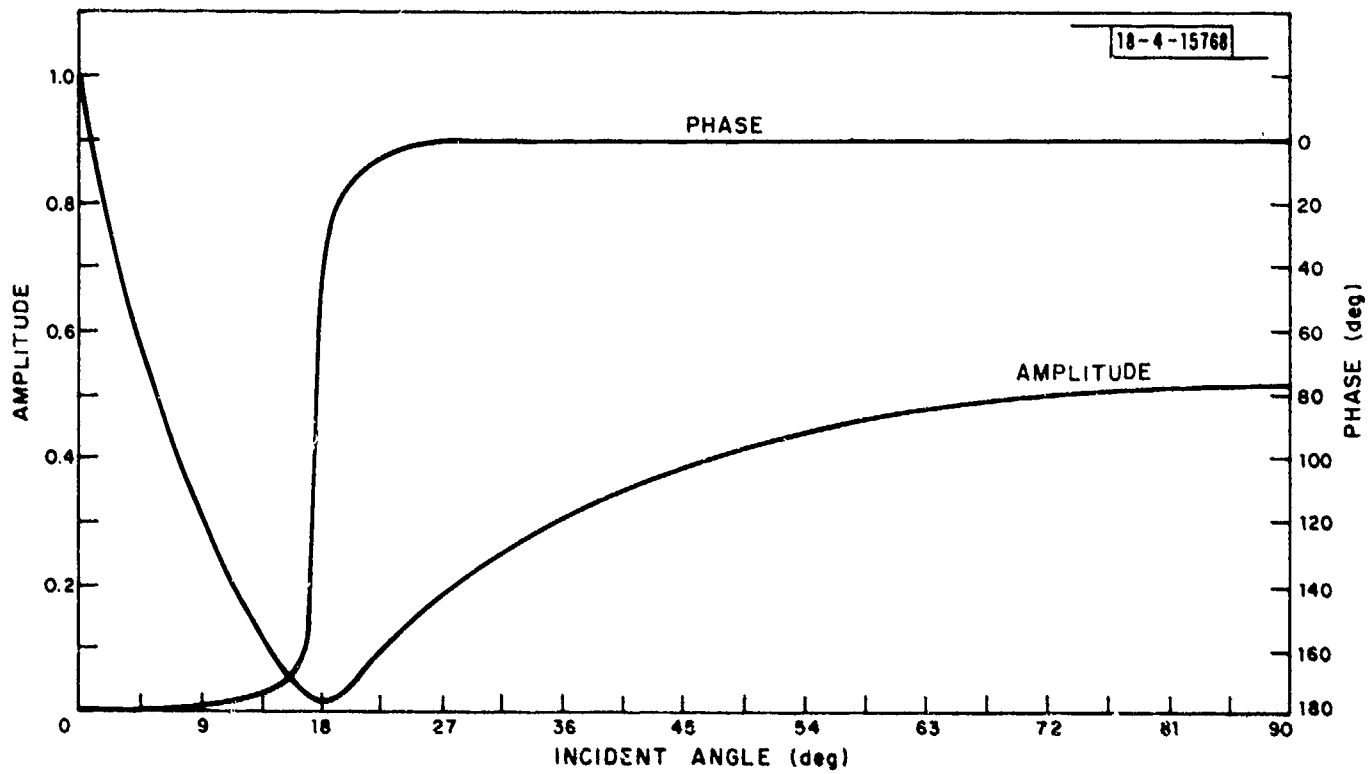


Fig. 10. Reflection coefficient.

reflection coefficient η_{D_i} for each surface. This coefficient has been determined by Beckmann [2] and it depends upon the angle of reflection, ξ , as does the Fresnel reflection coefficient. It also depends upon the statistical properties of the scattering surface. Specifically, if $z(x, y)$, the height of the surface at point x, y , is a zero mean Gaussian random variable with variance σ_h^2 , Beckmann shows that

$$\eta_{D_i} = \exp \left[- \left(\frac{4\pi \sigma_h \sin \xi}{\lambda_0} \right)^2 \right] . \quad (3.22)$$

For ξ close to 0 the coefficient is near unity. However, for very rough surfaces ($\sigma_h \gg \lambda_0$), this term decreases rapidly as the angle of incidence increases. In Fig. 11 we have sketched η_{D_i} for two different roughness ratios, σ_h/λ_0 , as a function of ξ .

3.2.3 Diffraction Effects

As the size of the reflecting surface decreases, diffraction becomes important and ultimately dominates the behavior. For example, it is well known that a rectangular surface illuminated by a plane wave from direction \underline{k} as shown in Fig. 12(a) diffracts the radiation into the specular direction and into other directions according to the $\sin x/x$ distribution. In Fig. 12(b) we have plotted the distributions of the diffracted amplitude of the field in the k_x, k_y directions. Note the central peak in the specular direction, \underline{k}' , and the presence of sidelobes in other directions. In Fig. 13 two representative specular reflectors, S_1 and S_2 , are shown with sketches of the diffraction pattern of the reflected radiation superimposed. The dimensions of surfaces

18-4-15769

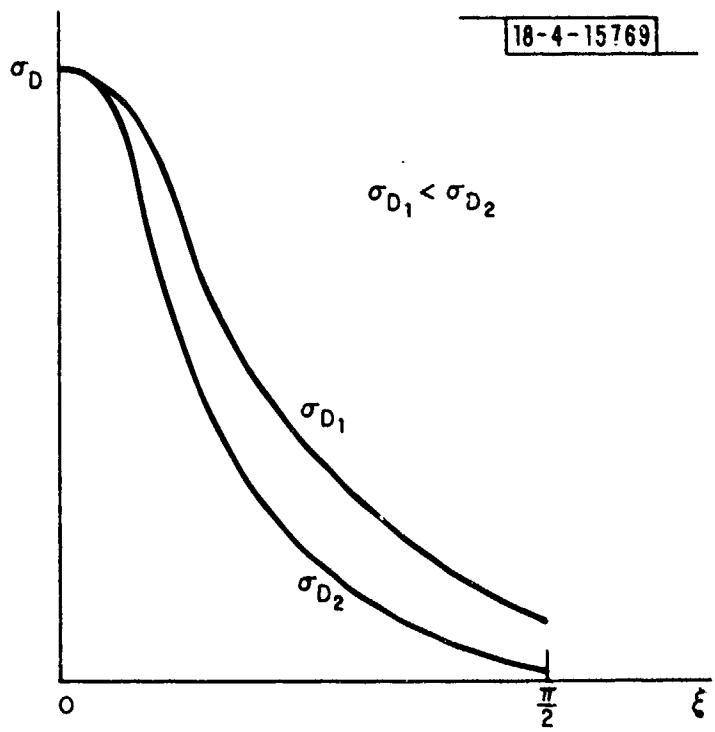


Fig. 11. Behavior of diffuse reflection Coefficient.

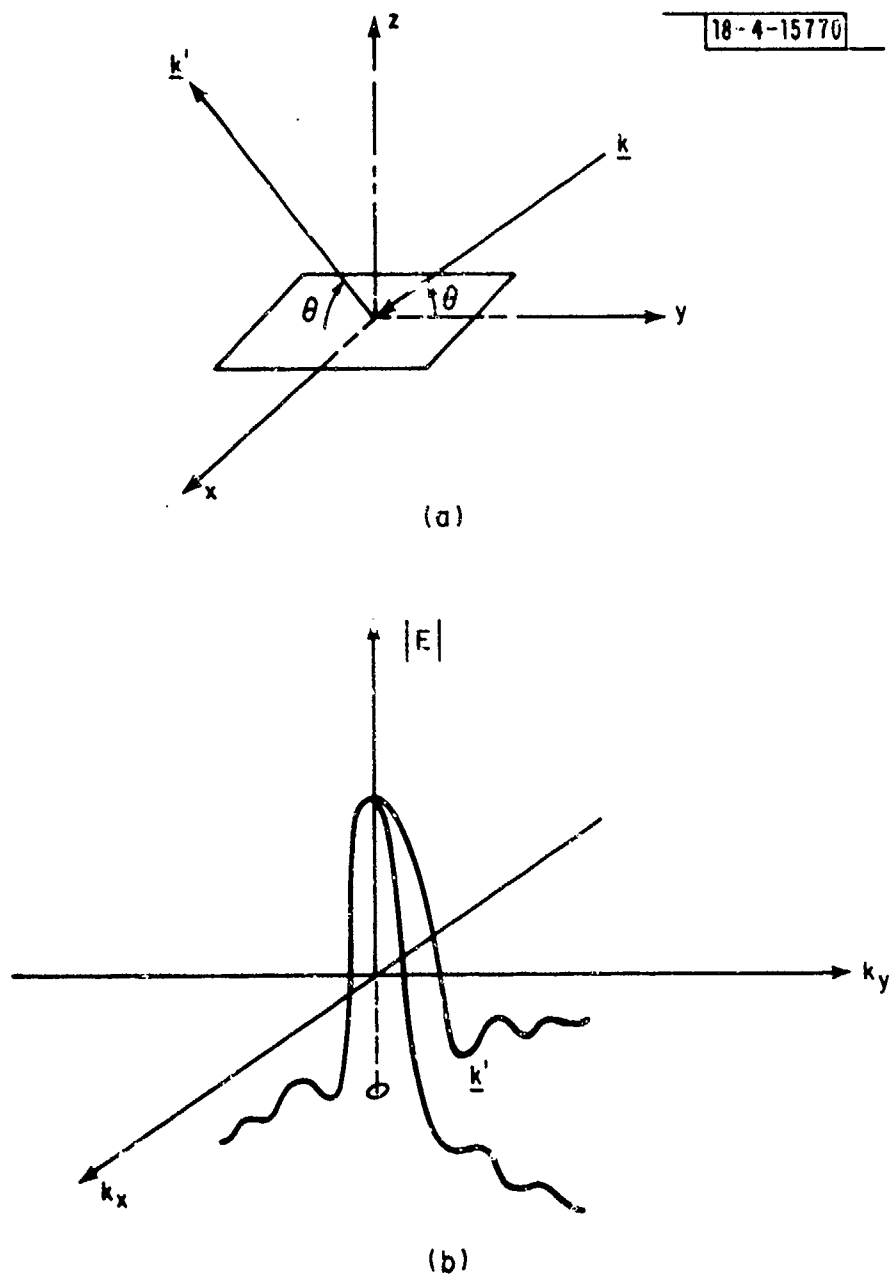


Fig. 12. Diffraction from a rectangular plane.

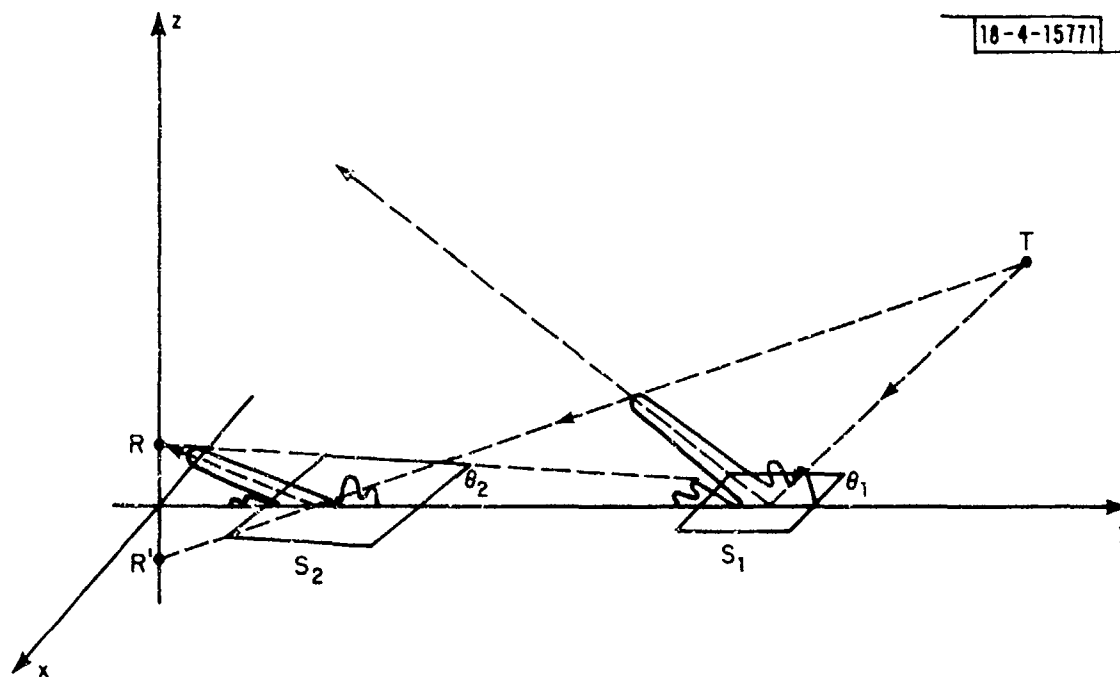


Fig. 13. Movement of diffraction plane and specular diffraction.

S_1 and S_2 are assumed to be small enough that the radius of curvature of the wavefront is large compared to the surface size. This allows us to say that the incident wave is coming from the direction joining the midpoint of the surface to T, and the surface is irradiated by a plane wave.

The amplitude of the field received from a reflector depends on the width and orientation of the diffraction pattern, which in turn depends on the size and location/orientation of the reflector, respectively.

From geometrical optics we know that if T emits a spherical wave and the wave is scattered by some plane, then the scattered wave is also spherical. Furthermore, the apparent direction of the radiation can be obtained by observing the direction of the ray passing through the desired point. Thus, in Fig. 14, we have drawn a ray diagram for a wave travelling from T and have shown seven receivers. The reflected wave is also shown to be spherical by drawing the normal to the rays. Now consider any one of the receiver points R_1 . For this case of an infinite reflecting plane, we see that there is a definite reflecting point, P_1 , at which the ray follows Snell's law. We now pose the question: If there is only a finite amount of scattering surface, and P_1 is not on that surface, what is received at R_1 ? To find the answer we must consider diffraction analysis. Thus, in Fig. 13, if R is in the sidelobes of that diffraction pattern of surface S_1 , its amplitude is decreased. Furthermore, we can consider the following experiment. If we fix R and T in Fig. 13, move the surface S and plot the amplitude of the received field as a function of y , the range, we will effectively plot out the diffraction pattern for that surface. This result is sketched in Fig. 15. When the surface is centered at a point y^* , the amplitude of the signal received at R reaches a maximum.

18-4-15772

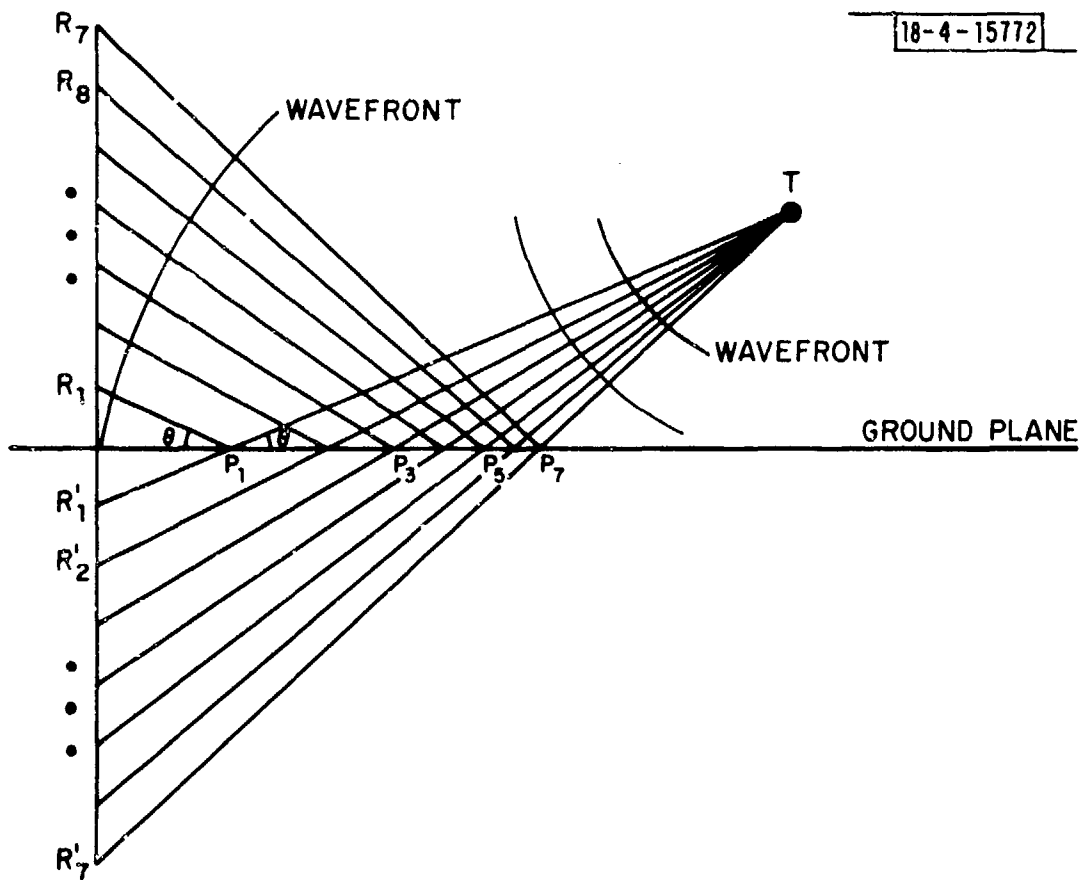


Fig. 14. Wavefront propagation.

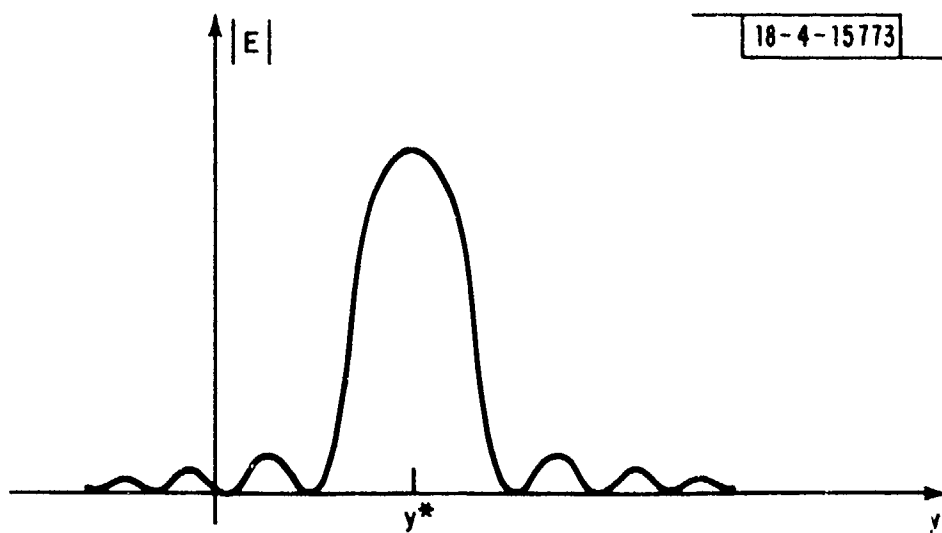
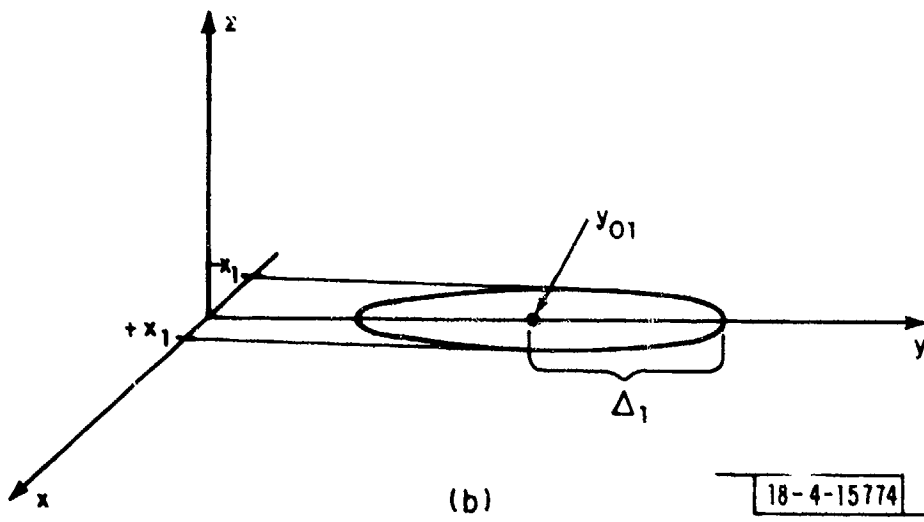
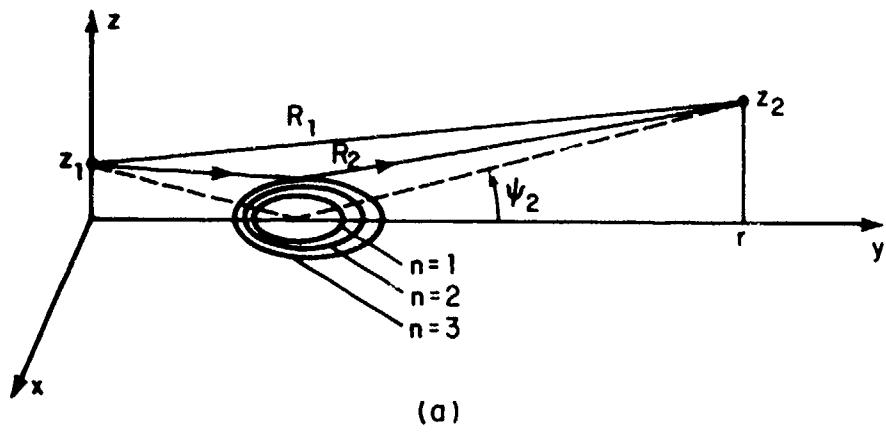


Fig. 15. Sketch of diffraction pattern.

Now if S is large enough (to have a narrow diffraction pattern) but not too large (small with respect to the radius of curvature) then the point y^* in Fig. 15 will, in some sense, correspond to the reflection points P_i in Fig. 14. That is, by positioning this small surface at the right point, we can effect a received wave that would appear to be coming from an infinite reflecting plane. This idea is the basis of the Fresnel zone concept. Furthermore, it can be rigorously shown that if one has many such planes, that only the one centered at the right position will contribute to the received field while all others will coherently cancel.

In view of the above discussion, we can consider what portion of an infinite reflecting plane dominates in the reflecting process. This area is called the first Fresnel zone and represents the region on the plane where the first π radians of phase shift occurs. The higher order Fresnel zones represent regions of increasing π radians of phase shift. These zones are depicted in Fig. 16(a). The first zone is shown in Fig. 16(b) in more detail. It is an elliptical surface located at a center point y_{01} with an extent $\pm \Delta_1$ about that point and $\pm x_1$ about the x axis. These quantities are given in terms of z_1 , z_2 , and r as follows:

$$y_{01} = \frac{\left[1 + \frac{2z_1(z_1 + z_2)}{\lambda_0 r} \right]}{\left[1 + \frac{(z_1 + z_2)^2}{\lambda_0 r} \right]} \frac{r}{2} \quad (3.23)$$



18-4-15774

Fig. 16. Geometry of Fresnel zones.

$$\Delta_1 = \frac{r}{2} \frac{\left[1 + \frac{2\delta_0 \pi/2}{\lambda_0} \right]}{\left(z_1 + z_2 \right)^2} \frac{1}{1 + \frac{\lambda_0 r}{\lambda_0 r}} \quad (3.24)$$

where δ_0 is defined by;

$$\delta_0 = \frac{2z_1 z_2}{r} \quad (3.25)$$

and

$$x_1 = \frac{1}{2} \left[\frac{\lambda_0 r}{2} \frac{1 + \frac{2\delta_0}{\lambda_0}}{\left(z_1 + z_2 \right)^2} \right]^{1/2} \quad (3.26)$$

The area of the Fresnel zone, A_F equals;

$$A_F = \pi x_1 \Delta_1 \quad (3.27)$$

With these values we can determine whether or not a surface will act as a source of reflection from the transmitter to receiver. Namely, if it is in the first Fresnel zone then it clearly will reflect an amount limited by the dilution of the main lobe of the diffraction pattern due to its finite size. If, however, it lies outside the first Fresnel zone then its contribution to the reflected signal will be limited to that portion which is in the zone. Thus, as the reflecting surface moves out of the Fresnel zone its reflected signal amplitude at

the receiver decreases, the amplitude being determined by the sidelobes of the diffraction pattern.

Thus an evaluation of the diffraction reflection coefficient, η_{D_i} , can be determined from the diffraction pattern of the surface being irradiated. However, such a calculation is often quite tedious. A reasonable approximation is let η_{D_i} equal the ratio of the amount of reflecting surface area in the first Fresnel zone to the area of the first Fresnel zone. This is a quantity that is easily calculated. That is, if A_i is the area of the i th reflector in the first Fresnel zone then;

$$\eta_{D_i} = \frac{A_i}{A_F} \quad (3.28)$$

Thus, (3.19), (3.22) and (3.28) provide all that is necessary for ρ_i in (3.17). Furthermore, this completes the specifications of all the parameters in the specular signal of (3.1).

3.3 EXAMPLES OF RECEIVED SIGNALS

The model developed at the beginning of this section for the specular portion of the received signal can be used to demonstrate the effect of certain terrains or structures on the signal. The dominant effect is that of fading, where the direct return and other multipath returns add coherently to cause a decrease in signal amplitude. This can produce a reduction in the signal-to-noise ratio which seriously affects detection and position estimation. Using the model just developed, it is possible to see what type of multipath environment will give rise to the more deleterious effects and how through proper siting and antenna design, they may be prevented.

The fading property of the signal is easily observed by evaluating the power in the specular returns. Thus, let $\tilde{\sigma}(t)$ be the magnitude squared of (3.1). It can be written as;

$$\begin{aligned} \tilde{\sigma}(t) = & E_s A \sum_{i=1}^N \frac{\rho_i^2}{R_i^2} G^2(\theta_i, \phi_i) \left| \tilde{f}\left(t - \frac{R_i}{c}\right) \right|^2 \\ & + E_s A \sum_{i=1}^N \sum_{\substack{j=1 \\ i \neq j}}^N \frac{G(\theta_i, \phi_i) G(\theta_j, \phi_j) \rho_i \rho_j}{R_i R_j} \\ & \tilde{f}^*\left(t - \frac{R_i}{c}\right) \tilde{f}\left(t - \frac{R_j}{c}\right) \cos(\psi_i - \psi_j) . \end{aligned} \quad (3.29)$$

Now if $\tilde{f}(t)$ has a width which is long in time with respect to the path differences then the time dependence may be neglected by integrating (3.29) and using the assumption in (2.5). The resulting time integrated function is called s and is (3.29) with the time dependence absent. The first terms are clearly independent of the path differences and are always positive. The second terms, those involving the double summation, depend on the path differences due to $\psi_i - \psi_j$ and can be negative. They represent the result of coherent addition of the wavefronts.

This phenomenon has been investigated by Spingler and Fig. 17 is a plot of these amplitudes versus aircraft elevation angle on a radial flight. One can note clearly the beat phenomenon and see the multiple beating. These results are for a typical ATC radar beacon interrogator antenna. Fades of 20 dB are not uncommon in this data set.

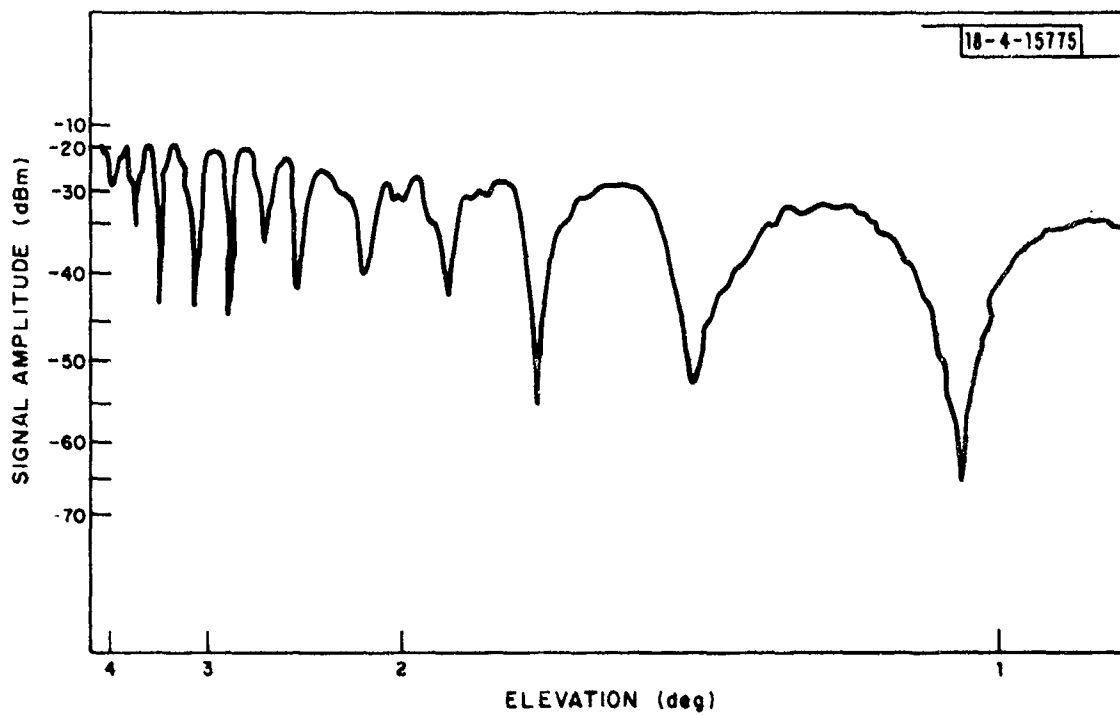


Fig. 17. Charleston, S. C., AN/FPS-27 site 1,000 ft flight test results on 53.6-degree radial.

Using the model developed in this section we have analyzed three specific cases in detail. Each case assumed a flat earth plus a single additional scattering plane. The three cases are depicted in Fig. 18. Case I is an example of a slightly sloping hill. Case II is a large vertical obstruction that is parallel to the y axis. Case III represents a moderately sloping rise. In all cases, the aircraft flew a radial out along the y axis at a fixed altitude.

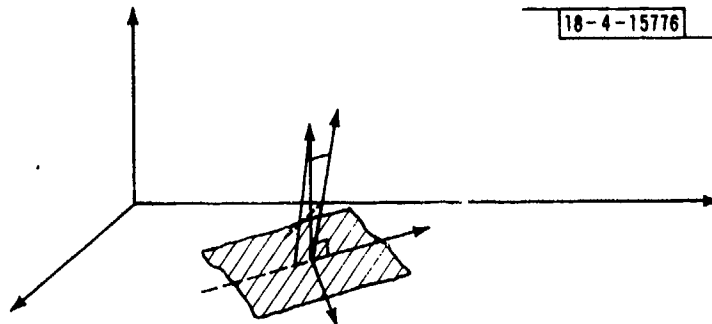
With each of these examples we also analyzed the effect of multipath on monopulse azimuth estimation and the performance of multipath-interference detectors (MID) (see McAulay and McGarty). For monopulse we have two responses $\tilde{\Sigma}$ and $\tilde{\Delta}$ corresponding to an antenna gain $G_{\Sigma}(\theta, \phi)$ or $G_{\Delta}(\theta, \phi)$ respectively. Using these gains in (3.1) and properly eliminating the time behavior (matched filter detection) one obtains $\tilde{\Sigma}$ and $\tilde{\Delta}$. It is clear that they are complex numbers. The estimated angle is given by

$$\hat{\theta} = k \operatorname{Re} \left[\frac{\tilde{\Delta}}{\tilde{\Sigma}} \right] \quad (3.30)$$

where k is the monopulse slope. The MID is given by τ where

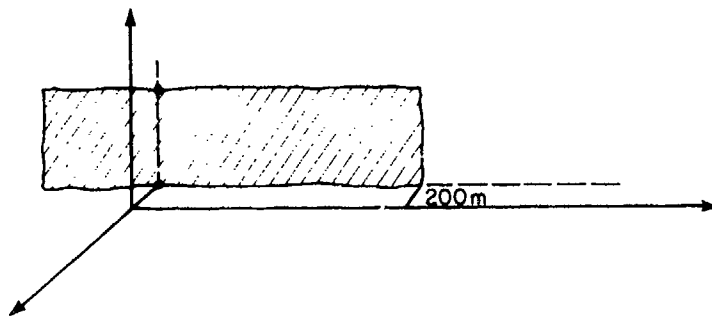
$$\tau = \left| \tilde{\Sigma} \right| \operatorname{Im} \left[\frac{\tilde{\Delta}}{\tilde{\Sigma}} \right] \quad (3.31)$$

In Figs. 19-21 we have plotted s , $\hat{\theta}$ and τ respectively versus $1/R$ (where R is range). The plot of s in this fashion shows the periodic nature of the received signal directly. The rapid beats are due to the extra reflecting plane while the lower frequency modulation is due to the flat earth reflection.



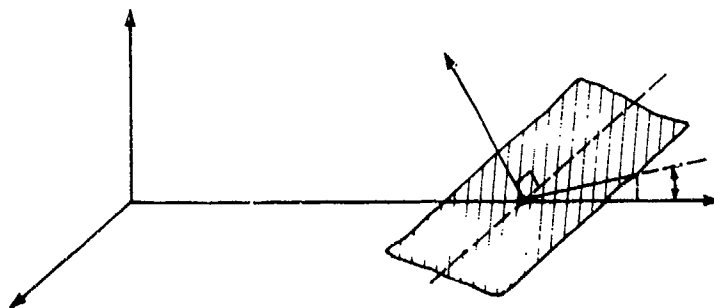
(a)

CASE I : $\alpha = \beta = 2^\circ$; $x_0 = 200\text{m}$, $y_0 = 1000\text{m}$, $z_0 = 0\text{m}$



(b)

CASE II : $\alpha = 0^\circ$, $\beta = 90^\circ$; $x_0 = -200$, $y_0 = 0$, $z_0 = 0$



(c)

CASE III : $\alpha = 4^\circ$, $\beta = 15^\circ$; $x_0 = 0$, $y_0 = 10,000\text{m}$, $z_0 = 0$

Fig. 18. Geometry of reflecting plane for cases discussed.

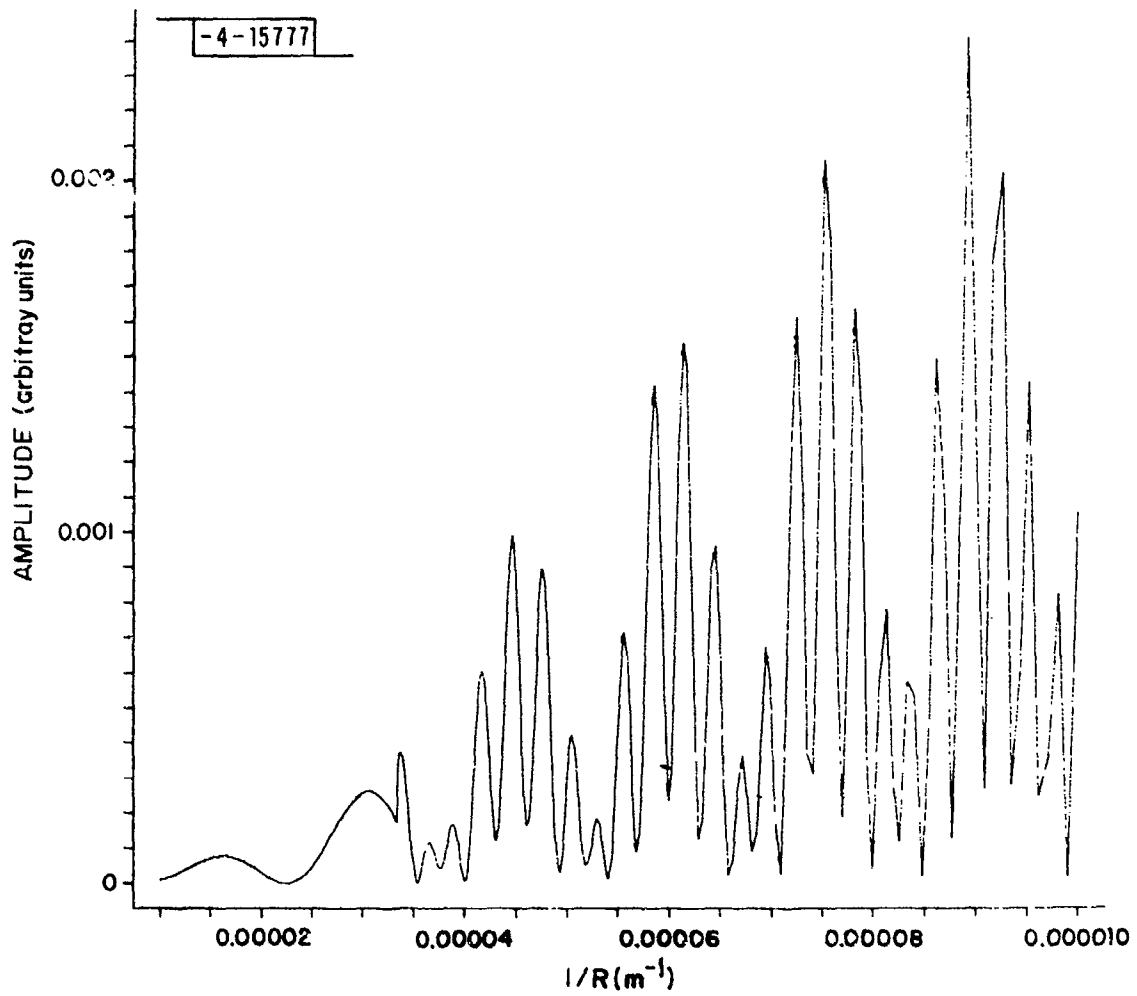


Fig. 19. Beam power vs inverse range; Case L.

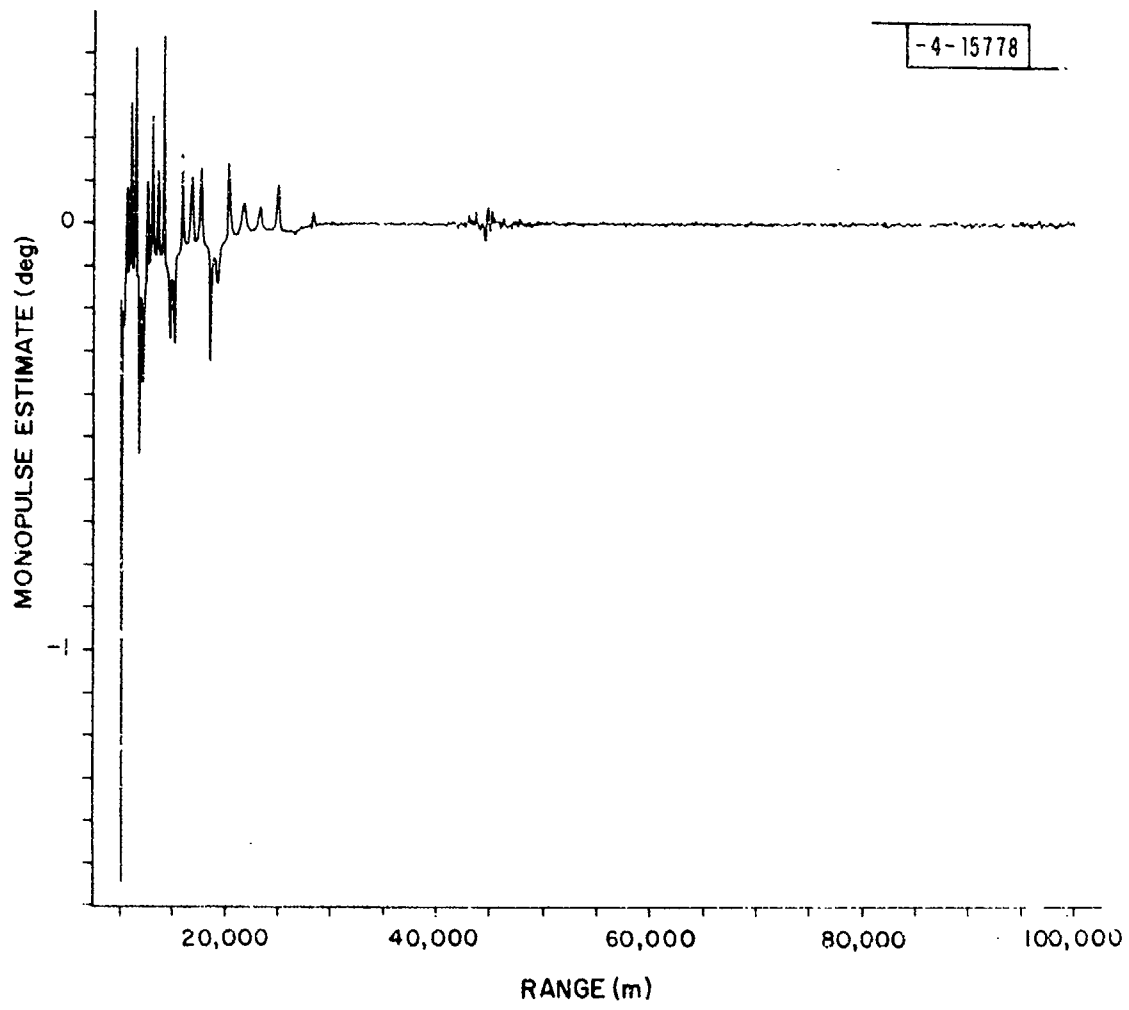


Fig. 20. Estimated angle vs range; Case I.

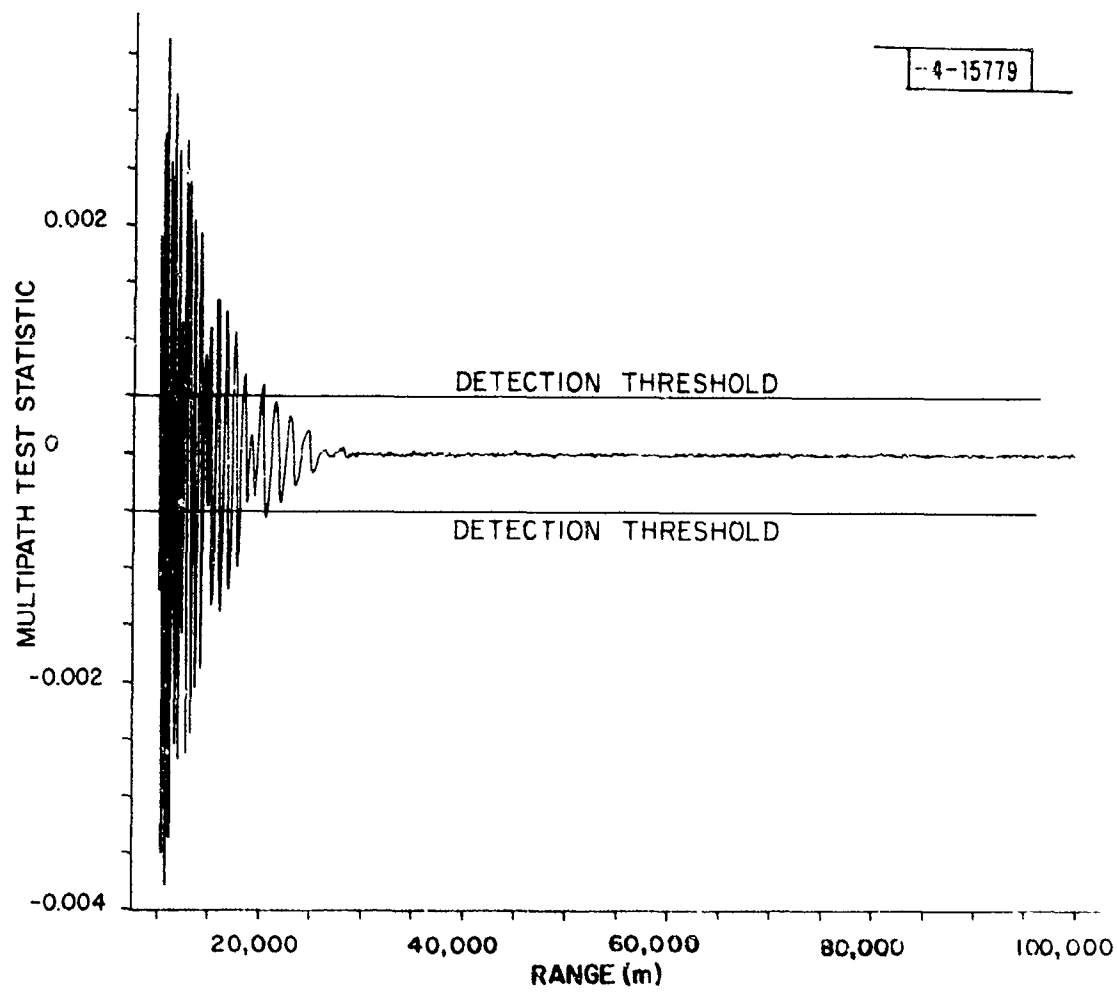


Fig. 21. Multipath test vs range; Case I.

The angle estimate in Fig. 20 for Case I shows the combination of both fading, SNR losses, and the multipath bias modulation effect noted by McAulay and McGarty. The plot of τ shows how such multipath is registered by this detector by its passage beyond the detection thresholds shown. These cases were done for 512 element dipole array that was tilted down 4° and had a 3 dB/degree vertical cutoff below the "horizon."

In a similar fashion, Case II is shown in Figs. 22-24. Here the multipath effect on angle estimates is more clearly pronounced in Fig. 23. Case III results are shown in Figs. 25-27 for a hogtrough antenna and in Figs. 28-30 for an antenna with vertical aperture. What is most clear here is that vertical aperture does help significantly in reducing the angle errors (Fig. 29). This is a result of increasing the effective SNR as is evidenced by comparing Figs. 25 and 28.

Various other analyses are possible that exhibit the effects of increased surface roughness, changes in the electrical properties and other reflecting plane orientations.

3.4 CONCLUSIONS

The effects of reflections from large smooth surfaces has been modeled as the coherent sum of plane waves incident on the antenna aperture. The waves can be completely characterized by their amplitude, phase, azimuth and elevation relative to the boresight of the antenna. In this section we presented a detailed model which could be used to develop a received signal which would be representative of specular multipath.

The specular multipath model developed depended upon the following points:

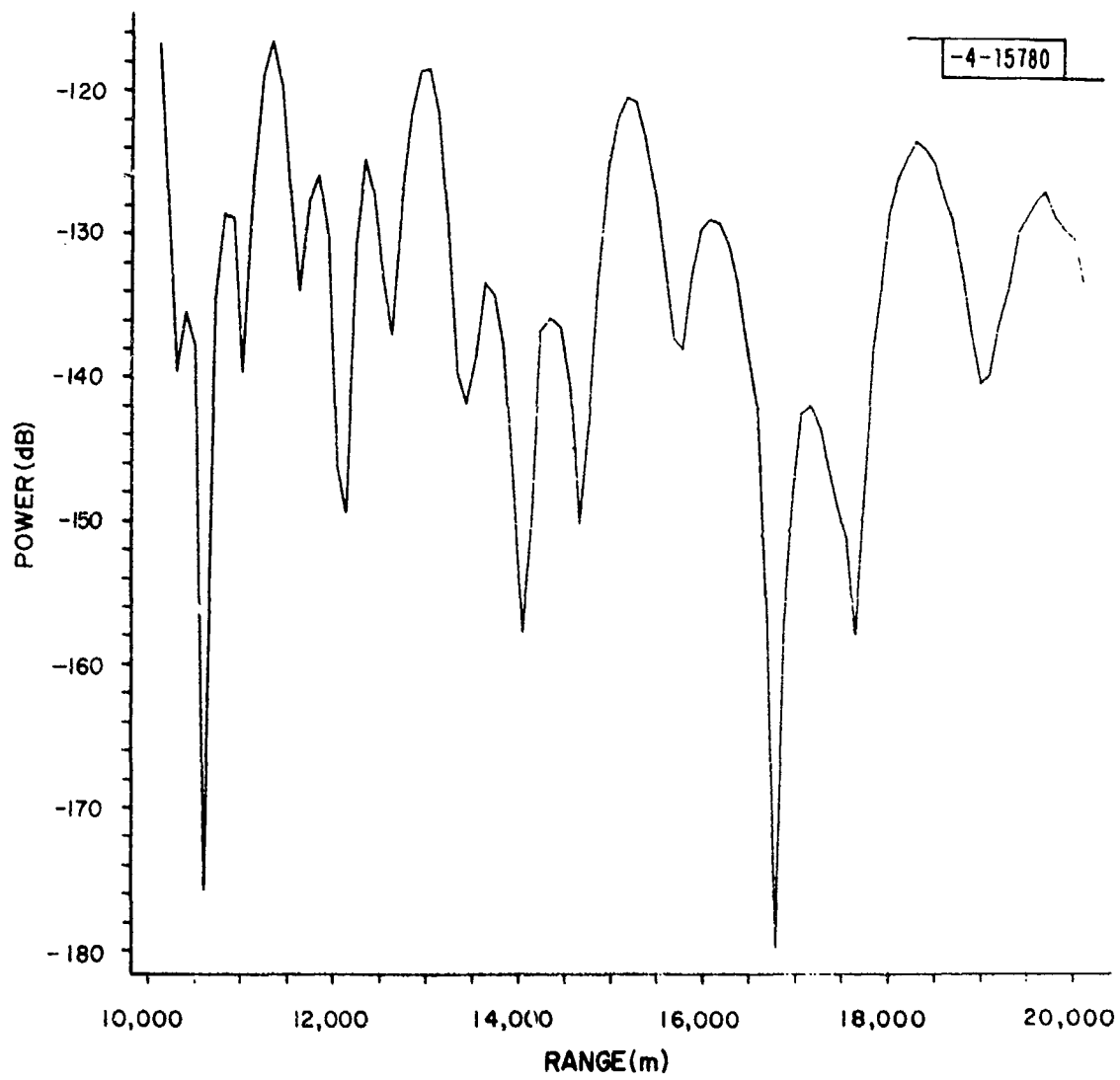


Fig. 22. Beam power in dB vs range; Case II.

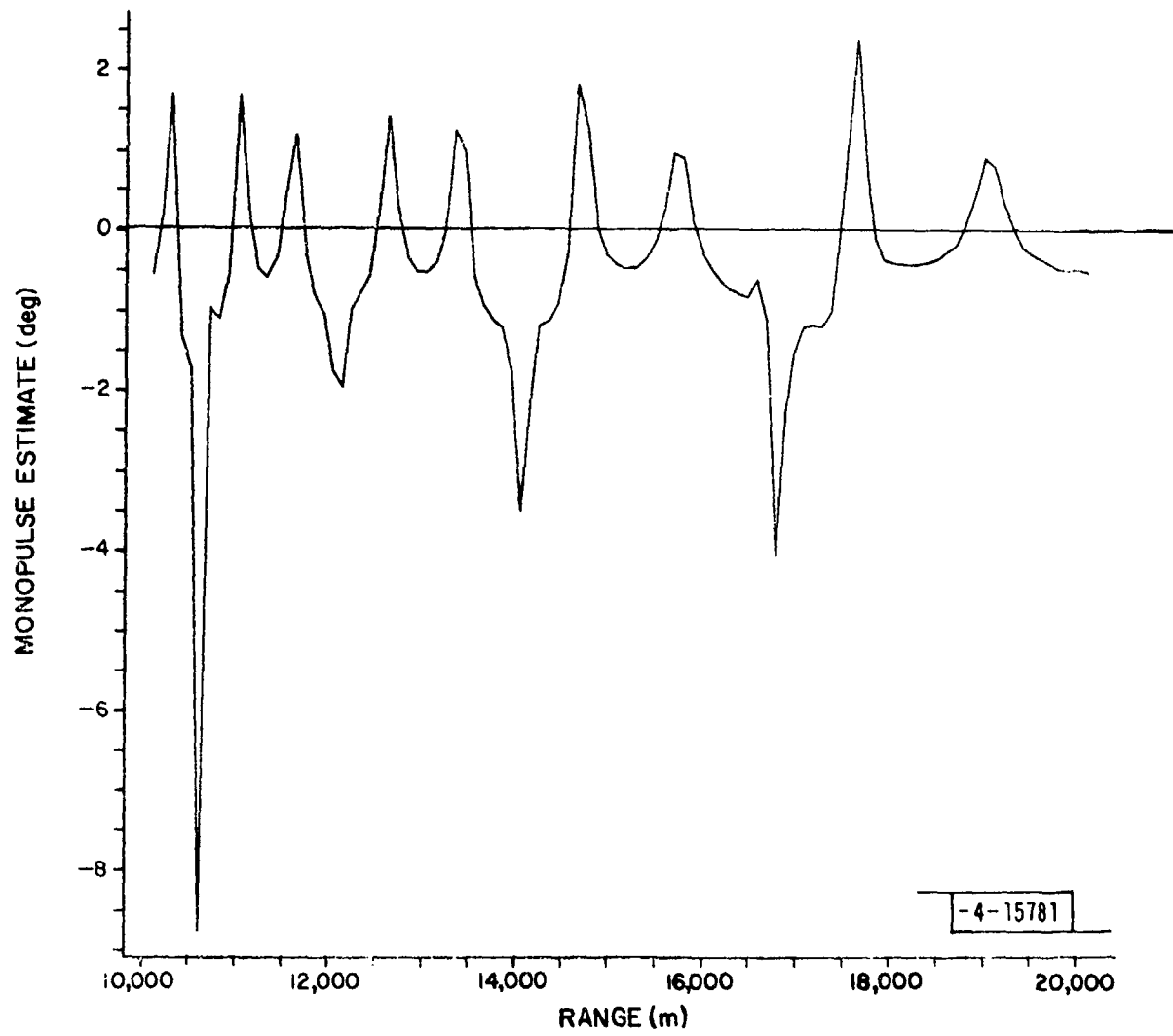


Fig. 23. Monopulse azimuth estimate; Case II.

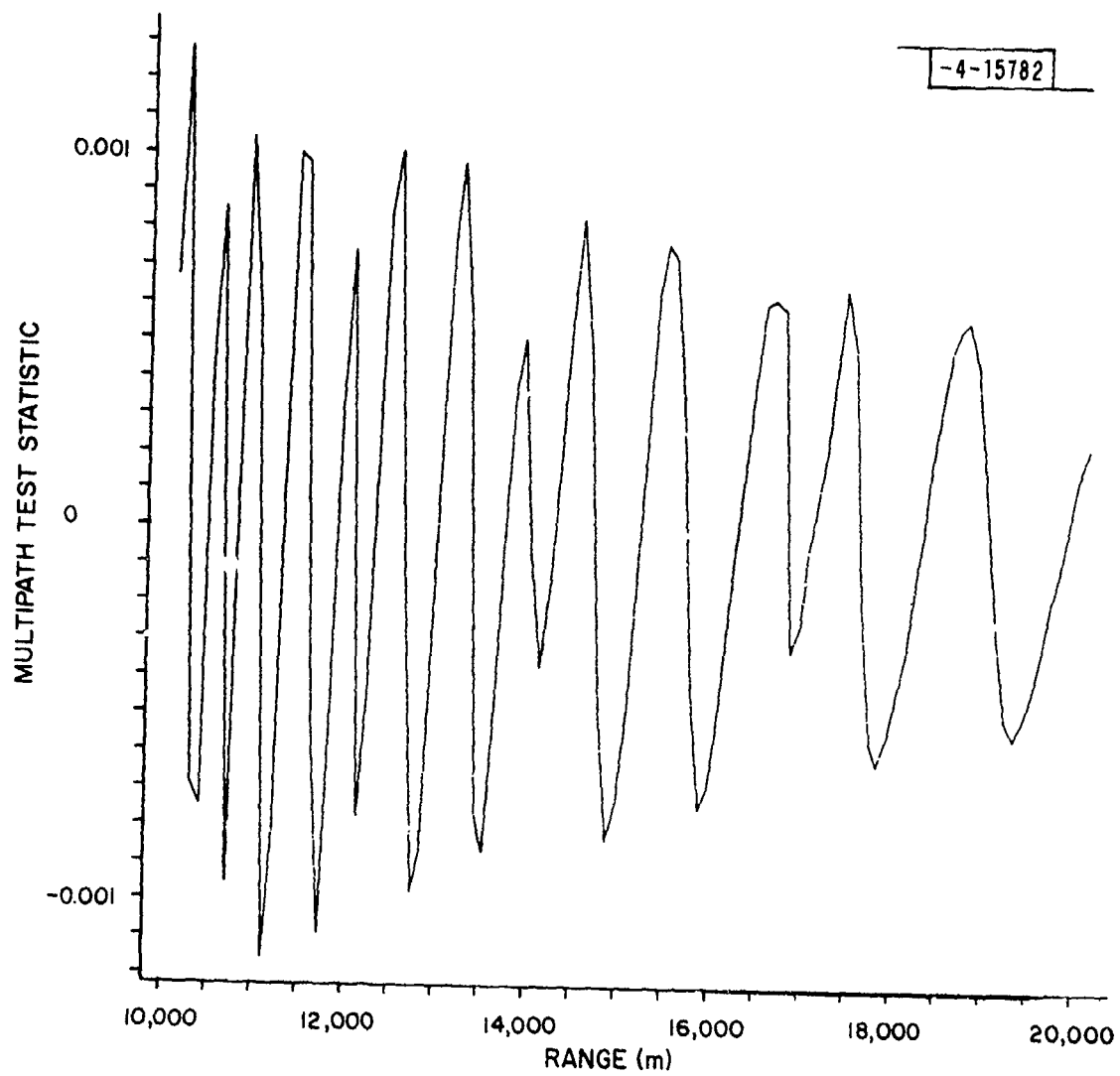


Fig. 24. Multipath detector output; Case II.

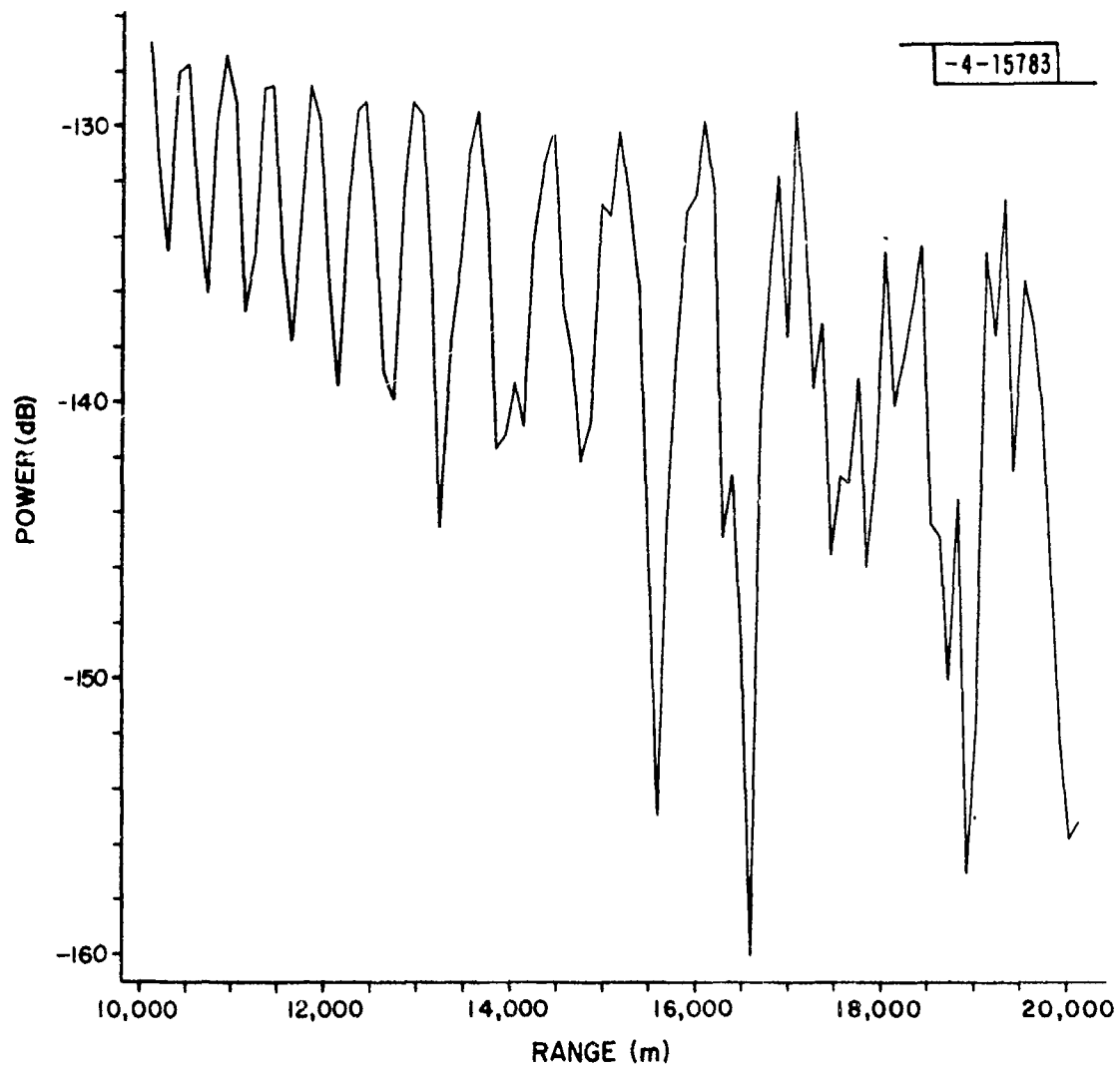


Fig. 25. Signal power vs range; Case III, no vertical aperture.

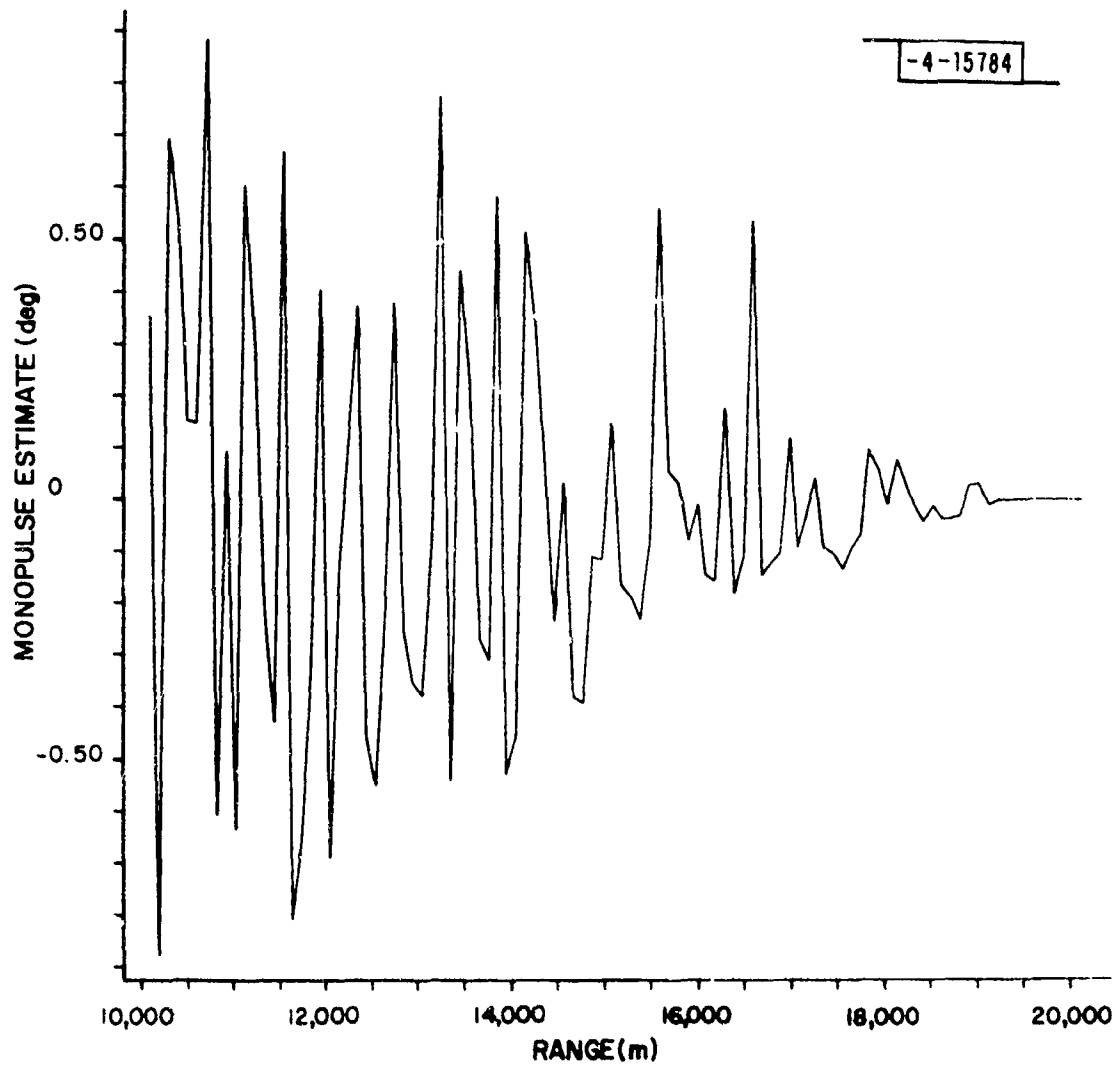


Fig. 26. Monopulse azimuth estimate; Case III, no vertical aperture.

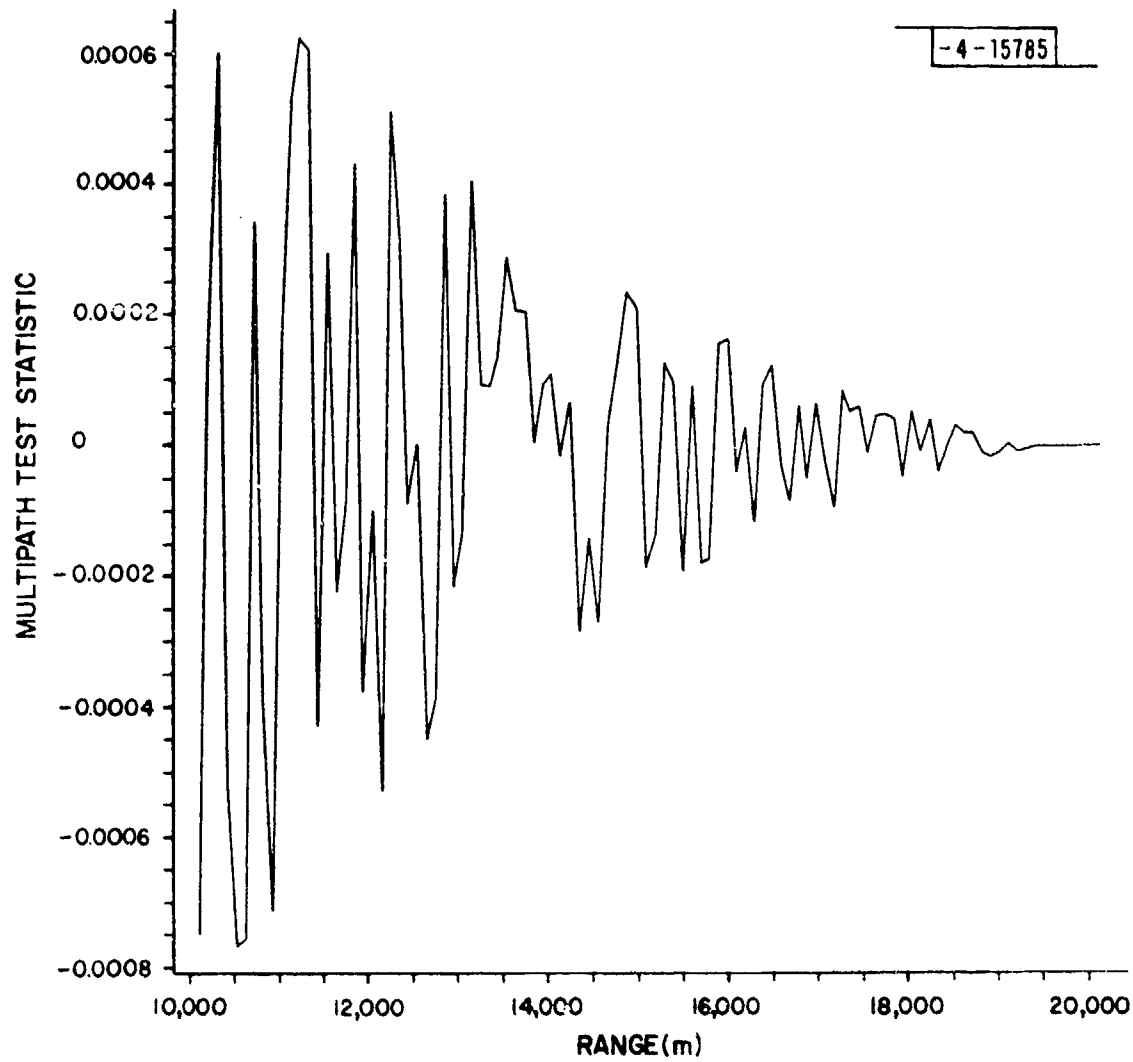


Fig. 27. Multipath detector statistic; Case III, no vertical aperture.

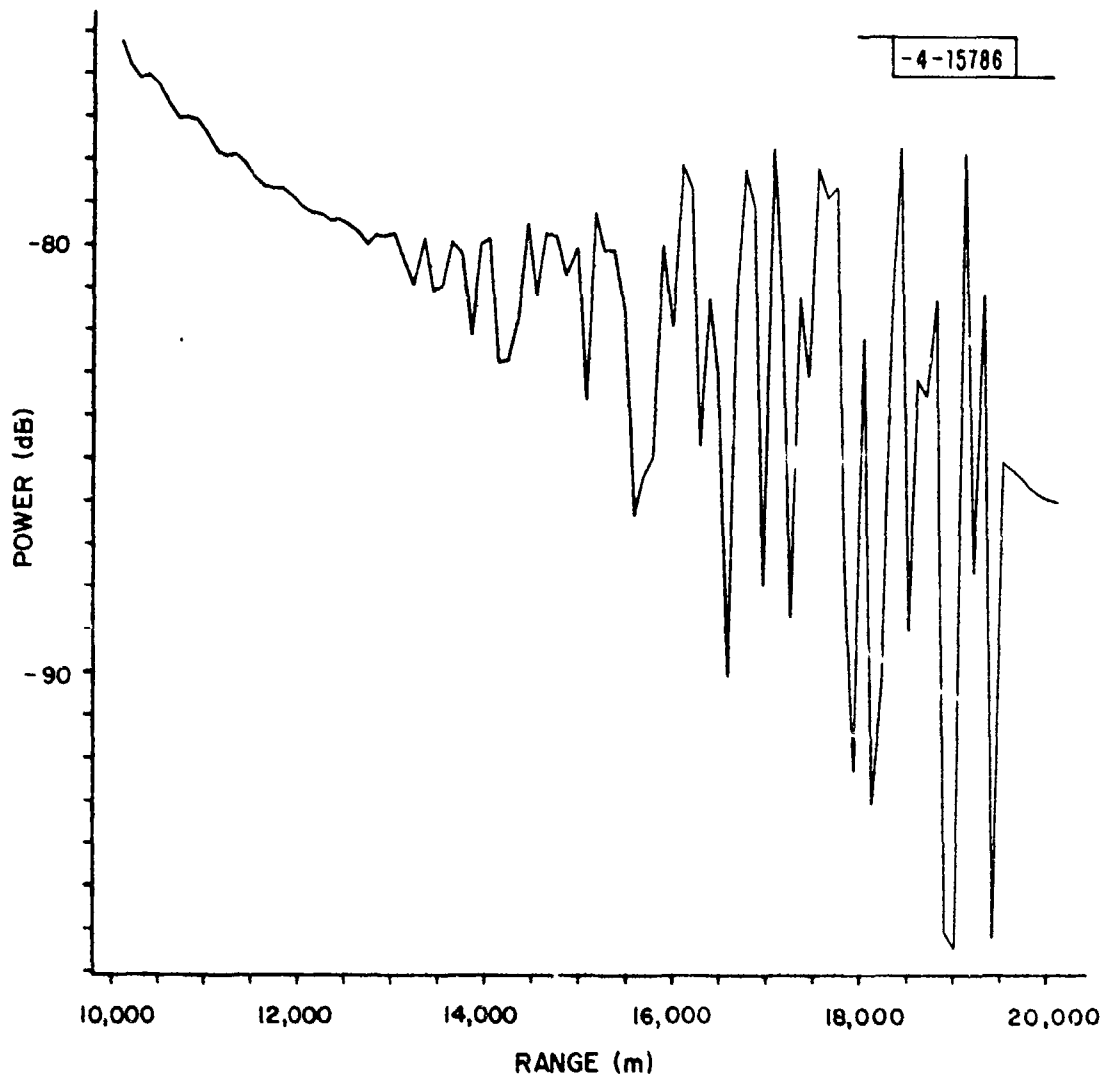


Fig. 28. Signal amplitude vs range; Case III, vertical aperture.

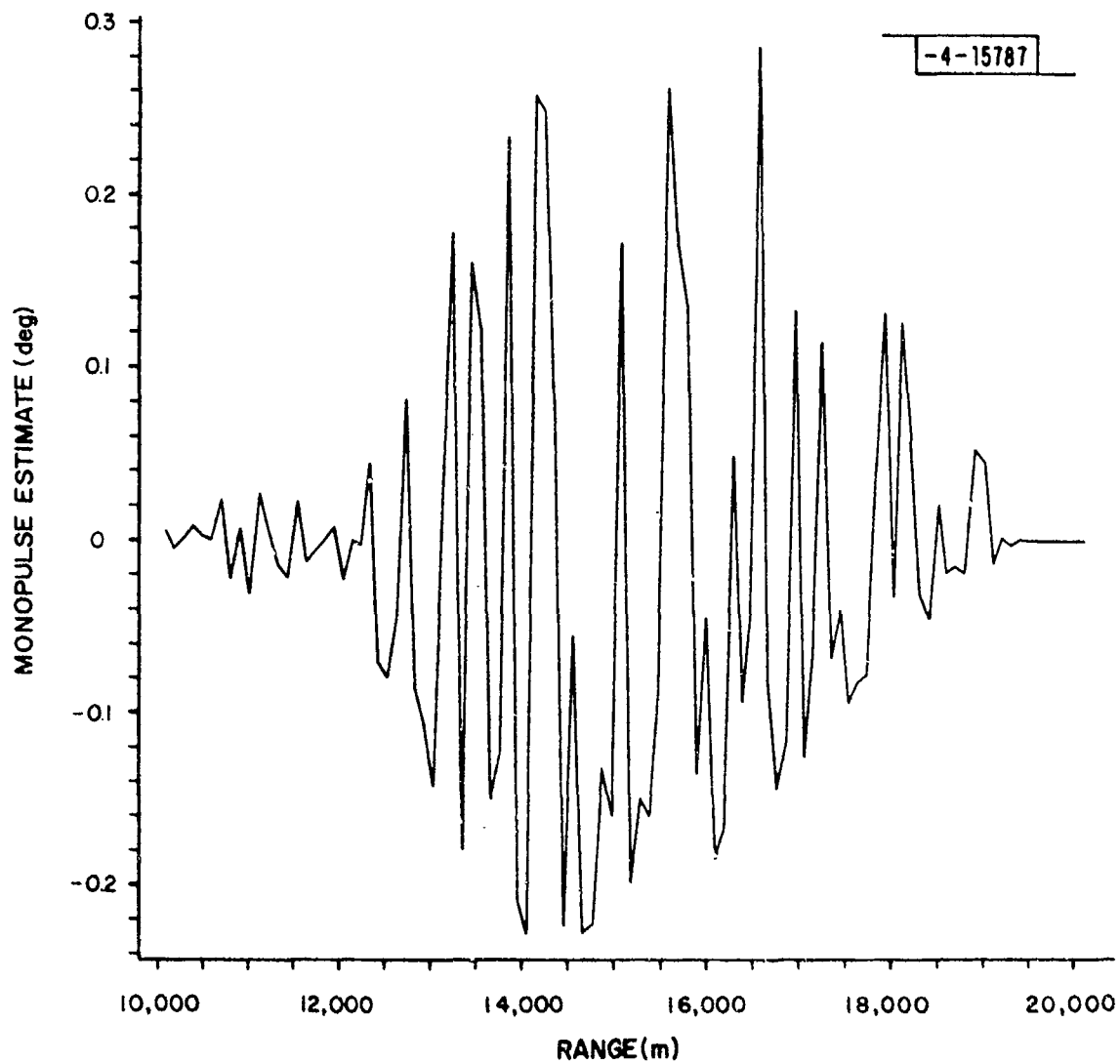


Fig. 29. Monopulse azimuth estimate; Case III, vertical aperture.

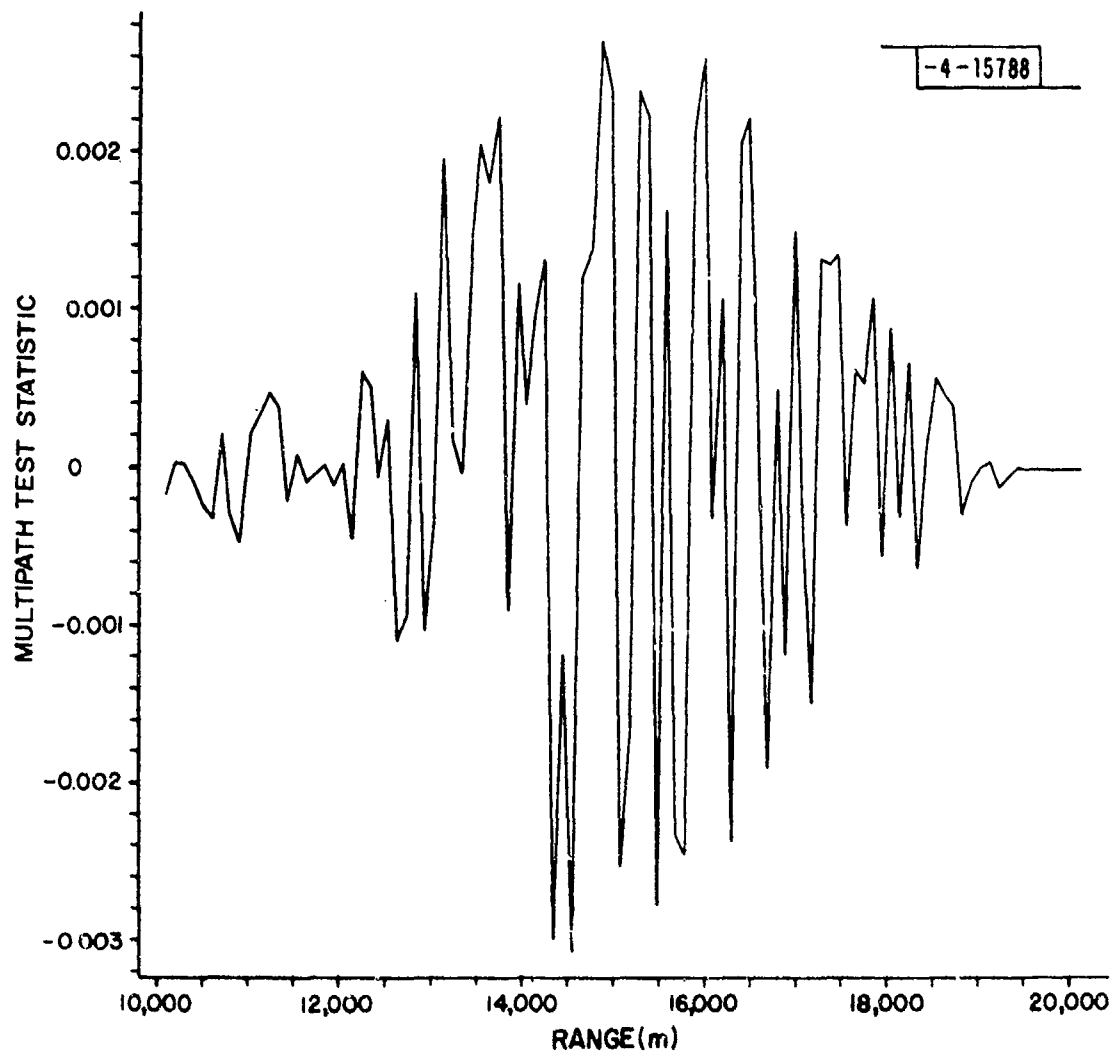


Fig. 30. Multipath detector; Case III, vertical aperture.

1. **Geometry:** For each multipath source a plane was positioned at the source location and tilted in both range and cross range directions to coincide with the actual surface. Evaluation of propagation distances could then be made directly knowing the location of the receiver and transmitter. All geometrical constants were determined for each multipath reflector in terms of the offset position of the plane, its range and cross range tilts and the locations of transmitter and receiver.
2. **Reflection Coefficient:** The effect of a multipath signal on azimuth estimation and link reliability depends directly upon how strong it is relative to the free space signal. The ratio of multipath to free space signal amplitudes is given by the reflection coefficient. These were
 - a. **Electromagnetic Reflection:** This is determined by the Fresnel reflection equation for a plane wave at the interface of two media with different electrical properties.
 - b. **Diffuse Multipath:** This represents the fraction of incident radiation that is not lost to other than the specular direction as a result of surface roughness.
 - c. **Diffraction:** If the surface is of finite size than its location and size must be considered. This results in a study of where the scattering aperture falls relative to the Fresnel zone projected on the scattering plane.

The inclusion of all these items leads to an analytical model which can be used to simulate what would be observed by an arbitrary antenna from a given terrain. Specific results for an antenna with the characteristics of the DABS experimental facility antenna (vertical aperture $8\lambda_0$, horizontal aperture, $26\lambda_0$) were evaluated. The antenna has a sum beam with a 3.2° beamwidth in azimuth difference beam and a sector beam in elevation with 3 dB/degree cutoff at the horizon. Plots of the sum beam, the monopulse azimuth estimate and the multipath-interference detector were plotted for three different multipath geometries. As a result of these simulations the following conclusions were reached.

1. The monopulse azimuth errors were in general quite small except when both fading from the flat earth and the multipath plane (tilted surface) occurred simultaneously. In those instances the effective free space signal was reduced resulting in an exceptionally large multipath to signal ratio and thus a large error. This effect can be countered however by using a large vertical aperture with a sharp cutoff below the horizon.
2. When the vertical aperture is reduced to λ_0 serious fades and monopulse errors occur.
3. The inclusion of a vertical aperture can reduce vertical lobe fades on the sum beam power from 20 dB with a λ_0 aperture to 6-8 dB with an $8\lambda_0$ aperture.
4. The MID shows strong correlation between large azimuth errors and its output. Therefore, it may be useful as a multipath detector.

The simulations discussed in this report represent only a small number of those that have been performed. Furthermore, recent comparisons of simulations with actual data obtained at DABSEF indicate that the model does represent the observed phenomena quite well in many cases.

SECTION FOUR

DIFFUSE MULTIPATH

Diffuse multipath is a random phenomenon, distinct from specular multipath, and must be treated as such. In contrast to the development in the last section, where exact descriptions of the scattering surface were given, in this section the nature of the scattering surface is describable in only a probabilistic sense. The reason for this is that the diffuse multipath arises from the roughness of the surface and is predominantly a diffraction effect. This will become important when we analyze the effects giving rise to the scattered field.

In the estimation of the azimuth of a cooperative signal source, the effects of multipath tend to degrade the performance of such estimates. The multipath encountered has been divided into two different categories, specular and diffuse. Specular multipath results from large smooth surfaces occupying a significant part of the first Fresnel zone. Diffuse multipath differs from the specular form in that when it is scattered, it does not propagate in a single direction but in a continuum of directions, depending on the roughness properties of the scattering surface. Diffuse multipath is a diffraction phenomenon where the element doing the diffracting is a small surface perturbation.

The effects of such scattering were discussed by Kerr(1951) in an attempt to analyze the effect of sea surface scattering on radar performance.

The approach used by Kerr was to obtain a scattering cross section for the surface. A more detailed approach was undertaken by Rice (1951) when he modeled the surface by means of a deterministic polynomial and then solved the random problem. His approach was quasi-deterministic and directed at sea surface scattering. A different approach using the Kirchoff approximation was presented by Eckart (1953) and was directed at acoustic scattering from rough surfaces. Equations for the field were obtained and then averaged. The resulting equations were then solved for the required quantities. This work was later followed by Ament (1953, 1956), using a similar approach.

Hoffman (1955) extended the analysis to the vector problem encountered in electromagnetic field problems, using the Kirchoff technique. Other attempts were made by Clark and Hendry (1964) to evaluate backscattering effects. The prime reference using the Kirchoff method is Beckmann and Spizzichino (1963). Their results give the field decomposition in terms of different scattered directions. They assume a Gaussian surface behavior with knowledge of surface standard deviations and correlation lengths. Experiments yielding these values have been discussed by Fung and Moore and Hayre and Moore.

Most of these previous results are not suitable for an analysis of azimuth estimator performance, however. It was shown by McGarty (1974), for the case of bearing estimation with a sonar array, that a function called the channel spread function was necessary to evaluate performance. This function gives the intensity of radiation incident at the receiver from all directions. This function cannot be obtained from the Beckmann and Spizzichino model. However, analyses by Kodis (1966) and Barrick (1968) provide exactly

what is necessary for the performance determination. Their analyses obtain a scattering cross section which relates the scattered radiation into a specific direction from a specified incident direction. The method of analysis differs greatly from others in that it solves the scattering problem first using a stationary phase technique (similar to Twersky (1957)), and then an averaging technique. The averaging technique yields a very physical formula for the scattering cross-section. It is in terms of the average number of scatterers, the average surface curvature (following Longuet-Higgins [1, 2]) and reflection coefficient.

4.1 THE SIGNAL MODEL

In Section 2, while discussing the nature of the total returned signal, we defined the diffuse multipath return as

$$\iint G(\theta, \phi) \tilde{b}(\theta, \phi, t) d\theta d\phi$$

where θ is azimuth, ϕ elevation and $G(\theta, \phi)$ the antenna gain for those angles. The terms $\tilde{b}(\theta, \phi, t)$ represents the random return from, θ, ϕ at time t . It is clear then that $\tilde{b}(\theta, \phi, t)$ is some form of a random process in time. Moreover, it is also a random process in space. Such processes are also called random fields.

We can motivate the structure of $\tilde{b}(\theta, \phi, t)$ by considering the geometry shown in Fig. 31. Here, as before, we have a transmitter at T and a receiver at R. We place, centered at (x', y') , an incremental surface dS . Energy is now transmitted from T and scattered from dS into all directions.

18-4-15789

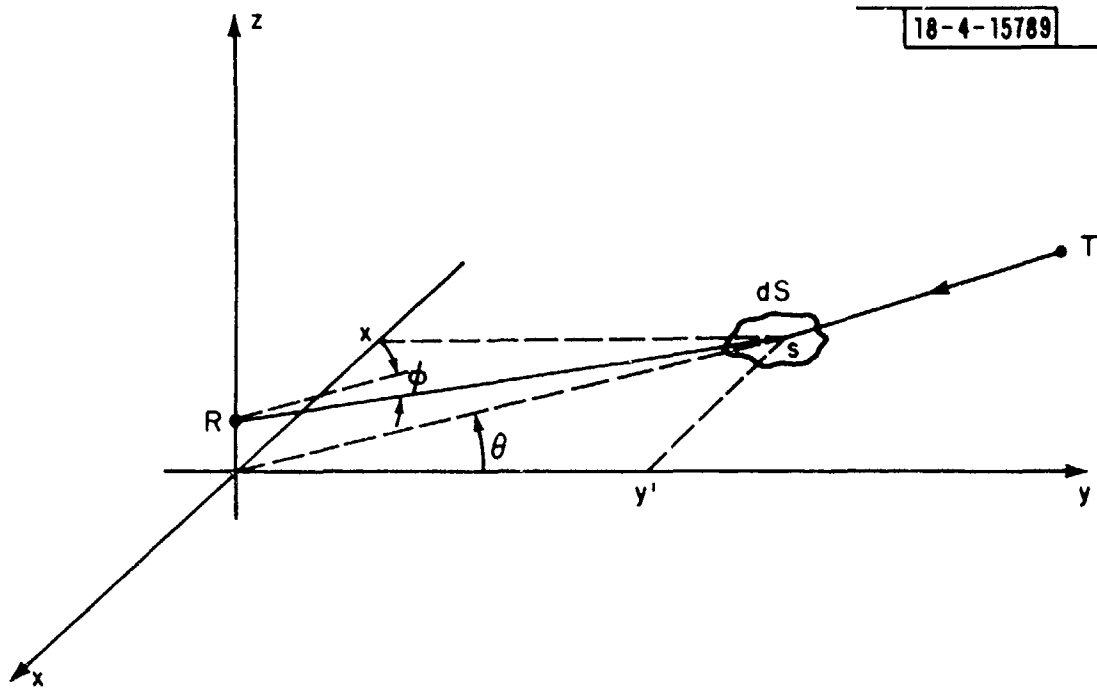


Fig. 31. Diffuse multipath geometry.

The amount arriving at R will depend on the diffraction nature of the surface (recall our discussion in Section 3.2.3).

The azimuth θ and elevation ϕ are shown in Fig. 31. It will be shown later that each (x', y') pair uniquely corresponds to a (θ, ϕ) pair, thus with this one-to-one transformation we can equivalently phrase the multipath in terms of these variables. Let us now also consider the temporal behavior of $\tilde{b}(\theta, \phi, t)$. Since we are assuming that the surface is not moving and that T is moving slowly compared to the measurements, the temporal behavior of the received signal is merely that induced by $\tilde{f}(t)$. Specifically, with these assumptions we have

$$\tilde{b}(\theta, \phi, t) = \tilde{b}(\theta, \phi) \tilde{f}(t - \frac{R}{c}) \quad (4.1)$$

where R is the path length \overline{TSR} . This then represents the effect at R at time t of the source at T radiating onto dS. The term $\tilde{b}(\theta, \phi)$ represents the random nature of the signal at R at time t.

Consider now some point \underline{r} which lies in the receiving aperture as shown in Fig. 32. Now the total reflecting surface can be viewed as the source of many waves incident on \underline{r} . Specifically, the surface dS generates a wave incident from direction \underline{k} as defined by the vector from \underline{r} to dS. Thus, we can consider each of the contributors from this surface to point \underline{r} as the contributor of a plane wave with an amplitude $\tilde{b}(\theta, \phi)$ or equivalently $\tilde{b}(\underline{k})$ where \underline{k} is uniquely defined by θ and ϕ . This allows us to write for an isotropic (omnidirectional) receiver at \underline{r} the observed signal as

18-4-15790

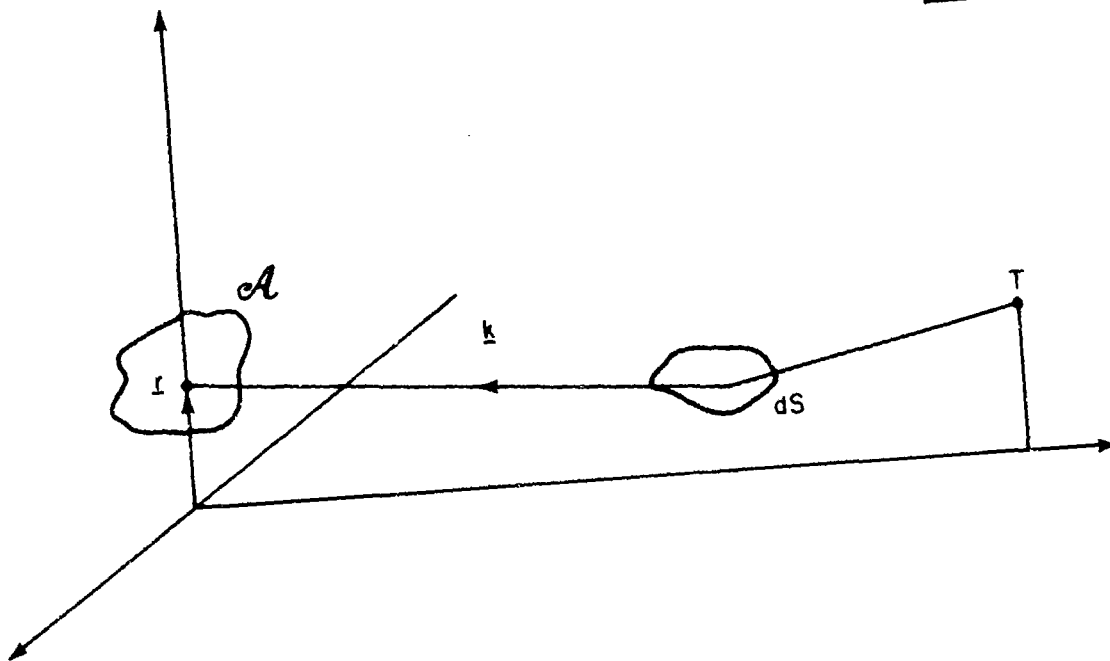


Fig. 32. Geometry of receiving aperture.

$$\tilde{s}(\underline{r}, t) = \iiint \tilde{b}(\underline{k}) \exp(j \underline{k} \cdot \underline{r}) \tilde{f}(t - \frac{R}{c}) d\underline{k} . \quad (4.2)$$

For simplicity, let us assume that the variation of $\tilde{f}(t)$ is small so it can be neglected. Thus we consider $\tilde{s}(\underline{r})$ where

$$\tilde{s}(\underline{r}) = \iiint \tilde{b}(\underline{k}) \exp(j \underline{k} \cdot \underline{r}) \quad (4.3)$$

Here $\tilde{b}(\underline{k})$ equals $\tilde{b}(\theta, \phi)$ and $\underline{k} \cdot \underline{r}$ is merely the projection of the incident direction vector on \underline{r} .

We now define the properties $\tilde{b}(\underline{k})$ should have to be consistent with properties of $\tilde{s}(\underline{r})$. Note that $\tilde{s}(\underline{r})$ is a random field in \underline{r} generated by $\tilde{b}(\underline{k})$. The first assumption on $\tilde{b}(\underline{k})$ is that it is a zero mean Gaussian random field. Thus

$$E[\tilde{b}(\underline{k})] = 0 . \quad (4.4)$$

This assumption is consistent with the roughness assumption leading to the definition of diffuse multipath. Since it is Gaussian, all we need for a complete statistical description is the covariance. That is, we need

$$E[\tilde{s}(\underline{r}) \tilde{s}^*(\underline{r}')] = K_s(\underline{r}, \underline{r}') . \quad (4.5)$$

This is written as;

$$K_s(\underline{r}, \underline{r}') = \iiint \iiint E[\tilde{b}(\underline{k}) \tilde{b}^*(\underline{k}')] \exp(j \underline{k} \cdot \underline{r} - j \underline{k}' \cdot \underline{r}') d\underline{k} d\underline{k}' . \quad (4.6)$$

It is convenient at this point to assume that $\tilde{s}(\underline{r})$ is a homogeneous random field over the aperture so that;

$$K_s(\underline{r}, \underline{r}') = K_s(\underline{r} - \underline{r}') \quad (4.7)$$

This implies (see Yaglom) that;

$$E[\tilde{b}(\underline{k}) \tilde{b}^*(\underline{k}')] = K(\underline{k}) \delta(\underline{k} - \underline{k}') \quad (4.8)$$

where $\delta(\underline{k} - \underline{k}')$ is a two dimensional impulse function. The function $K(\underline{k})$ or $K(\theta, \phi)$ is called the channel spread function and it is a measure of the energy coming from direction (θ, ϕ) to the point \underline{r} .

It is the channel spread function that defines the angle estimation performance of antennas (see McGarty [1]) and thus plays a dominant role in determining the effects of random multipath phenomena. It is the evaluation of this function from first principles and the use of it in system performance evaluation which will interest us in this section.

4.2 THE CHANNEL SPREAD FUNCTION

To evaluate the effect of diffuse radiation on azimuth estimation performance, it is necessary therefore to determine the channel spread function. To obtain this function, we must first evaluate the time behavior of the irradiated surface and also the radiation pattern of incremental portions of the surface. Once these two relationships are obtained, the spread function can be obtained directly.

Consider a point source located at position $(0, r, z_2)$ on the flat earth model as shown in Fig. 33. A receiver is located at $(0, 0, z_1)$. The source emits a spherical wave which begins at time t_0 and is received by the receiver at time t_1 where

$$t_1 = t_0 + \frac{d_0}{c} \quad (4.9)$$

where d_0 is the distance between the source and the receiver and is given by;

$$d_0 = \sqrt{r^2 + (z_2 - z_1)^2} \quad (4.10)$$

The power density of the wave received at the receiver is $P_0/(4\pi d_0^2)$ where P_0 is the power of the source.

The source also irradiates a portion of the surface of the earth and this surface scatters the radiation in all directions. The fraction of the incident power scattered to the receiver from the i th incremental area is given by σ_i , the scattering cross-section per unit area. Assume that there are N such areas. Then, the total amount of power per square meter received at the receiver due to the N discrete incoherently radiating surface areas is, S_N , where;

$$S_N = \sum_{i=1}^N \frac{\sigma_i P_0 A_i}{(4\pi)^2 R_{1i}^2 R_{2i}^2} \quad (4.11)$$

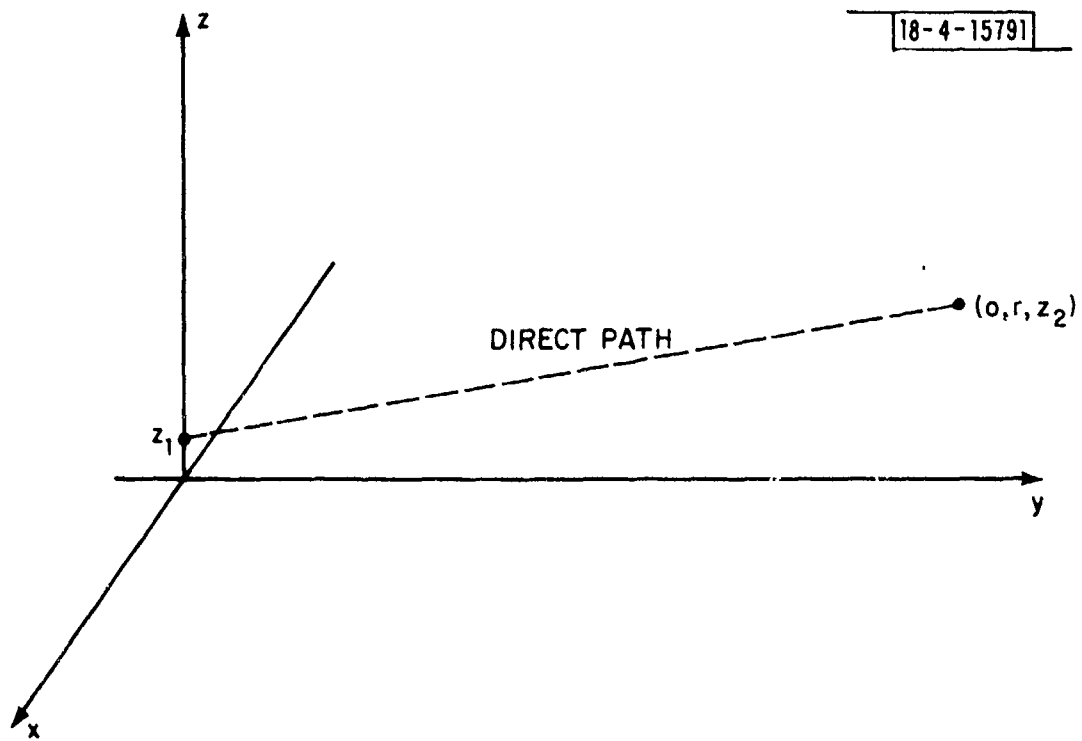


Fig. 33. Geometry of direct path.

where A_i is the area of the i th scattering section, R_{1i} is the distance from the receiver to the i th scatterer, and R_{2i} is the distance from the transmitter to the i th area.

Now, at any one instant of time, not all of the ground is illuminated by the source. For example, at $t = t_0$ the wave has just begun to propagate. The minimum amount of time it takes for a wave to propagate from the source to the receiver via a reflection from the earth's surface is,

$$t_s = \frac{\sqrt{r^2 + (z_1 + z_2)^2}}{c} \quad (4.12)$$

where c is the speed of propagation. At this instant, the area of the scattering plane illuminating the receiver is only a point. For $t > t_s$, we can find the area by finding the equations of all (x, y) such that the distance $R_1 + R_2$ equals ct . The resulting area is that area from which the receiver obtains power at time t . This follows directly from the fact that R_1 is the distance from the scattering point to the receiver and R_2 the distance from the scattering point to the source.

From the geometry of Fig. 34, it is clear that

$$R_1^2 = x^2 + y^2 + z_1^2 \quad (4.13)$$

and

$$R_2^2 = x^2 + (r - y)^2 + z_2^2 \quad (4.14)$$

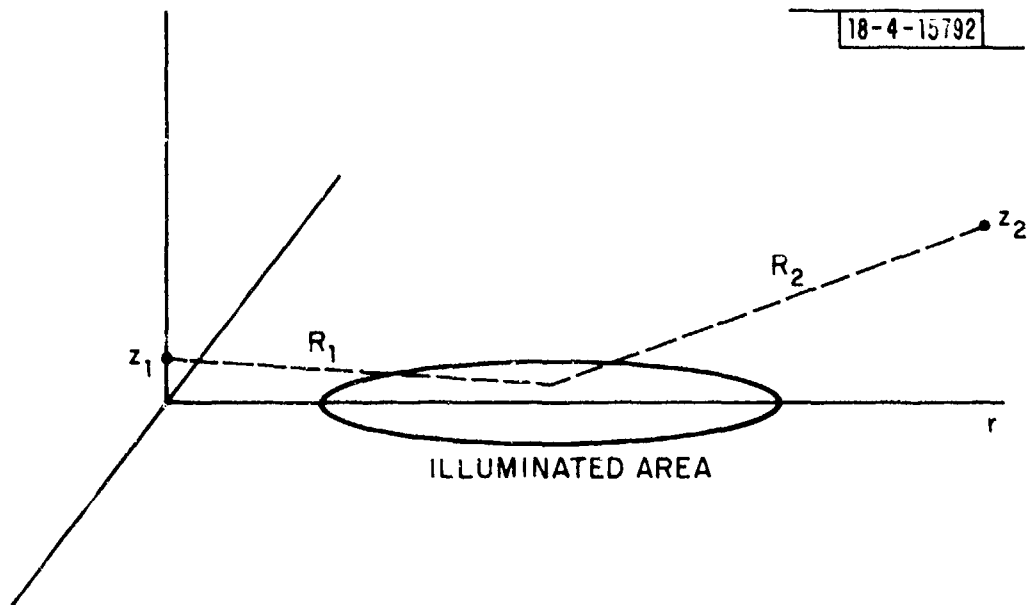


Fig. 34. Time variation of area.

Then, if we define for each time, t , a distance ρ as;

$$\rho = ct \quad (4. 15)$$

we can show that the area irradiated which gives rise to signals received at the receiver at time $t > t_s$ is bounded by the ellipse given by (see Appendix I)

$$a^2(y - y_0)^2 + b^2 x^2 = r_0^2 \quad (4. 16)$$

where

$$a^2 = r(\rho^2 - r^2) \quad (4. 17)$$

$$b^2 = 4\rho^2 \quad (4. 18)$$

$$y_0 = \frac{(\rho^2 - r^2 + z_1^2 - z_2^2)r}{2(\rho^2 - r^2)} \quad (4. 19)$$

and

$$r_0^2 = \rho^2 \frac{\left[(\rho^2 - r^2 + z_2^2 - z_1^2)^2 - 4z_2^2(\rho^2 - r^2) \right]}{(\rho^2 - r^2)} \quad (4. 20)$$

Thus, for any time t , the surface from which radiation is received is bounded by the ellipse given by (4. 16). We shall call the area of the elliptical surface $A(t)$. It is easily shown that as $t \rightarrow \infty$, the ellipse turns into a circular region.

Now, if we assume that the receiver is omnidirectional, then we can calculate the total power density at the receiver. This can be obtained directly from (4. 11) as a limiting case. Namely, if $\sigma(x, y)$ is the fraction of incident power scattered from (x, y) into the receiver, then the total power density at the receiver at time t is given by $S(t)$ where

$$S(t) = \frac{P_0}{(4\pi)^2} \iint_{A(t)} \frac{\sigma(x, y) dx dy}{R_1^2 R_2^2} \quad (4. 21)$$

where $A(t)$ is the bounding ellipsoid.

There is an important interpretation of Eq. (4. 21) worth noting. Consider the special case of a reflector which scatters the incident radiation uniformly in all directions. For this case we let $\sigma(x, y)$ equal σ_0 and obtain for $S(t)$;

$$S(t) = \frac{\sigma_0 P_0}{(4\pi)^2} \iint_{A(t)} \frac{dx dv}{R_1^2} \quad (4. 22)$$

$S(t)$, now in Eq. (4. 22), is the power per square meter at the receiver at time t . As t increases, the ellipse grows; however, the inverse distance squared values weight contributions less and less. It can be shown that (4. 22) approaches a limiting value at $t \rightarrow \infty$. An exact calculation is shown in Fig. 35. Here, we have plotted $S(t)$ versus time for $r = 15$ km, $z_1 = 10$ m and $z_2 = 3$ km. Note how rapidly $S(t)$ approaches almost a steady-state value. What this

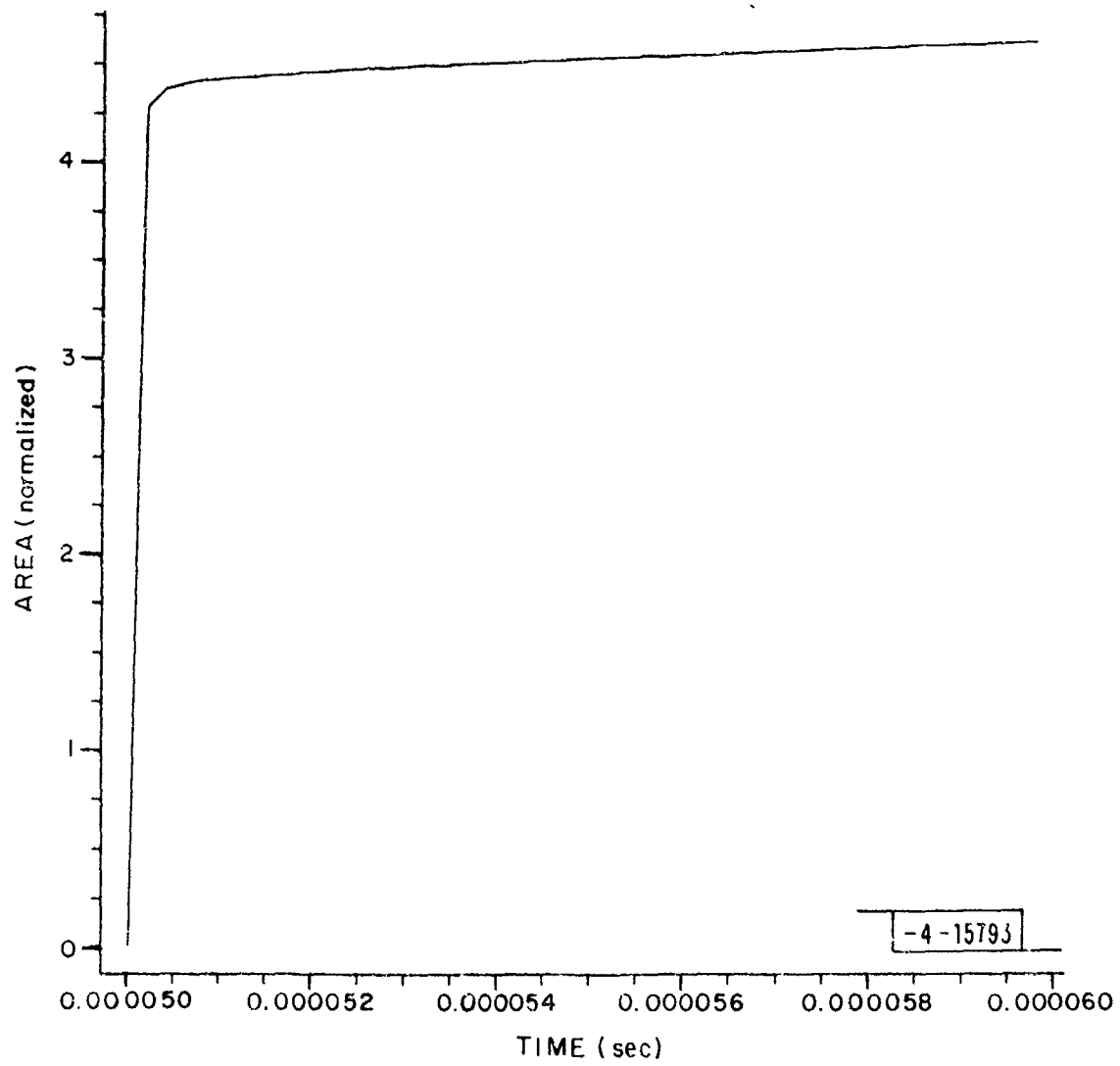


Fig. 35. Area, $S(t)$, vs time ($z_1 = 10$ m, $z_2 = 3$ km, $R = 15$ km).

implies is that there will be little time fluctuation in the diffuse field due to this effect.

The response $S(t)$ due to pulses is shown in Figs. 36 and 37. Here, the source emits a 1 μsec and 1.6 μsec pulse respectively. The corresponding power density is plotted. Again, note the sharp rise and cutoff values for the diffuse radiation. The rise time is about 0.5 μsec while the decay time is about 0.25 μsec .

To complete the analysis, the scattering cross section per unit area $\sigma(x, y)$ must be determined. To do this, we shall follow Kodis and Barrick and obtain the function $\sigma(\theta_s, \phi_s; \phi_i)$. This is the fraction of the incident power incident on a surface S from an angle ϕ_i and scattered into direction (θ_s, ϕ_s) . These directions are shown in Fig. 38. Here, it is assumed that the incident field is a plane wave, making an angle ϕ_i with the z axis and having a wave vector lying in the y - z plane.

To obtain this function, we write the scattered field as

$$\underline{E}_{sc}(\underline{r}) = -j\omega\mu \int_S \underline{\Gamma}(\underline{r}, \underline{r}') \underline{J}(\underline{r}') dS \quad (4.23)$$

where $\underline{\Gamma}(\underline{r}, \underline{r}')$ is the dyadic Green's function given by (see Silver, p. 132)

$$\underline{\Gamma}(\underline{r}, \underline{r}') = \left(\underline{I} + \frac{1}{k^2} \nabla \nabla \right) (\exp[jk|\underline{r} - \underline{r}'|] / (4\pi|\underline{r} - \underline{r}'|)) \quad (4.24)$$

and $\underline{J}(\underline{r}')$ is the surface current density and j is $\sqrt{-1}$.

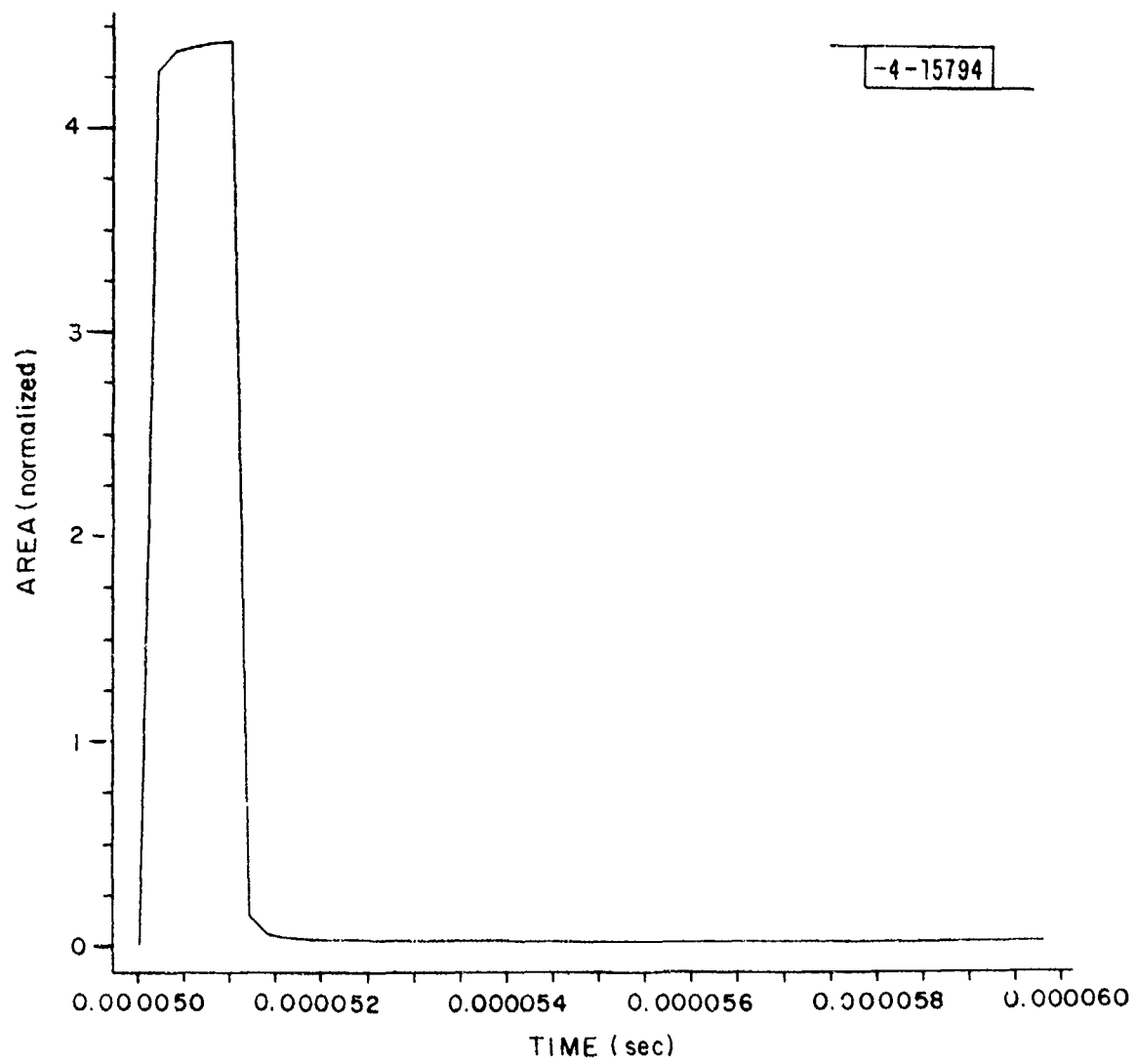


Fig. 36. Differential area vs time $(S(t + T) - S(t))$;
 $T = 1 \mu\text{sec}$; $z_1 = 10 \text{ m}$, $z_2 = 3 \text{ km}$, $R = 15 \text{ km}$.

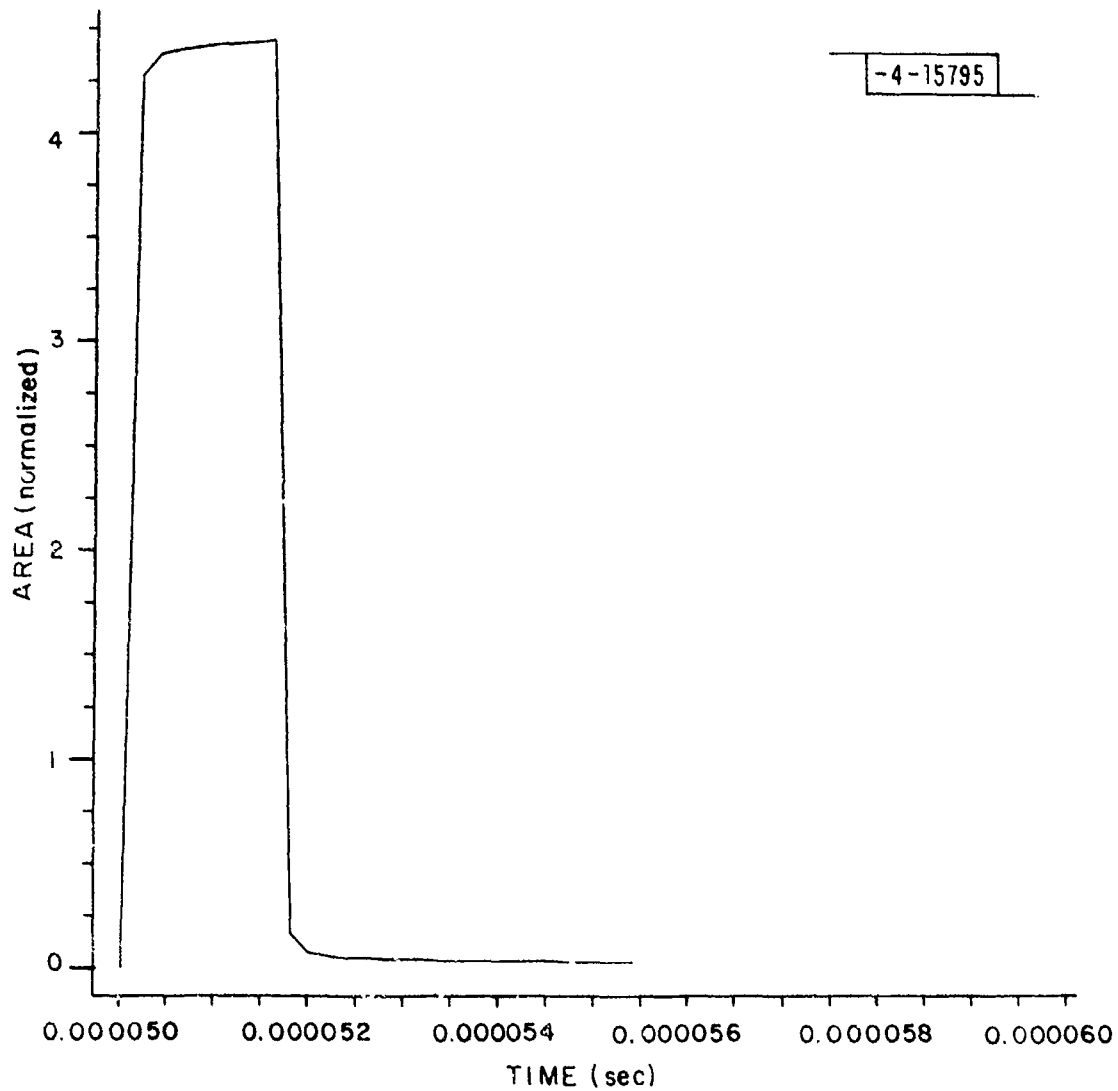


Fig. 37. Differential area vs time $(S(t + T) - S(t))$;
 $T = 1.6 \mu\text{sec}$; $z_1 = 10 \text{ m}$, $z_2 = 3 \text{ km}$, $R = 15 \text{ km}$.

18-4-15796

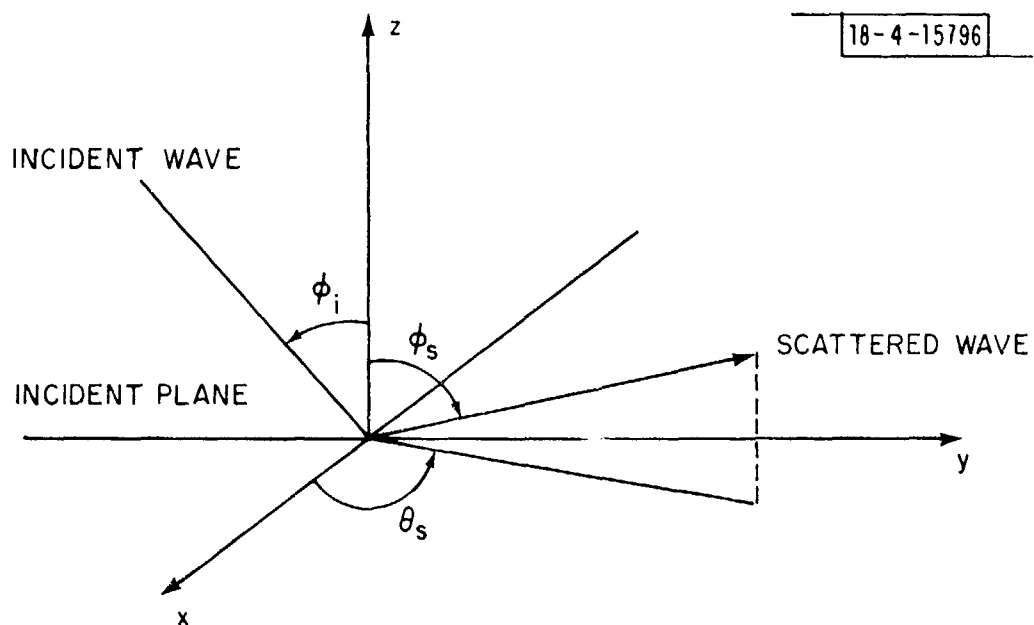


Fig. 38. Scattering geometry.

Using the Kirchoff approximation, Kodis shows that the field scattered in direction \underline{k}_s due to a source from \underline{k}_i is given by

$$\underline{E}_{sc}(\underline{k}_i, \underline{k}_s) = \frac{2jk}{2\pi r} e^{jkr} \int dS' (\underline{I} - \underline{k}_s \underline{k}_s) (\underline{h} \times \underline{\hat{n}}) \cdot \exp[j(\underline{k}_i - \underline{k}_s) \cdot \underline{r}'] \quad (4.25)$$

where

$$\underline{h} = \underline{k}_i \times \underline{\hat{e}} \quad (4.26)$$

and $\underline{\hat{n}}$ is the unit normal directed into the scattering plane at every point and $\underline{\hat{e}}$ is the polarization vector of the incident field. Using the method of stationary phase and then averaging, Kodis shows that the scattering cross section is given by

$$\sigma(\theta_s, \phi_s; \phi_i) = \pi n_A \langle |r_1 r_2| \rangle |R(\xi)|^2 \quad (4.27)$$

where n_A is the average number of specular points per unit area, $\langle |r_1 r_2| \rangle$ the average absolute value of product of principal radii of curvature, and $R(\xi)$ the reflection coefficient. The angle ξ is the local angle of incidence at the specular point and is given by the relationship;

$$\cos \xi = \frac{1}{2} \sqrt{1 - \sin \phi_i \sin \phi_s \cos \theta_i + \cos \phi_i \cos \phi_s} \quad (4.28)$$

Barrick has shown that

$$n_A = \frac{7.255}{\pi^2 2\sigma_l^2} \exp\left[-\left(\frac{\tan^2 \gamma}{s^2}\right)\right] \quad (4.29)$$

with

$$s^2 = 4 \frac{\sigma_h^2}{\sigma_l^2} \quad (4.30)$$

where σ_l is the correlation length of the surface and σ_h^2 is the variance of the surface height. $\tan \gamma$ is given by

$$\tan \gamma = \frac{\sqrt{\sin^2 \phi_i - 2 \sin \phi_i \sin \phi_s \cos \theta_s + \sin^2 \phi_s}}{\cos \phi_i + \cos \phi_s} \quad (4.31)$$

The curvature has also been shown by Barrick to be

$$\langle |r_1 r_2| \rangle = 0.1387 \pi \frac{\sigma_l^2}{s^2} \sec^4 \gamma \quad (4.32)$$

Finally, for vertical polarization over a perfectly conducting plane, we have for the reflection coefficient

$$R(\xi) = \frac{-\sin \phi_i \sin \phi_s \sin^2 \theta_s + a_2 a_3}{4 \sin^2 \xi \cos^2 \xi} \quad (4.33)$$

where

$$a_2 = \cos\phi_i \sin\phi_s + \sin\phi_i \cos\phi_s \cos\theta_s \quad , \quad (4.34)$$

$$a_3 = \sin\phi_i \cos\phi_s + \cos\phi_i \sin\phi_s \cos\theta_s \quad . \quad (4.35)$$

If we define a constant C as the product of 0.1378 and 7.255 then we can combine (4.28) - (4.35) to yield;

$$\sigma(\theta_s, \phi_s; \phi_i) = C \frac{\sec^4 \gamma}{s^2} \exp\left[-\frac{\tan^2 \gamma}{s^2}\right] |R(\xi)|^2 \quad . \quad (4.36)$$

This is the resulting scattering cross-section. We can observe its behavior easily in this form. By using (4.31) we first see that for positive ϕ_i and ϕ_s , $\tan \gamma$ increases as the azimuth θ_s increases or decreases from zero. This implies that the angle γ is increasing as an absolute value of the azimuth. Thus for fixed ϕ_i and ϕ_s the azimuth behavior of the scattering cross-section is dominated by γ which in turn is reflected in the two terms; $\exp(-\tan^2 \gamma/s^2)$ and $\sec^2 \gamma$. The former term decreases with increasing γ , the rate of increase depending on the value of s^2 . The latter term, increases with $\sec^4 \gamma$, independent of s^2 . Now two distinct regions are possible. The first is for large s : In that case, the $\sec^4 \gamma$ behavior dominates a scattering cross-section which increases with azimuth. Large s implies that σ_l , the correlation length, is small compared to the surface roughness. This can be called a very rough surface. For example, if σ_h is 10 m, then the value of σ_l needed

to insure this condition is on the order of 10 m. A second effect to note is that the amplitude about zero azimuth depends inversely on s^2 . Thus, a very rough surface scatters less in the forward direction. The second region is that in which s^2 is small, i. e., $\sigma_l \gg \sigma_h$, so that $\exp(-\tan^2 \gamma/s^2)$ dominates the profile of the scattering cross-section. Figs. 39-42 depict results for varying cases. Note that in Fig. 40 we have almost a specular scatter surface with minimum spread. This results from a very large value of σ_l , the surface correlation length.

The assumptions that must be made concerning the surface in order that the analysis leading to (4.34) be consistent are (see Barrick):

1. The radius of curvature, ρ , everywhere on the reflecting surface be much greater than the wavelength. Thus $\rho \gg \lambda_0$.
2. Multiple scattering effects can be neglected.
3. The mean square surface height is much greater than a wavelength, that is $\sigma_h^2 \cos^2 \phi_i \gg \lambda_0^2$.

Condition (1) and (3) are direct limitations on the types of surfaces. Specifically, (1) requires that the surfaces be very rounded since λ_0 at 1090 Mhz is about one foot. Furthermore, (3) states that unless h is very large, the approximations breakdown at grazing angles; $\phi_i \rightarrow \pi/2$. That is most surfaces "look" like specular reflectors at grazing angles such that $\phi_i \approx \pi/2$.

Further limitations concerning the surface correlation coefficient are discussed in Barrick [2]. He notes that the correlation must be quadratic about the origin. Specifically, the result in (4.36) assumes that the surface height z is a Gaussian random variable with a correlation, $E[z(x, y) z(x', y')]$,

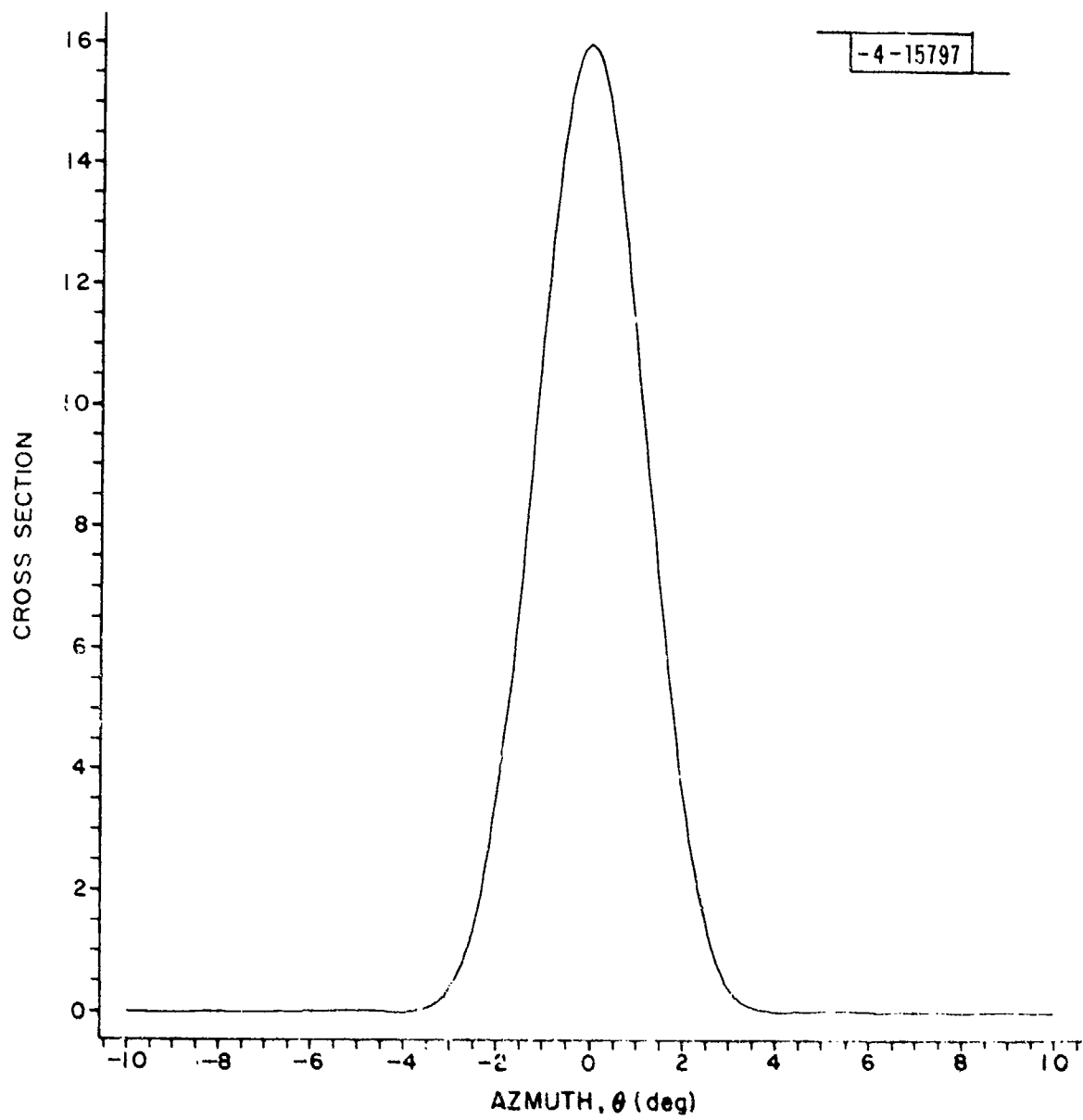


Fig. 39. Scattering cross-section vs azimuth ($\phi_i = \phi_s = 88^\circ$, $s = 1/2$).

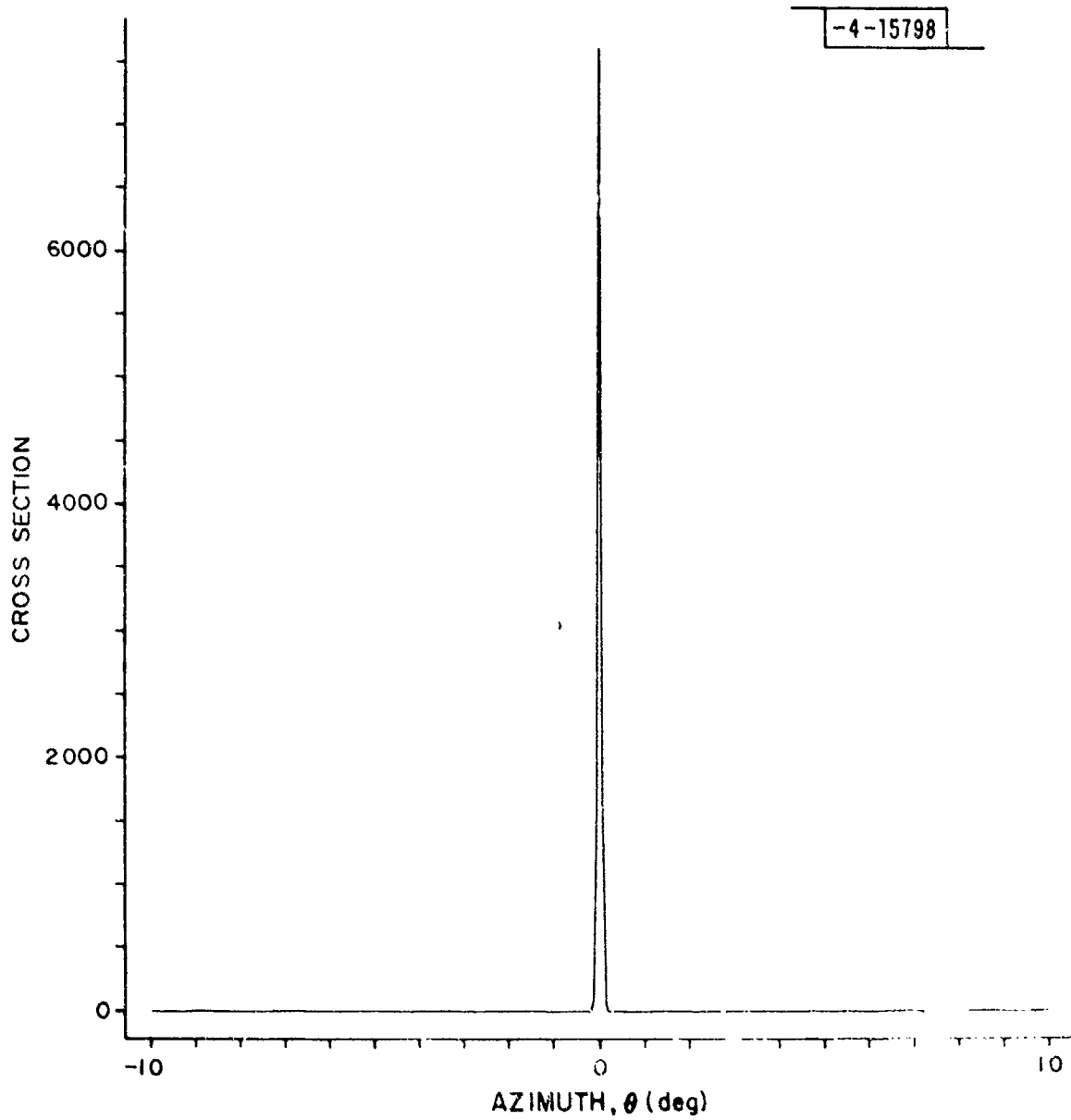


Fig. 40. Scattering cross-section vs azimuth ($\phi_1 = \phi_2 = 88^\circ$, $s = 1/2^6$).

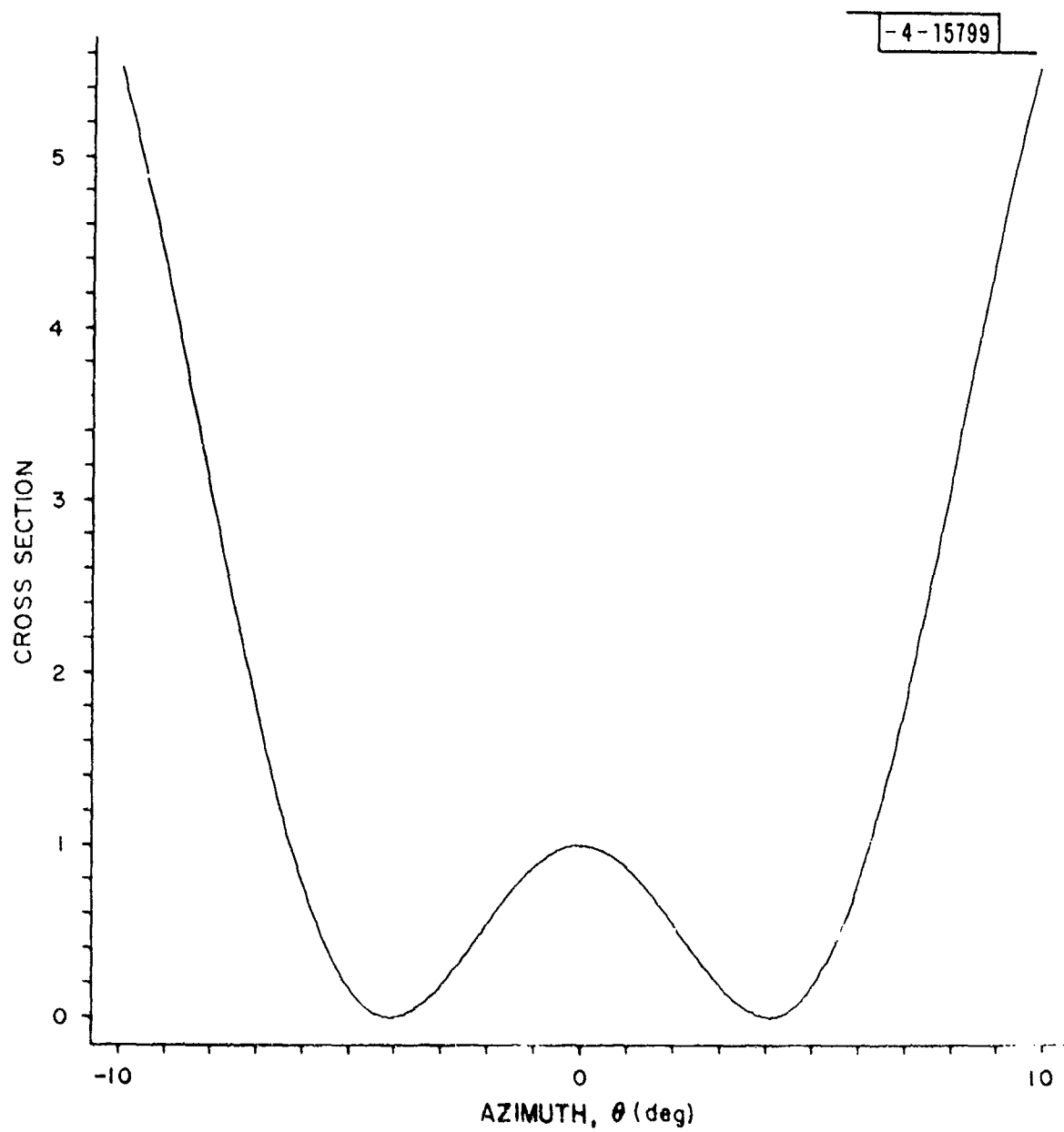


Fig. 41. Scattering cross-section vs azimuth ($\phi_i = \phi_s = 88^\circ$, $s = 2$).

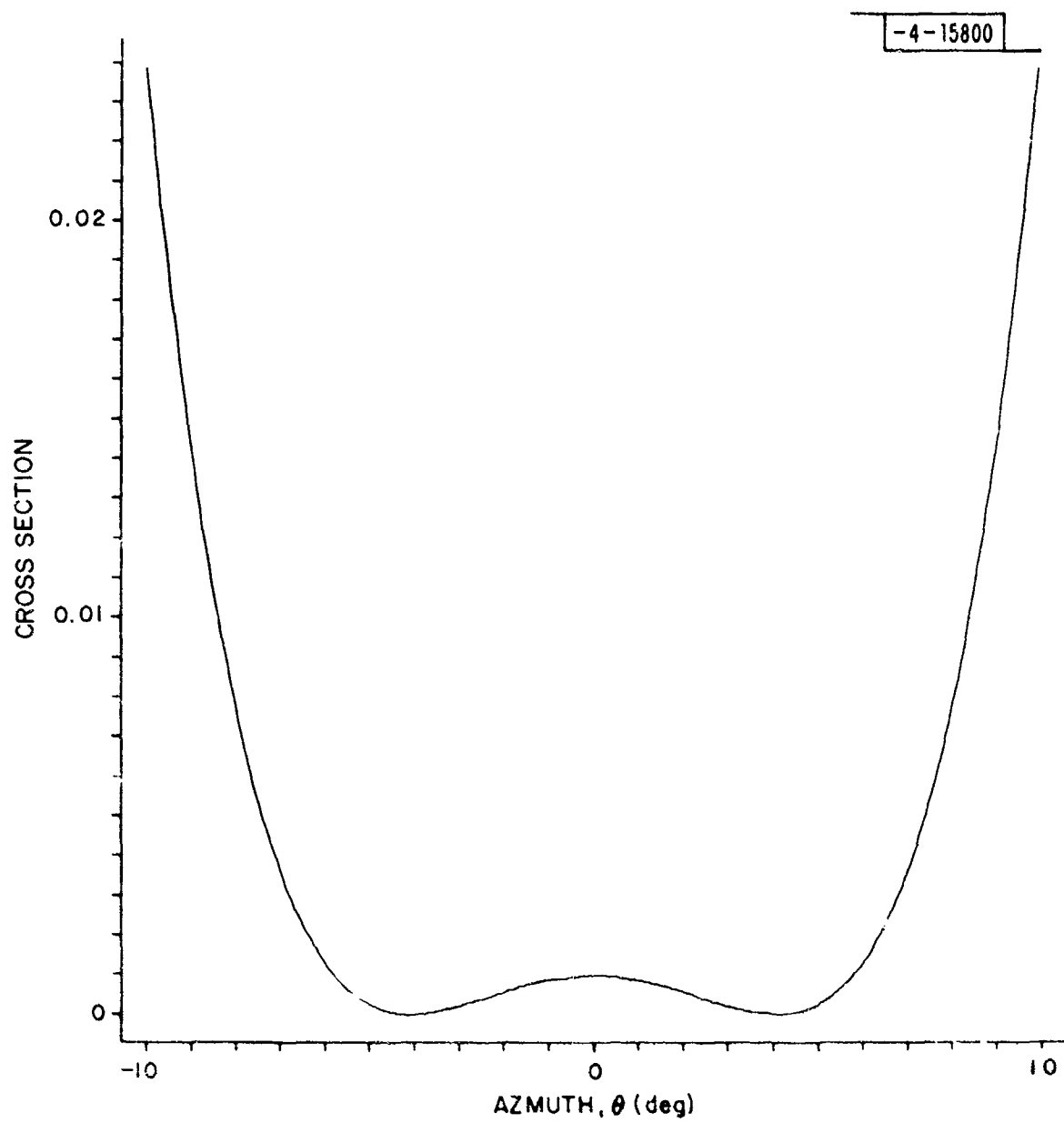


Fig. 42. Scattering cross-section vs azimuth ($\phi_i = \phi_s = 88^\circ$, $s = 2^6$).

having the form, $\exp(-\alpha \rho_s^2)$, where ρ_s^2 is $(x - x')^2 + (y - y')^2$. This form ensures power conservation and correct behavior as the ray optics limit is approached.

We now want to evaluate the spread function $K(\theta, \phi)$ which represents the power per unit area per square radian incident at the receiver coming from directions ϕ in elevation and θ in azimuth. To do this, consider an incremental area $\Delta S'$ as shown in Fig. 43. Draw a line from the origin at an angle θ in the x, y plane, bounding dS' on one side and a line at angle $\theta + \Delta\theta$ bounding $\Delta S'$ on the other side. Now ϕ is given by

$$\phi = \tan^{-1} \left[\frac{\sqrt{x^2 + y^2}}{z_1} \right]. \quad (4.37)$$

The loci of constant ϕ for constant z_1 are circles in the x, y plane. Circles for ϕ and $\phi + \Delta\phi$ are shown also in Fig. 43. The cross hatched area in this figure represents the region of the scattering plane from which the source receives radiation coming from the solid angle $\phi, \phi + \Delta\phi$, and $\theta, \theta + \Delta\theta$. The power per unit area received from this area is $K(\theta, \phi) \Delta\theta \Delta\phi$. Also, ΔS is directly defined by the bounding region.

For any point in the area from Fig. 44, we see that

$$\phi_i = \tan^{-1} \left[\frac{\sqrt{y^2 + (r - y)^2}}{z_2} \right]. \quad (4.38)$$

The scattered angle ϕ_s is given by (4.37). The angle θ , the angle used for the scattering cross-section is given by

18-4-15804

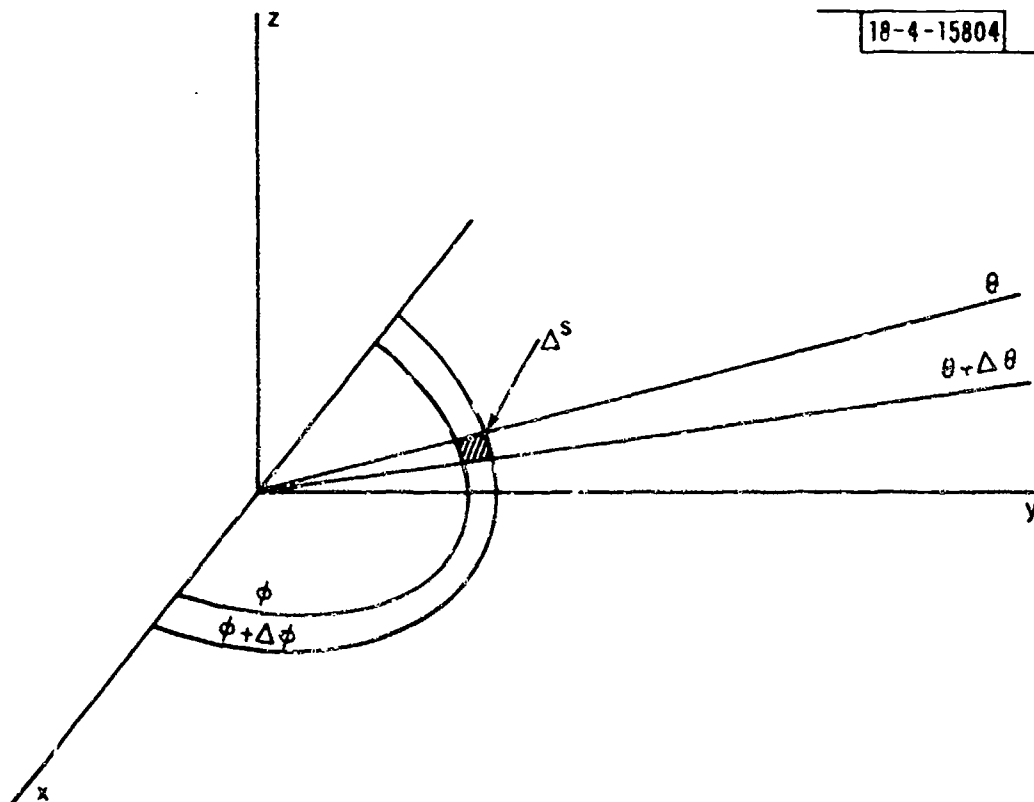


Fig. 43. Spread function geometry.

$$\theta' = \theta + \psi \quad (4.39)$$

where

$$\psi = \tan^{-1} \left| \frac{x}{r-y} \right| \quad (4.40)$$

Thus, we have for any θ, ϕ pair

$$K(\theta, \phi) = \lim_{\substack{\Delta\theta \rightarrow 0 \\ \Delta\phi \rightarrow 0}} \left[\frac{P_0 \iint_{\mathcal{S}} \sigma(\theta + \psi, \phi; \phi_i) dx dy}{(4\pi)^2 R_1^2 R_2^2} \right]_{\Delta\theta \Delta\phi} \quad (4.41)$$

where \mathcal{S} is the intersection of the region formed as in Fig. 43 and the area of illumination at time t . Note that x, y and ϕ_i are functions of θ and ϕ so that by using the Jacobian of the transformation some simplification of (4.41) may result. However, another simplifying tool can be used if we introduce variable ρ_0 where

$$\rho_0 = \sqrt{x^2 + y^2} \quad (4.42)$$

But, from (4.37) and Fig. 44 we note that

$$\rho_0 = z_1 \tan \phi \quad (4.43)$$

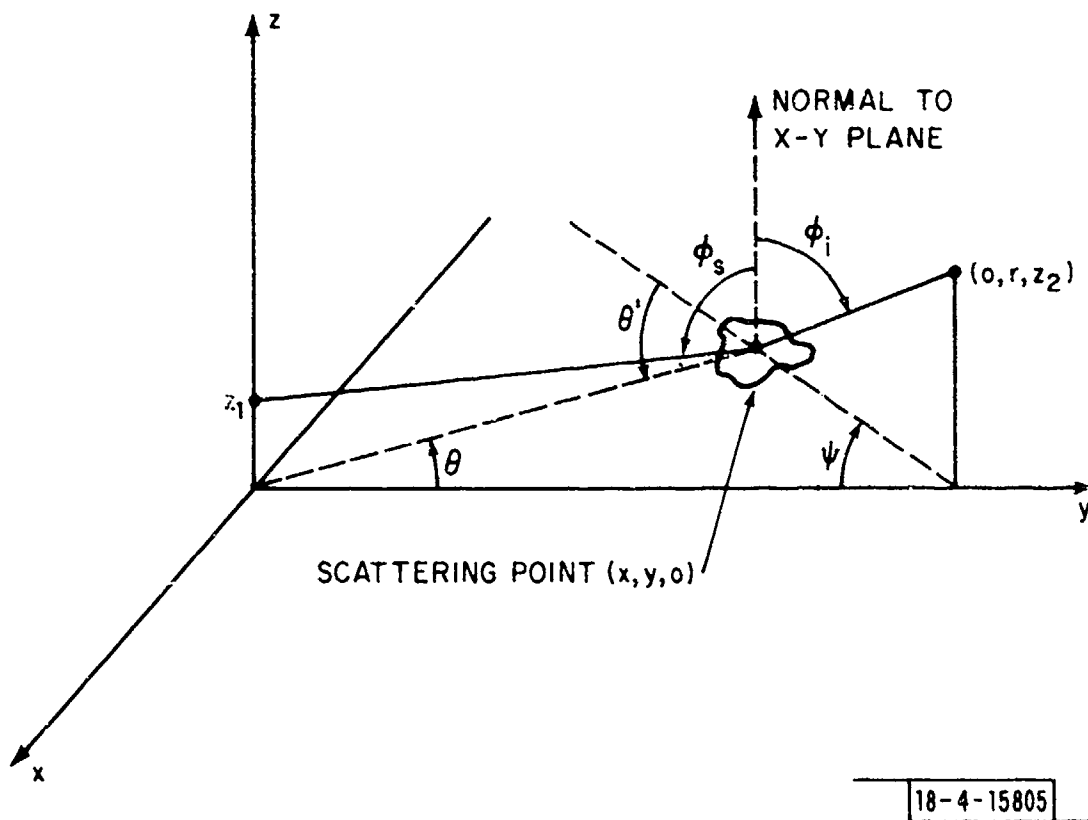


Fig. 44. Scattering geometry.

Here ρ_0 is the radius of a circular coordinate system in the x, y plane. Then

$$x = \rho_0 \sin\theta = z_1 \tan\phi \sin\theta \quad (4.44)$$

$$y = \rho_0 \cos\theta = z_1 \tan\phi \cos\theta \quad (4.45)$$

With these substitutions we can write ψ as in (4.40);

$$\psi = \tan^{-1} \left[\frac{z_1 \tan\phi \sin\theta}{r - z_1 \tan\phi \cos\theta} \right] \quad (4.46)$$

and

$$R_1^2 = z_1^2 (1 + \tan^2\phi) \quad (4.47)$$

$$R_2^2 = z_1^2 \tan^2\phi + r^2 - 2r z_1 \tan\phi \cos\theta + z_2^2 \quad (4.48)$$

Then using the transformation from x, y into ρ_0, θ the integral in (4.41) can be written using

$$dx dy = \rho_0 d\rho_0 d\theta \quad (4.49)$$

as;

$$K(\theta, \phi) = \lim_{\substack{\Delta\theta \rightarrow 0 \\ \Delta\phi \rightarrow 0}} \left[\frac{P_0}{(4\pi)^2} \frac{\iint_{\Delta S} \frac{\sigma(\theta + \psi(\theta, \phi), \phi; \phi_i(\theta, \phi)) \rho_0 d\rho_0 d\theta}{R_1^2(\theta, \phi) R_2^2(\theta, \phi)}}{\Delta\theta \Delta\phi} \right] \quad (4.50)$$

where we have assumed that $A(t)$ is large enough ($t \gg t_0$) and have explicitly stated, ψ , R_1 and R_2 in terms of θ and ψ . Now using (4.49) and (4.43) we can take the limit to yield;

$$K(\theta, \phi) = \frac{P_0}{(4\pi)^2} \frac{\sigma(\theta + \psi(\theta, \phi), \phi; \phi_i(\theta, \phi)) z_1^2 \sec^2 \phi \tan \phi}{R_1^2(\theta, \phi) R_2^2(\theta, \phi)} \quad (4.51)$$

as the resulting channel spread function for this diffuse multipath field.

An evaluation of the channel spread function has been performed and the results are shown in Figs. 45 to 48. This is for a time large enough so that all the surface is irradiated. The ground antenna is assumed to be at 20 m and the aircraft at 1 km. The value of s varies as does the range of the aircraft. In these figures, we have normalized (4.51) by $P_0/4\pi d_0^2$ and have plotted $10 \log_{10}$ of that ratio.

In Fig. 45, we have a fairly smooth surface ($s = 0.5$). We note the bright spot near the horizon and a rapid decrease as θ goes from broadside. A similar plot is shown in Fig. 46 but now the aircraft has quintupled its range. We note the narrowing of the peaks. This narrow area is the glistening surface mentioned in Beckmann and Spichizzino. The remaining two plots

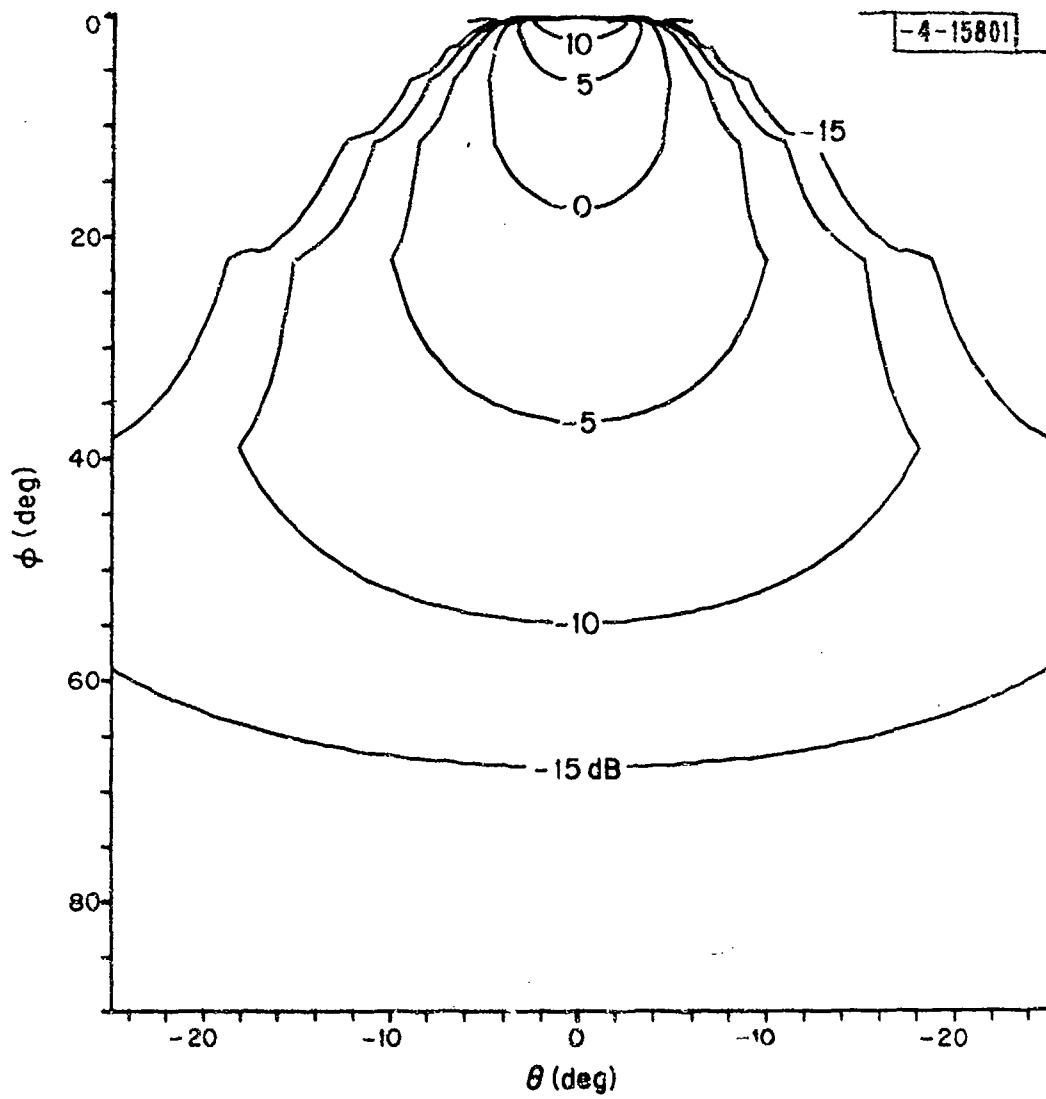


Fig. 45. Contour plot of scattering cross-section ($R = 10$ km, $z_2 = 1$ km, $s = 0.5$).

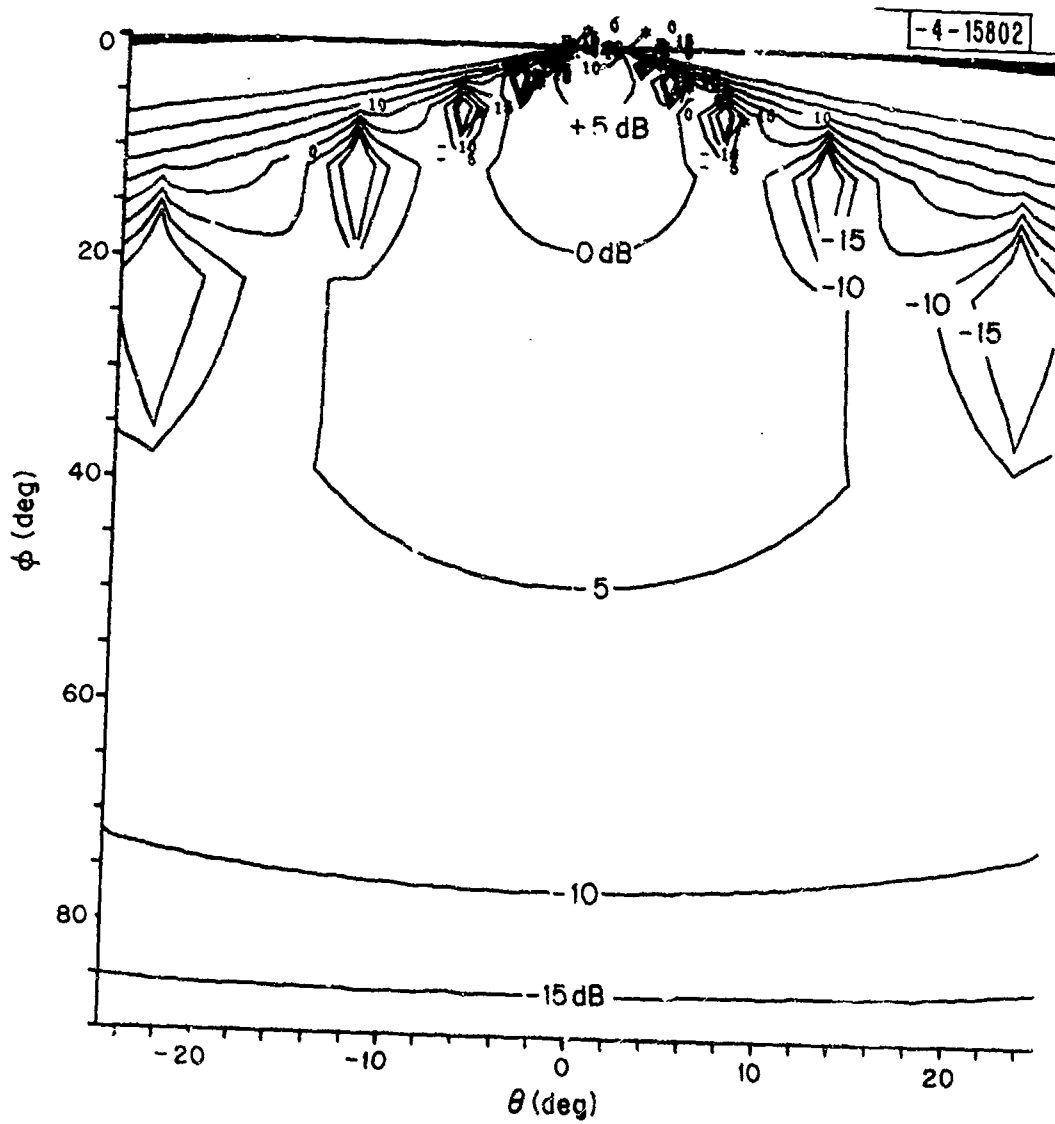


Fig. 46. Contour plot of scattering cross-section ($R = 50$ km,
 $z_2 = 1$ km, $s = 0.5$).

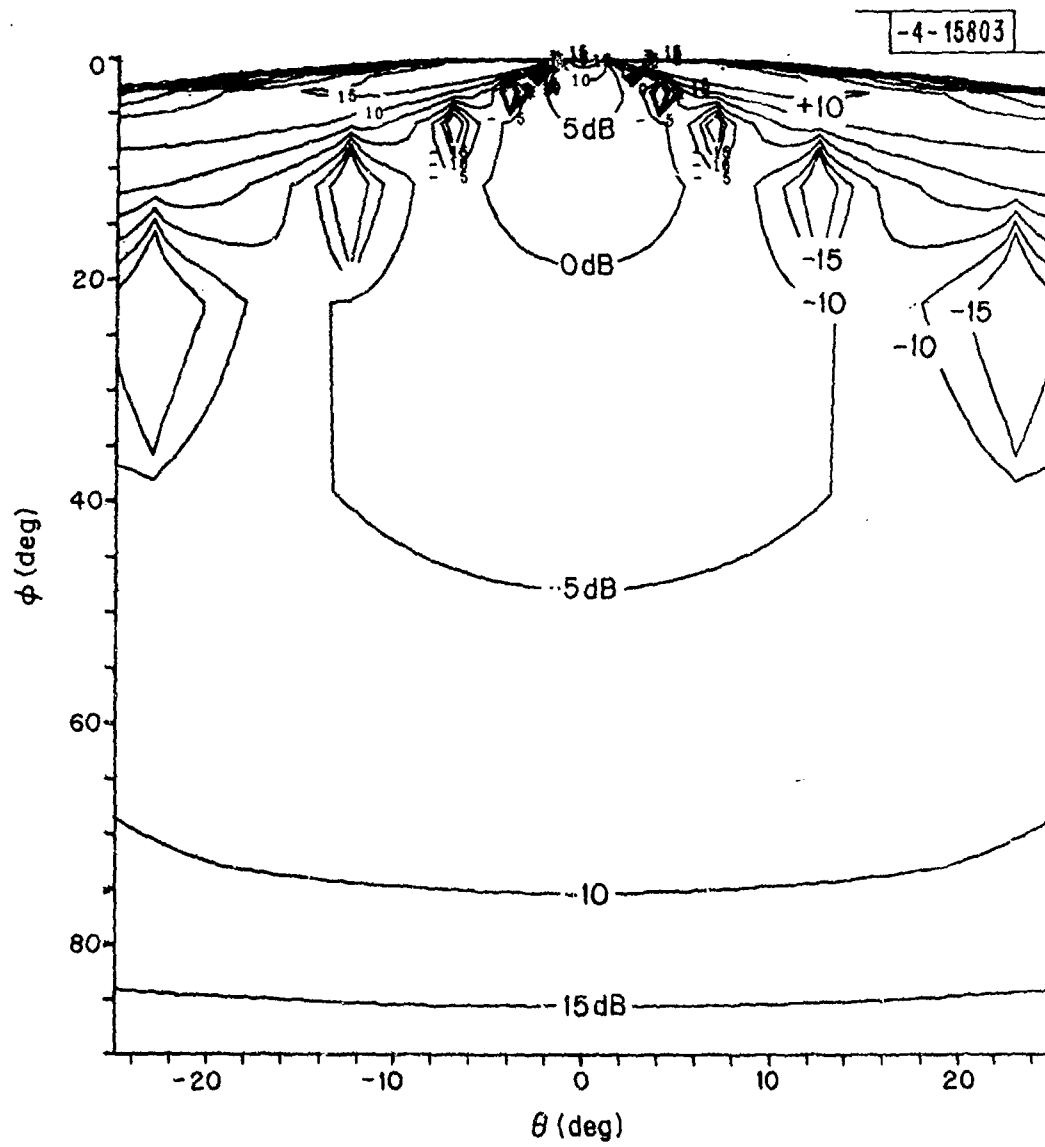


Fig. 47. Contour plot of scattering cross-section ($R = 50$ km, $z_2 = 1$ km, $s = 2.0$).

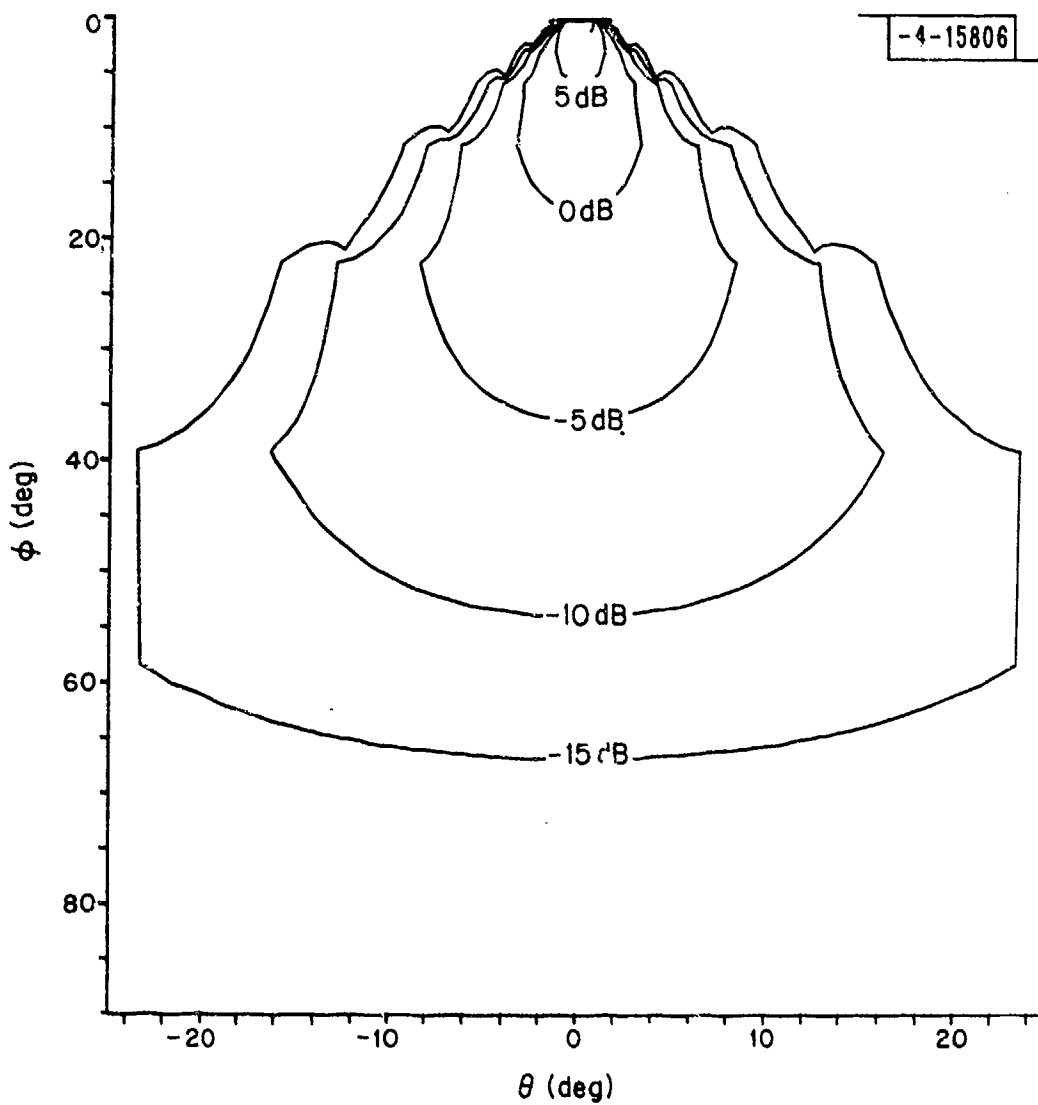


Fig. 48. Contour plot of scattering cross-section ($R = 50$ km, $z_2 = 1$ km, $s = 4.0$).

show how sidelobes appear as the surface becomes more rough. This is a result of the increase in the radius of curvature term as well as a slow decrease in the average number of scatters as appear in (4.51).

With $K(\theta, \phi)$, the azimuth spread for a given antenna vertical gain can be evaluated. Let $G(\phi)$ be the vertical gain of the antenna; then, azimuth spread $K(\theta)$ is given by

$$K(\theta) = \int_{-\frac{\pi}{2}}^{\frac{\pi}{2}} G(\phi) K(\theta, \phi) d\phi \quad (4.52)$$

As before, this is a function of $\sigma_l, \sigma_h, z_1, z_2, r$, and time. A sample plot for $r = 30$ km using the vertical array proposed for the DABS antenna is shown in Fig. 49. Note the sharp central peak and the drop of 6 orders of magnitude as the azimuth increases. This profile is called the glistening surface by Beckmann and Spizzichino.

It is also possible to use the gain in azimuth. Thus, if $G(\theta, \phi)$ is the gain of an antenna in elevation and azimuth then, the quantity

$$\eta = \frac{\int_{-\frac{\pi}{2}}^{\frac{\pi}{2}} \int_{-\pi}^{\pi} G(\theta, \phi) K(\theta, \phi) d\theta d\phi}{\frac{P_0}{4\pi d_0^2}} \quad (4.53)$$

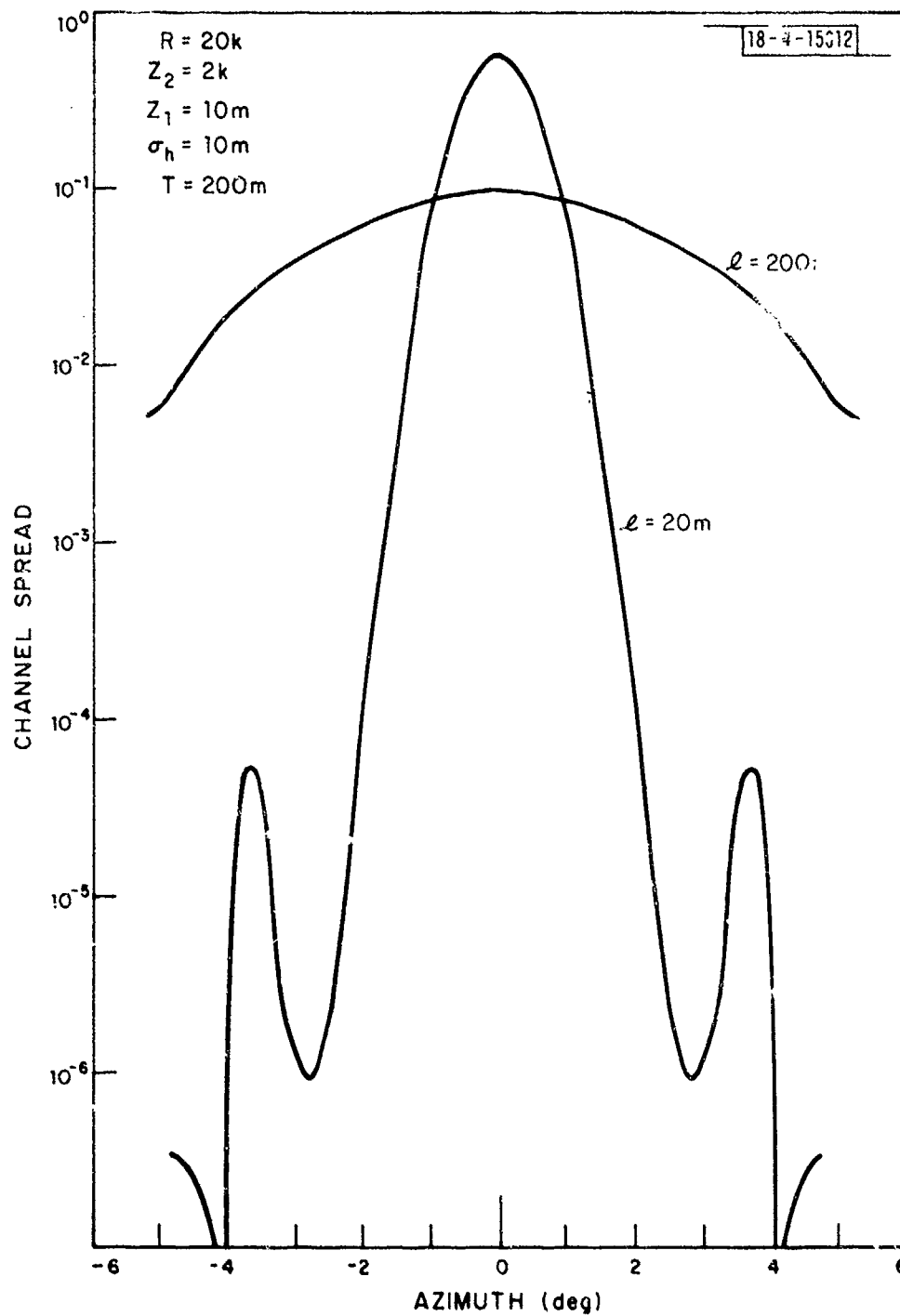


Fig. 49. Plot of channel spread function vs azimuth for two correlation lengths.

represents the diffuse energy-to-signal value for the given antenna gain $G(\theta, \phi)$. This has been evaluated in Fig. 50 versus range for the DABS antenna. From this plot, we see that the diffuse multipath is quite low and would predict that it should not cause any difficulty in azimuth estimation.

4.3 PERFORMANCE

The azimuth estimation performance of an array is determined by its beam pattern or ambiguity pattern, the inherent system noise, and also the effect of multipath interference. For diffuse multipath, as the type discussed in Section 4.2, the performance can be given in terms of the ambiguity function and the azimuth spread function. We have the azimuth spread in terms of

$$K(\theta) = \int_{-\frac{\pi}{2}}^{\frac{\pi}{2}} G(\phi) K(\theta, \phi) d\phi \quad (4.54)$$

For the performance analysis we want K as a function of μ which is $\cos\theta$ where $\theta = 90^\circ$ represents broadside. Furthermore, we want $K(\mu)$ to have unit area. Thus, we define the constant;

$$\sigma_i^2 = \int_{-\pi}^{\pi} K(\theta) d\theta \quad (4.55)$$

as a normalization factor. Then, in terms of the function $K(\theta)$, we have

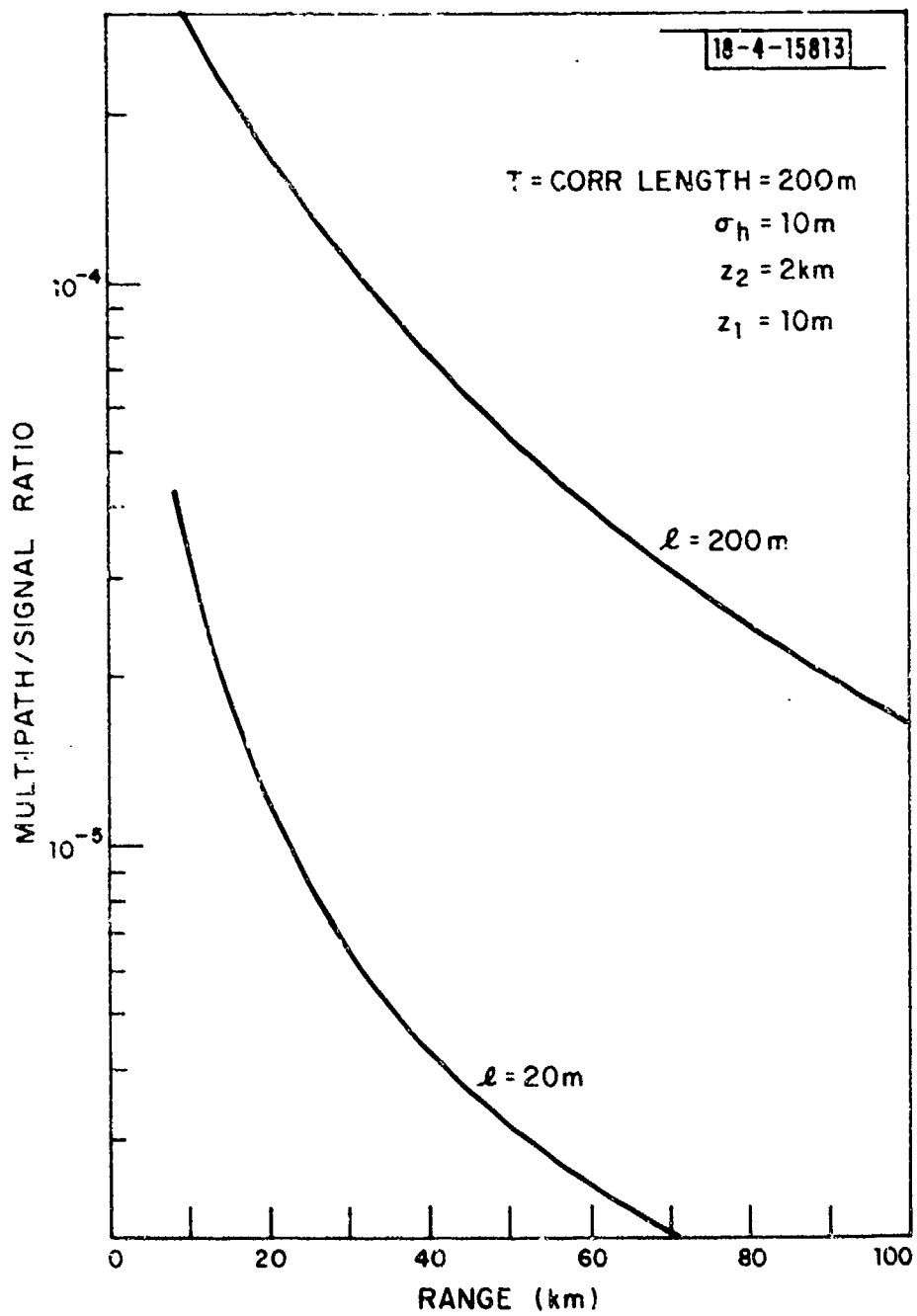


Fig. 50. Plot of multipath energy to signal vs range.

$$K(\mu) \triangleq \frac{K(\theta)}{\sigma_i^2} ; \mu = \cos\theta . \quad (4.56)$$

The ambiguity function of array is defined as $\mathcal{B}(\mu)$ and is given by

$$\mathcal{B}(\mu') = \left| \underline{\tilde{m}}^\dagger(\mu) \underline{\tilde{m}}(\mu + \mu') \right|^2 \quad (4.57)$$

where $\underline{\tilde{m}}(\mu)$ is the $N \times 1$ complex vector

$$\underline{\tilde{m}}(\mu) = \begin{bmatrix} \exp(-j2\pi d_1 \mu / \lambda_0) \\ \vdots \\ \exp(-j2\pi d_N \mu / \lambda_0) \end{bmatrix} . \quad (4.58)$$

Here, d_i is the displacement from the origin of the i th dipole receiver (for a dipole array), λ_0 is the wavelength, and N is the number of dipoles.

The total signal energy is given by

$$\sigma_s^2 = \sigma_b^2 E_s \quad (4.59)$$

where E_s is the energy of the transmitted pulse and σ_b^2 represents channel attenuation effects. The total diffuse multipath signal level is

$$\sigma_I^2 = E_s \sigma_i^2 \quad (4.60)$$

since we assume the signal due to diffuse multipath has been generated by the source. The noise is assumed to be a zero mean Gaussian white noise process, independent from element to element in the array and has a variance given by

$$\sigma_n^2 = \frac{N_0}{2} \quad (4.61)$$

For analytical purposes it becomes convenient to define two ratios, the multipath-to-signal ratio, ξ , and the noise-to-signal ratio, γ . These are

$$\xi = \frac{\sigma_I^2}{\sigma_s^2} \quad (4.62)$$

$$\gamma = \frac{\sigma_n^2}{\sigma_s^2} \quad (4.63)$$

Now it has been shown elsewhere that the Cramer-Rao bound for estimating μ is given by (McGarty [1]);

$$\text{var}(\mu - \hat{\mu}) \geq -\frac{1}{J} \quad (4.64)$$

where

$$J = C \left[\sigma_s^2 \frac{\partial^2 \mathcal{B}(\mu)}{\partial \mu^2} \Big|_{\mu=0} + \sigma_I^2 \int_{-1}^1 K(\mu') \frac{\partial^2 \mathcal{B}(\mu - \mu')}{\partial \mu^2} d\mu' \right] \quad (4.65)$$

where

$$C = \frac{N^2 \sigma_s^2 + \sigma_I^2 \Phi}{N \sigma_n^2 (\sigma_n^2 + \sigma_s^2 N^2 + \sigma_I^2 \Phi)} \quad (4.66)$$

$$\Phi = \int K(\mu') \mathcal{B}(\mu - \mu') d\mu' \quad (4.67)$$

By using (4.63), we can rewrite (4.66) as

$$C = \frac{(N^2 + \xi \Phi)}{\gamma N (N^2 + \xi \Phi + N \gamma)} \quad (4.68)$$

and the term in the brackets in (4.65) becomes

$$\frac{\partial^2 \mathcal{B}(\mu)}{\partial \mu^2} \Big|_{\mu=0} + \xi \int_{-1}^1 K(\mu') \frac{\partial^2 \mathcal{B}(\mu - \mu')}{\partial \mu^2} d\mu' \quad (4.69)$$

The bound on σ_μ^2 can be shown to relate to σ_θ^2 as;

$$\sigma_{\theta}^2 = -\tan^2 \theta + \tan^2 \theta \sqrt{1 + 2 \frac{\cot^2 \theta}{\sin^2 \theta} \sigma_{\mu}^2} \quad (4.70)$$

where θ is the pointing angle. Note that $\theta = 90^\circ$ implies broadside.

Now the evaluation of (4.65) can be facilitated by using Fourier transform relationships. This has been discussed elsewhere but the evaluation of the performance curves in Fig. 51 have been evaluated using this technique. (See McGarty [1].)

We can express the performance as a function of the beamwidth of the array as follows. Recall that for a linear array, we have for the ambiguity pattern

$$B(\mu) = \left[\frac{\sin \frac{Nd}{2} \mu}{\sin \frac{d}{2} \mu} \right] \quad (4.71)$$

where d equals $2\pi d_0/\lambda_0$, d_0 being the interdipole spacing and λ_0 the wavelength. The first null in this pattern occurs at μ_B where

$$\frac{Nd}{2} \mu_B = \pi \quad (4.72)$$

The center of the beam is at $\mu = 0$ so that the beamwidth between nulls is given by

$$\mu_B = \sin^{-1} \frac{\lambda_0}{Nd_0} \quad (4.73)$$

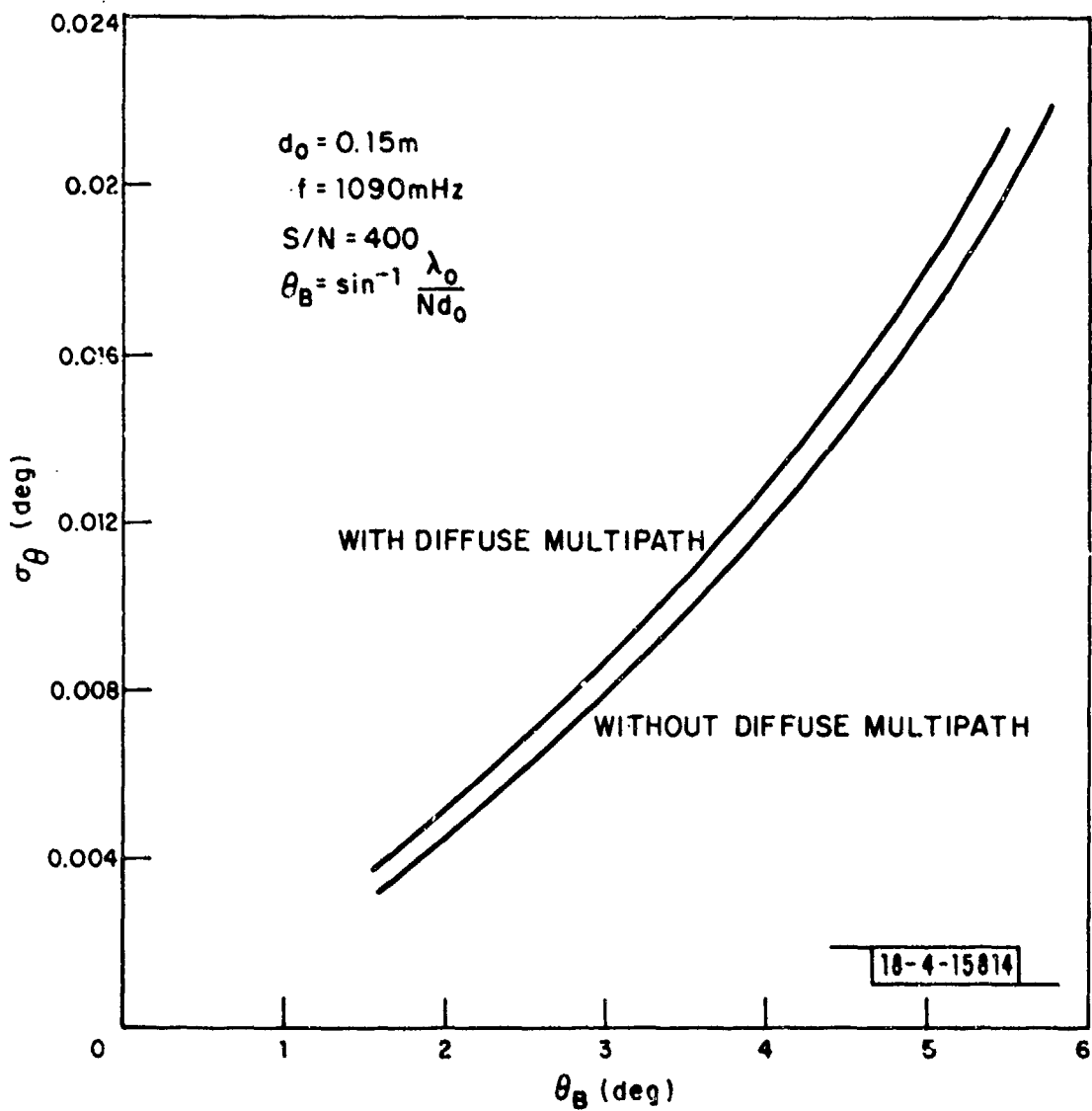


Fig. 51. Standard deviation of angle estimate.

From McGarty [1], we have the performance bound in the absence of multipath which yields the standard deviation of the azimuth estimate, σ_θ in terms of the signal-to-noise ratio and the number of elements. It is

$$\sigma_\theta(\text{radians}) = \sqrt{\frac{12}{\sigma^2(N^3 - N)}} \quad (4.74)$$

where σ^2 is the signal-to-noise ratio. Now, using (4.73) for N we have

$$\sigma_\theta = \left[\frac{12}{\sigma^2 \left[\left(\frac{d_0}{\lambda_0 \sin \theta_B} \right)^3 - \left(\frac{d_0}{\lambda_0 \sin \theta_B} \right) \right]} \right]^{1/2} \quad (4.75)$$

Assuming $\theta_B \ll 1$, we can approximate this by

$$\sigma_\theta = \sqrt{\frac{12}{\sigma^2 \left(\frac{d_0}{\lambda_0} \right)^3}} \theta_B^{3/2} \quad (4.76)$$

where σ_θ is in radians as is θ_B .

That is, in the absence of multipath the standard deviation of the angle estimate is proportional to the three-halves power of the beamwidth. This curve, along with the curve including multipath, is shown in Fig. 51.

Also, if the multipath effect is small (i. e., $\xi \gg 1$), then the error with multipath can be written as;

$$\sigma_{\theta}^2 = \sigma_{\theta}^2, \text{ no multipath} \left(1 + \xi \int_{-1}^1 K(\mu') \frac{\partial^2}{\partial \mu^2} \mathcal{B}(\mu - \mu') d\mu' \right) \quad (4.77)$$

That is, the variance is increased by a factor which depends on the multipath to signal ratio, ξ , and the nature of the spread channel, $K(\mu)$.

Plotted in Fig. 51 is σ_{θ} versus θ_B , the beamwidth in degrees for d_0 equal 0.152 m, a frequency of 1090 MHz, a signal-to-noise ratio of 25 dB, and the interference-to-signal ratio of -20 dB. We use the spread function for z_1 equal to 10 m, z_2 equal to 2 km, range equal to 20 km. σ_h was 10 m, and σ_l , 200 m (as shown in Fig. 49). Note the behavior of the variance. As θ_B decreases, σ_{θ} decreases almost linearly. The bound actually is dominated by S/N behavior and is only slightly affected by the diffuse multipath. This implies that for an array, with an $8\lambda_0$ vertical aperture and a $26\lambda_0$ horizontal aperture diffuse multipath will not be a significant problem.

4.4 CONCLUSIONS

Diffuse multipath can be modelled as a random phenomenon which results from the rough and random nature of the scattering surface. In this section we consider the effects of such randomness in detail. We first reviewed the rather large body of work that already exists on scattering from random surfaces and discussed the shortcomings or usefulness of several of the models that have been proposed.

A specific model for diffuse scattering was then proposed. First an analysis of the area irradiated as a function of time was performed. The result of this analysis was that for μ sec type signals the effects of finite time propagation could be neglected. Then using the Kodis-Barrick model the scattering cross-section per unit area was obtained for a Gaussian surface with a Gaussian correlation function. The resulting scattering cross-section $\sigma(\theta_s, \phi_s; \phi_i)$ was evaluated in terms of the mean square surface height, σ_h , the correlation length of the surface, σ_l , and the geometrical parameters of the point of scattering.

It has been shown that to evaluate the effects of random signals coming from a continuum of directions, as is the case for diffuse multipath, the channel spread function, $K(\theta, \phi)$, must be obtained. This function represents the fraction of diffuse energy received from a given azimuth, θ , and elevation, ϕ . Using the Kodis-Barrick scattering cross-section and the geometry of the ground-to-air surveillance link the spread function was obtained.

This section concluded with an evaluation of the effects of diffuse multipath on azimuth estimation. Several different types of surfaces were considered and a simplified closed form analytical result for azimuth errors was obtained.

As a result of this study the following specific conclusions were reached.

1. The Kodis-Barrick model for diffuse scattering cross-sections is most appropriate for performance evaluations.
2. Time dispersion effects are not important for MHz data rate transmissions with respect to diffuse multipath effects.

3. The channel spread function for $\sigma_h < \sigma_l$ shows a distinct glistening surface effect that has been noted by other investigators.
4. The errors on azimuth estimation due to diffuse multipath are negligible and orders of magnitude smaller than those observed for specular multipath. Thus diffuse multipath presents no serious limitations in direction finding capabilities in DABS.
5. The effects of earth curvature and shadowing can be included but their net effect is of second order and discussed in the next section.

SECTION FIVE

OTHER EFFECTS

In the past two sections, we have discussed the effects of specular and diffuse multipath and have presented models with which the effects of these sources of interference on system performance could be determined. In so doing, we neglected certain factors which in some circumstances can become important. It is the purpose of this section to discuss these factors and place them in their proper perspective relative to the general model.

5.1 REFRACTION

The model developed in this report for specular multipath considered the scattering plane to be flat. However, the earth is not flat, it has curvature. If we consider any scattering point x, y and let r_2 be the distance from the transmitter to x, y and r_1 the distance from the receiver to that point, then Beckmann and Spizzichino (pp. 222-224) show that we must reduce the reflection coefficient derived in Section 3 by a factor D where

$$D = 1 + \left[\frac{2r_1 r_2}{R_e (r_1 + r_2) \sin \gamma} \right]^{1/2} \quad (5.1)$$

where R_e is the effective radius of the earth and γ is $(\pi/2) - \phi_i$ where ϕ_i is as in Section 4. Then, for $r_1, r_2 \ll R_e$, this is close to unity and it can be neglected. In our analysis, we had also included the attenuation of $1/r_1^2 r_2^2$ which, combined with D , would imply for large R_e that

$$\frac{D}{r_1^2 r_2^2} \approx \frac{1}{r_1^2 r_2^2} \quad (5.2)$$

For the angles of interest ($\gamma \approx 3^\circ$) and $r_1, r_2 < 10$ km, D is sufficiently close to one to be neglected. However, for a more general analysis, its effect must be included.

In the same context of this problem is the evaluation of the line-of-sight. Namely, for a given antenna height and aircraft height, how far from the antenna must the aircraft fly to fall below the horizon. If $z_1 \ll z_2$ then, R_h , the range to the horizon can be shown to be

$$R_h = \sqrt{2z_2 R_E} \quad (5.3)$$

where z_2 is the altitude of the aircraft and R_E the effective radius of the earth. R_E equals $4/3 R_{E_0}$ where R_{E_0} is the geometrical radius of the earth. A plot of R_h vs z_2 appears in Fig. 52. As seen for an altitude of 1 km, the range to the horizon is 130 km.

5.2 SHADOWING

A second effect to be considered is that of shadowing. Here, we are interested in the decrease in area irradiated due to the surface irregularities themselves. This was first discussed by Beckmann [3] who developed an approximate expression for the fractional effective area. Due to an error in his analysis (see Shaw), Beckmann's theory underestimates the effects of shadowing. A geometrical approach was suggested by Brockelman and Hagfors

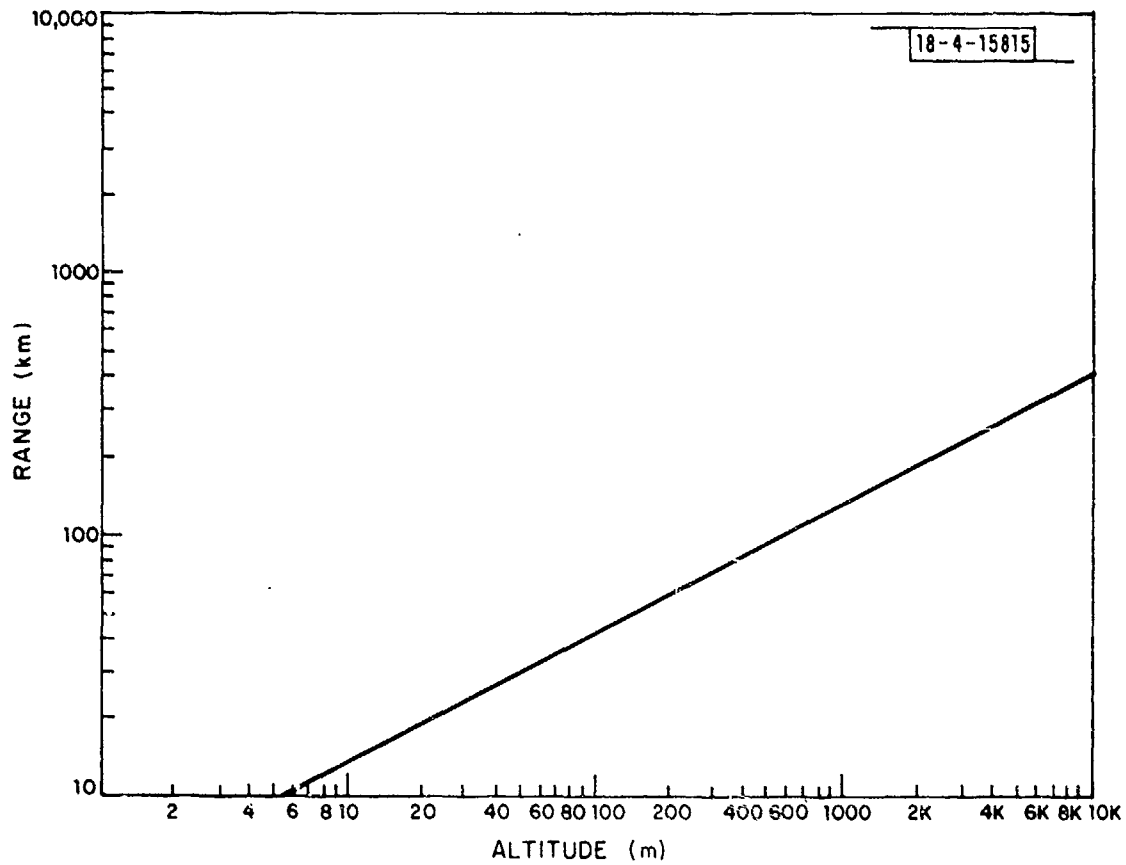


Fig. 52. Plot of aircraft altitude vs maximum range to horizon.

and later by Smith. All of these analyses are predominantly for back scattering. A bistatic shadowing function was developed by Wagner. It represents the effective fraction of the incident field scattered to the output direction. It is given by

$$S(\phi_1, \phi_2) = [1 - \exp(-2B_1 + B_2)] \cdot (\operatorname{erf} v_1 + \operatorname{erf} v_2) / 4 (B_1 + B_2) \quad (5.4)$$

where

$$\phi_1 = (\pi/2) - \phi_i \text{ and}$$

$$\phi_2 = (\pi/2) - \phi_s, \text{ with:}$$

$$B_i = [\exp(-v_i^2) - \sqrt{\pi} v_i \operatorname{erfc} v_i] / 4 \sqrt{\pi} v_i \quad (5.5)$$

$$v_i = |\eta_i| / \sqrt{2|\psi_0''|} \quad (5.6)$$

$$\eta_i = \tan \phi_i \quad (5.7)$$

$$\psi_0 = E[\xi(t) \xi(t)] \quad (5.8)$$

$$\psi_0'' = \left[\frac{\partial^2}{\partial \tau^2} E[\xi(t) \xi(t + \tau)] \right]_{\tau = 0} \quad (5.9)$$

and $\xi(t)$ is the surface height (e. g., $z(x, y)$). Depending on the surface correlation, (5.6) and (5.7) are directly evaluated. Wagner shows, that for the range of values discussed in Section 4, $S(\phi_1, \phi_2)$ is about 0.1 This indicates an order

of magnitude decrease in the values of the field intensity evaluated there. Since there appears to be little data to substantiate these results, we did not include them in the analysis.

5.3 SEA SURFACE SCATTERING

The scattering of electromagnetic waves from a sea surface is much more complex than that from land. A great deal of both the theoretical and experimental work has been done in this area but none as of yet directly applicable to the DABS problem. The theoretical work by Beard [1]-[2], Beard, et al., Barrick [1]-[3] and the experimental work of Bass, et al., [1]-[2] provide some insight into the problem. In particular, it has been noted that specular type reflections can arise in other than the expected specular direction. Furthermore, the difference between diffuse and specular reflections is not as clear as that developed in Sections 3 and 4.

The work by DeLorenzo and Cassedy has shown how one might analyze and interpret the results. Their model assumes that the surface of the ocean is a narrowband zero mean Gaussian random process. They assume that the height of the ocean, $z(x, y)$, depends only on x and that (see Fig. 53)

$$E[z(x)] = 0 \quad (5.10)$$

$$E[z(x_1) z(x_2)] = K_z(x_1 - x_2) \quad (5.11)$$

The field, $z(x)$, is homogeneous.

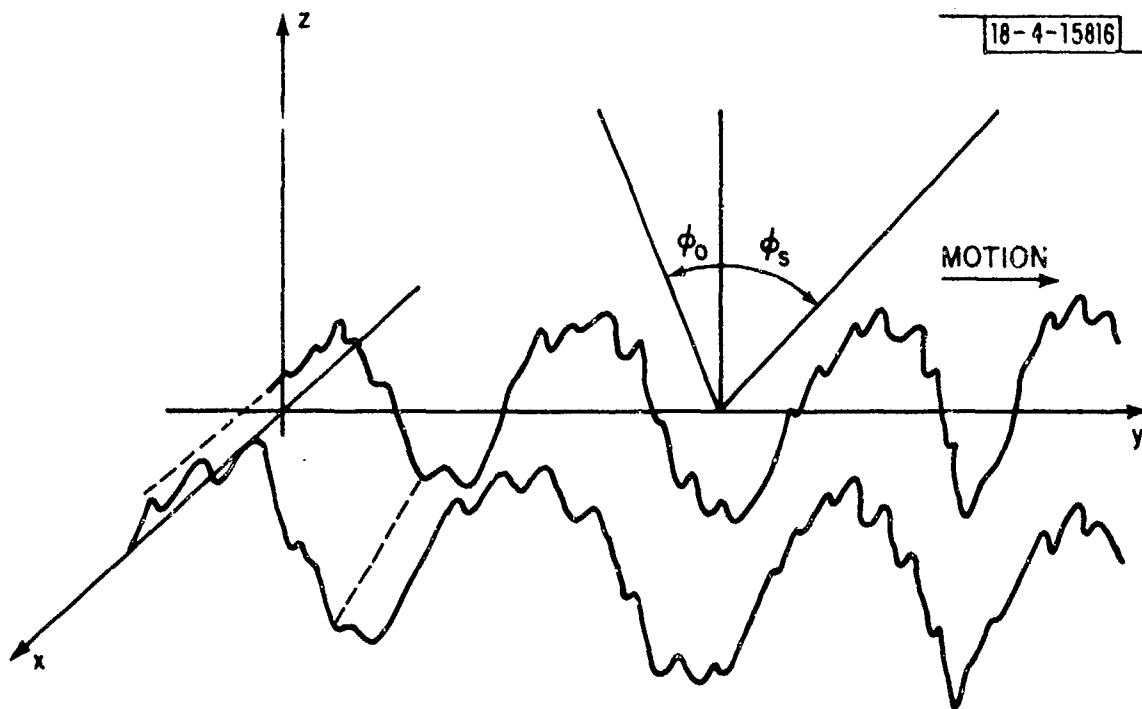


Fig. 53. Model of ocean waves.

Using a Floquet analysis based upon Cassedy, they proceed to identify the specular nature of the average intensity of the scattered field. They do this by assuming that a length $2L$ of the ocean is illuminated and write the normalized scattered field as;

$$\rho = \int_{-L}^L \exp(j\nu_x x - j\nu_z z(z)) dx \quad (5.12)$$

where

$$\nu_x = k(\sin\phi_0 - \sin\phi_s) \quad (5.13)$$

$$\nu_z = k(\cos\phi_0 + \cos\phi_s) \quad (5.14)$$

where k equals $2\pi/\lambda_0$. Clearly, $\nu_x = 0$ defines the classical specular direction since ϕ_0 is the angle of incidence and ϕ_s the scattering angle.

By assuming that $K_z(\tau)$ equals

$$K_z(\tau) = \sigma_R^2 \exp(-\tau^2/\tau_0^2) \cos(2\pi f_s \tau) \quad (5.15)$$

where σ_R^2 is the variance of the surface height, τ_0 the correlation length and f_s the spatial periodicity of the waves, they find that for the case $\tau_0 \gg L$;

$$E[\rho\rho^*] = \exp(-\nu_z^2 \sigma_R^2) \cdot \sum_{n=-\infty}^{\infty} I_n(\nu_z^2 \sigma_R^2) 4L^2 \frac{\sin^2(\nu_x + n2\pi f_s)L}{[(\nu_x + n2\pi f_s)L]^2} \quad (5.16)$$

This expression shows the scattered power to be strongly peaked at

$$\nu_x + 2\pi n f_s = 0 \quad . \quad (5.17)$$

Obviously, $\nu_x = 0$ is one of these values but so too are other directions. DeLorenzo and Cassedy show data which substantiates their model. Other variations of the surface parameters introduce diffuse-like scattering along with multiple specular scattering directions.

Thus, the analysis of the effects of multipath over the sea appears to be quite complex and still an open area on many issues.

5.4 COMPOSITE SCATTERING

The fourth and final extension would be the scattering from composite surfaces as discussed by Beckmann [1]. Basically, a composite rough surface is one having several σ_h and σ_l . Beckmann shows that the total energy from such a surface is the sum from all of its composites. To do this in practice requires a better understanding of the surface topography. The studies by Fung and Moore and Hayre and Moore do not seem to indicate however, that such composite behavior is common.

5.5 CONCLUSIONS

Those other effects that were not considered in the analysis of specular and diffuse multipath in Sections 3 and 4 respectively represent only second order perturbations on the results. The earth's curvature giving rise to divergence alters the result only slightly. The only serious limitation of having a

curved earth is that of line of sight limitations. These can be easily included as a cutoff at maximum range.

The effects of shadowing are also only second order and only tend to further reduce the effects of diffuse multipath. However, sea surface scattering does present a phenomenon for which little data in the L band regions exist. This effect will undoubtedly be important at airports which are adjacent to the ocean. To a first order the sea surface can be considered as a slightly rough flat plane with no tilts. This would indicate that azimuth errors would be small.

There are two other effects which may be dominant in certain locations and for which at present little is known. They are;

1. **Vegetation Effects:** The effect of trees and other forms of vegetation must be considered when evaluating the reflection coefficient. However, trees at L band represent a random, finite thickness, lossy, dielectric scatterer. At present no adequate theory is available to analyze this effect. DABSEF data indicate that a reduction in reflection coefficient results.
2. **Low Angle Effects:** When the aircraft is at very low elevation angles, theory for flat surfaces indicate that ρ approaches unity and very deep nulls occur. However, actual topography is not perfectly flat. There are many different, albeit large in area, surfaces of various tilts. Thus as the elevation angle gets smaller the Fresnel zone gets larger and encompasses many independently oriented surfaces. The coherent sum of the plane waves from these surfaces tend to cancel and

the resultant deep nulls do not appear. Again no adequate theory exists to model this phenomenon nor are adequate data available on large scale correlation effects.

SECTION SIX

APPLICATIONS

The models that have been developed for both diffuse and specular multipath are useful in evaluating many of the important aspects of DABS. In this section we shall discuss five areas in which these analytical methods find application and discuss how the results may be applied. These areas have in common an interest in how the signal behaves as a function of sensor type, sensor location and aircraft location. In general, the resulting analyses and conclusions will be based solely upon the specular multipath model, for, as we have shown in Section 4, diffuse multipath is a second order effect.

6.1 PERFORMANCE

There are two aspects of DABS performance that are impacted upon by multipath. The first is the communication link performance. The link performance depends upon SNR which in turn can be seriously degraded whenever the signal fades due to coherent multipath cancellation. The depths of these fades can be evaluated for various terrain conditions and the link performance obtained. In Section 3, we found that fading depended upon geometry, surface roughness antenna gains and sensor and aircraft locations. In contrast to a simple flat earth, single plane model, the model developed in Section 3 was based upon a more robust set of conditions. It allows fade calculations and performance predictions to be made from multiple reflecting planes of finite size and varying surface interface properties.

The second performance issue is that of azimuth estimation performance. As was shown in Section 3, the errors in monopulse azimuth estimation are dependent upon two effects. The first was a pure SNR fade and the second was a coherent cancelling by the off-azimuth multipath plane. Similarly, ATCRBS angle estimating schemes have also been analyzed and similar error behavior has been observed.

6.2 LOCALIZATION

Section 2 was basically an analytical approach to specular multipath in that, for a given geometrical configuration, the resulting output signal could be formed. The inverse of this technique, going from an observed output to a given geometry, is the synthesis portion of the analysis and has been termed localization. That is, by observing the output of an antenna and knowing the model it is possible to obtain the angles α_i, β_i as well as the offset location of the planes giving rise to that signal. In such a fashion we can localize the source of each specular multipath signal and identify it in the terrain.

From Section 3 we know that the specular multipath signal power, sampled in time and normalized by the intensity of the direct path, is given by

$$s^2 = 1 + \sum_{i=1}^n \rho_i^2 + 2 \sum_{i=1}^n \rho_i \cos(\delta \psi_i) + 2 \sum_{\substack{i=1 \\ i \neq j}}^n \sum_{j=1}^n \rho_i \rho_j \cos(\delta \psi_i - \delta \psi_j) \quad (6.1)$$

Here the ρ_i represents path effects, range effects and antenna effects. It is not the reflection coefficient of Section 3 but a conglomerate of all effects normalized by the conglomerate of all direct path effects. The factor n represents all paths except the direct free space path. The phase $\delta\psi_k$ represents the phase difference due to geometry between the direct path and the k th multipath. Note, that for convenience, we have neglected the Fresnel reflection coefficient phase factor.

Let the aircraft be at a position $(r \sin\gamma, r \cos\gamma, z_2)$ and the receiver at $(0, 0, z_1)$ where r is the horizontal ground range. Then for reflecting planes with small range and cross range slopes (less than about $\pm 10^\circ$) it can be shown that $\delta\psi_k$ is

$$\delta\psi_k = \frac{2\pi f_k}{r} + \tilde{\psi}_k \quad (6.2)$$

where

$$f_k = \frac{2}{\lambda_0} f^2(x_k, y_k, z_k) + (z_1 + z_2) \cos(\alpha_k) \cos(\beta_k) f(x_k, y_k, z_k) \quad (6.3)$$

$$\tilde{\psi}_k = -2\left(\frac{2\pi}{\lambda_0}\right) [f(x_k, y_k, z_k) + z_1 \cos(\alpha_k) \cos(\beta_k)] \cdot [\sin(\beta_k) \cos(\gamma) + \cos(\beta_k) \sin(\alpha_k) \sin(\gamma)] \quad (6.4)$$

and where;

$$f(x_k, y_k, z_k) = x_k \sin(\alpha_k) \cos(\beta_k) + y_k \sin(\beta_k) - z_k \cos(\alpha_k) \cos(\beta_k). \quad (6.5)$$

Thus s^2 is a periodic function of $1/r$ with frequencies f_k , $k = 1, \dots, n$, and phases $\tilde{\psi}_k$, $k = 1, \dots, n$. Thus if s^2 is spectrum analyzed, f_k and $\tilde{\psi}_k$ can be determined. It can be shown that by suitably varying γ and z_2 the parameters α_k , β_k and $f(x_k, y_k, z_k)$ can be obtained. The three parameters uniquely define the k th specular multipath source.

In Section 3, Fig. 19, we plotted a return with $n = 2$ as a function of $1/r$. The multiple sinusoids were quite evident. We have plotted in Fig. 54 the real part of the Fourier transform, in Fig. 55 the imaginary part and in Fig. 56 the power spectrum of the range corrected waveform of Fig. 19. The three peaks in the power spectrum are quite evident. The lower peak is due to the ground reflection and the upper peak is due to the tilted plane reflection. The central peak is a result of beating between these two multipath signals.

6.3 ANTENNA DESIGN

The effects of multipath strongly impact on the choice of an antenna for DABS. The discussion of azimuth estimation performance in Section 3 demonstrated that the effect of loss of SNR could be quite serious. This loss was due to the coherent interference between the direct path and the vertical lobing path. This effect can be lessened by using an antenna with vertical aperture which in effect will have a cutoff below the horizon. That is, the signal coming in at negative elevation angles will be attenuated. This results in an effective decrease in the reflection coefficient and increase in minimum SNR.

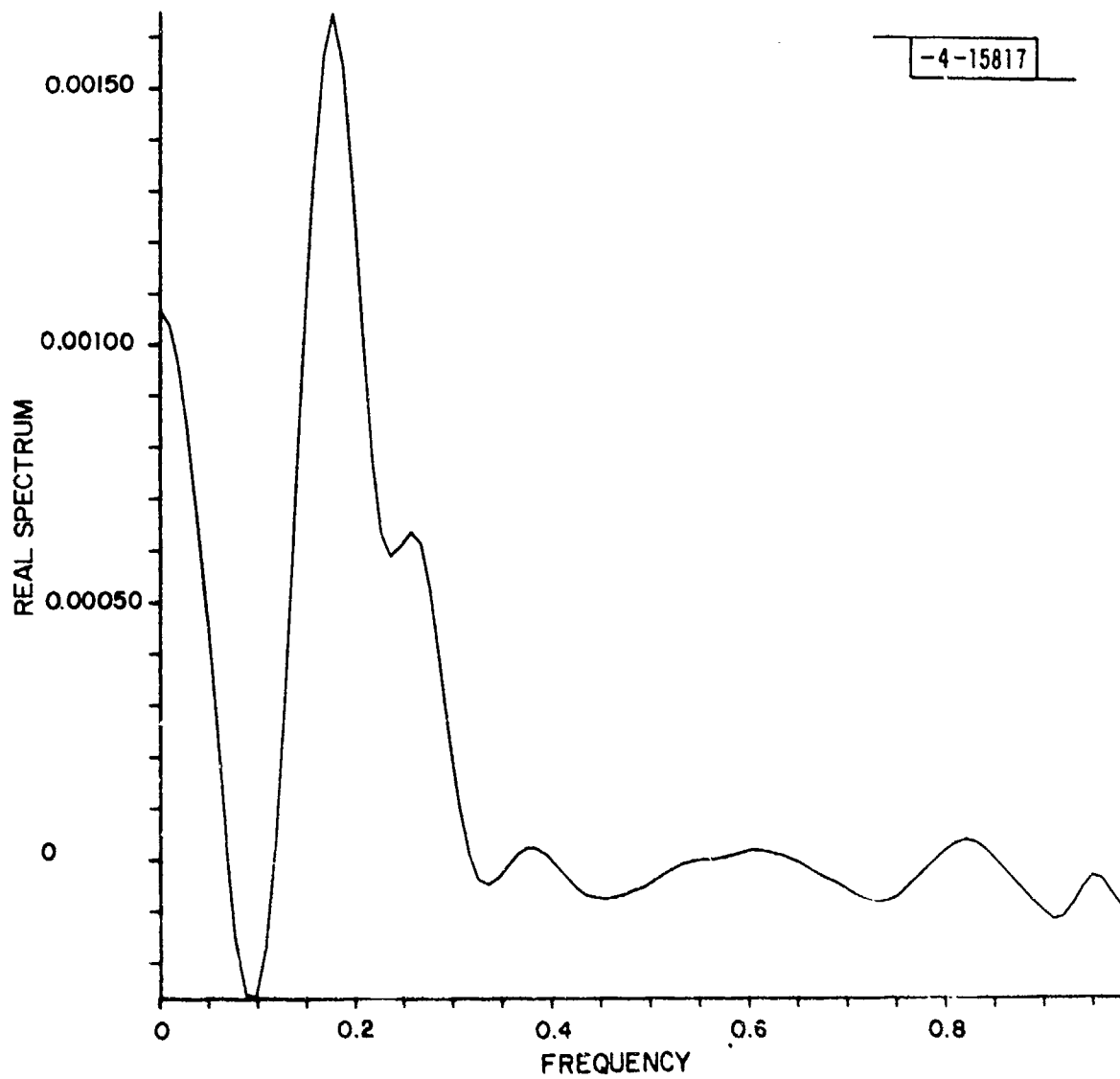


Fig. 54. Real part of Fourier transform.

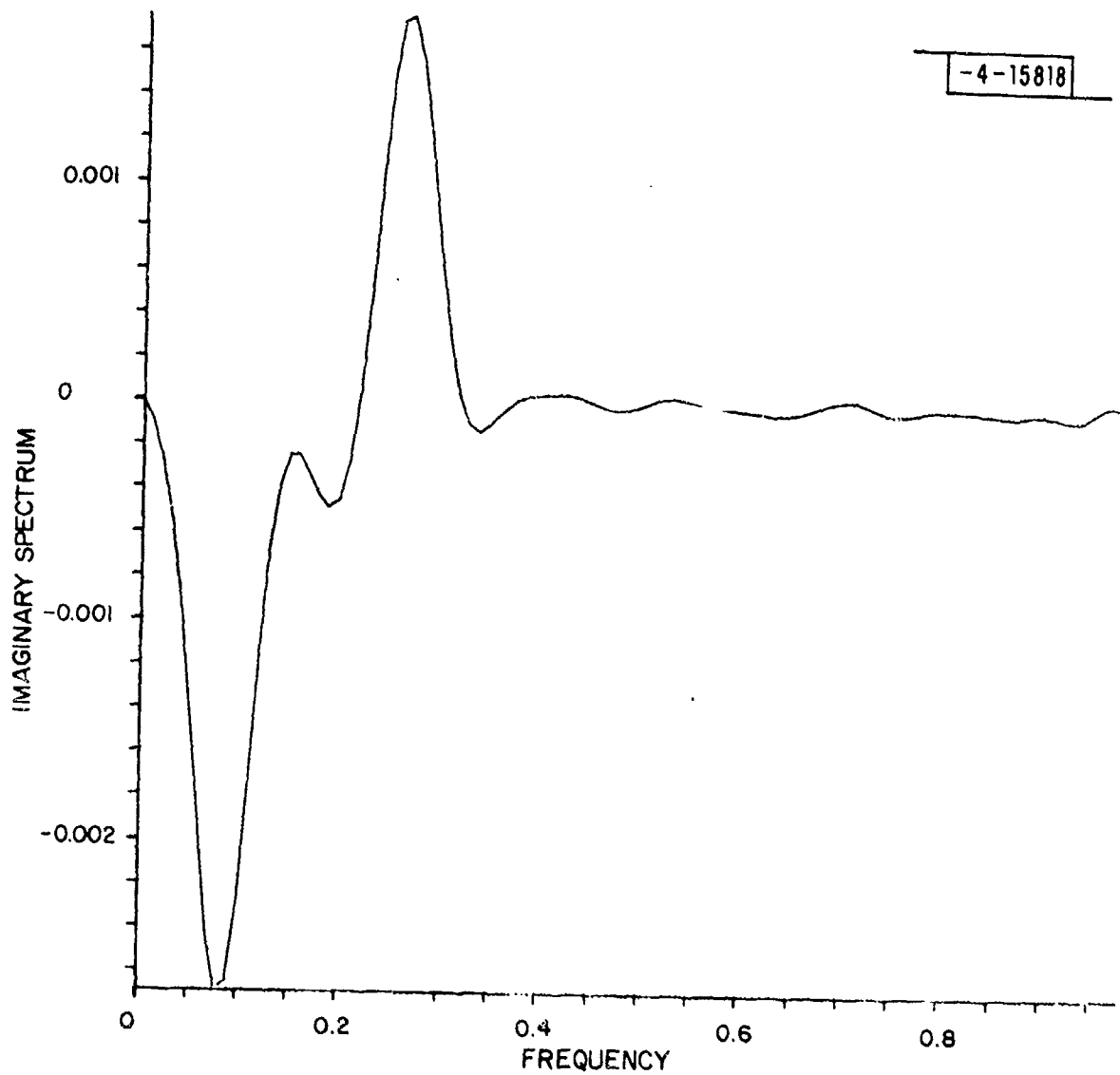


Fig. 55. Imaginary part of Fourier transform.

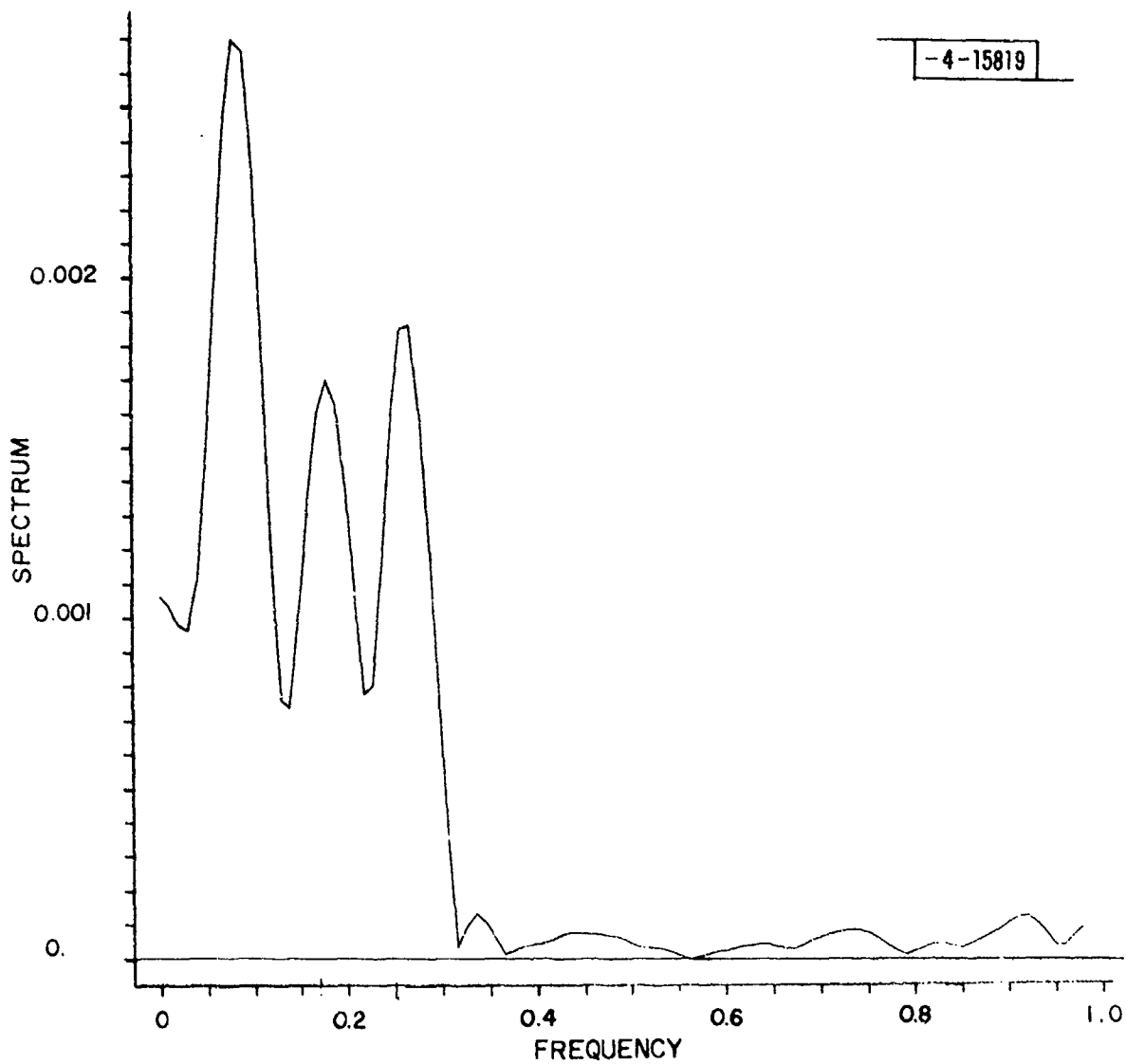


Fig. 56. Power spectrum.

Other effects can also be studied. For example, the choice of horizontal aperture and the nature of the sidelobes is also influenced by the type of multipath present.

6.4 SIGNAL PROCESSING

The fade margins can be determined by the depths of the nulls that occur. If these nulls are quite large then more sophisticated methods of coding and signal processing techniques will be necessary.

6.5 SITING

An important issue in the determination of the implementation of a DABS sensor is its siting. For example, where should it be, how high, and what type of tilts should be used. The effect of specular multipath on these issues is significant. Signal fading and coverage as well as angle estimation performance are often dominated by the multipath environment. At the present, there seems to be no cohesive measure of optimum siting performance but possibly, through a detailed study of the many multipath effects, one may evolve.

6.6 CONCLUSIONS

The models that we have proposed and developed can be used to evaluate and analyze the effects of multipath on system performance and design. Specifically, as we have observed, the effects of specular and diffuse multipath on azimuth errors can be evaluated in detail. Furthermore, link reliability can be deteriorated by specular fading. The effects of antenna gains and cutoffs in eliminating deep fades and serious azimuth errors can be ascertained.

The localization algorithm has been found to provide a useful tool in determining the source of specular returns. By the nature of the signal processing involved an effective increase in aperture can be obtained thus increasing resolution. The use of this technique on the analysis of DABSEF data is presently under way.

SECTION SEVEN

CONCLUSIONS

The ability to obtain azimuth information and communicate data over an air-to-ground surveillance link depends quite strongly on the different types of multipath effects. To determine the influence of multipath, we have in this report, developed models for the signals that are received after having propagated over multipath channels. The models include the effects of the topographical and electrical properties of the reflecting surfaces as well as the position of aircraft and sensor.

As a result of this study we have reached the following set of conclusions:

1. The most serious cause of azimuth angle of arrival estimate errors at the ground terminal will be specular multipath signals in the main beam. These will tend to cause bias errors in the estimate. The seriousness of the errors as measured by their magnitude will depend upon the angle made by the ray from the aircraft to the multipath reflecting surface and the beam pattern of the receiving antenna. If this angle is small, then the Fresnel reflection coefficient may be near unity which can only be reduced by the antenna pattern. The magnitude of the azimuth estimation error also depends on the total phase difference between the direct path and the reflected path. This

can be obtained from the geometry of the aircraft, sensor and reflecting surface.

The time delays for main beam multipath may vary significantly, from a few nanoseconds to several microseconds, as observed from DABSEF data. Again, this depends upon geometrical considerations. The nature of the surface will also affect the reflected signal. By using the concept of Fresnel zones, diffraction effects can be included in a first order manner.

2. Diffuse multipath will have a minimal effect upon ground terminal direction finding accuracy. The analysis of Section 4 has shown that diffuse multipath azimuth errors, as measured in standard deviations, have magnitudes less than noise errors. Furthermore, it has been shown by McGarty [1] that diffuse multipath in certain cases contains information on the azimuth of the target. This is in sharp contrast to the analysis of Kulke, et al., who employed results from Barton and Ward to compute the deleterious effect of diffuse multipath.
3. For most cases of interest, neither specular nor diffuse multipath will seriously limit either the direction finding or communication capabilities of DABS. There are certain pathological situations concerning specular multipath however, in which the effect will be quite deleterious. These have been analyzed in detail by McAulay.

4. The second order effects, such as shadowing and multiple oriented surfaces, could possibly dominate the signal behavior at low angles. To answer this question adequately, extensive experimental data are necessary.

As a result of the preceding analysis it becomes evident that a substantial experimental program should be initiated to provide a data base against which the proposed models can be compared. Part of this program is included in the DABSEF (DABS Experimental Facility) presently in operation at Lincoln Laboratory. A more extensive program is also envisioned which would include a portable system.

APPENDIX I

In the Appendix, we evaluate in closed form the bounding ellipse discussed in Section 4. Further, we relate this to several other physical parameters, namely, the minimum distance between the source and the receiver via a multipath reflection. The basic equality to evaluate the ellipse, which represents the locus of all points on the scattering plane whose total path length from receiver to transmitter is ρ , is;

$$R_1 + R_2 = \rho \quad (\text{I. 1})$$

where R_1 and R_2 are given by (4. 13) and (4. 14) respectively, and ρ equals ct. Now rearranging and squaring, we obtain

$$R_1^2 = \rho^2 - 2\rho R_2 + R_2^2 \quad (\text{I. 2})$$

Substituting the values for these quantities we obtain,

$$\begin{aligned} x^2 + y^2 + z_1^2 &= \rho^2 - 2\rho \sqrt{(r-y)^2 + x^2 + z_2^2} \\ &\quad + y^2 + x^2 - 2yr + r^2 + z^2 \end{aligned} \quad (\text{I. 3})$$

Cancelling and rearranging, we obtain

$$2\rho\sqrt{(r-y)^2 + x^2 + z_2^2} = \rho^2 - z_1^2 + z_2^2 + r^2 - 2yr. \quad (\text{I. 4})$$

Squaring yields

$$4\rho^2[(r-y)^2 + x^2 + z_2^2] = (\rho^2 - z_1^2 + z_2^2 + r^2)^2 - 4yr(\rho^2 + z_2^2 - z_1^2 + r^2) + 4y^2 r^2. \quad (\text{I. 5})$$

Now,

$$\begin{aligned} & 4\rho^2 y^2 - 4r^2 y^2 - 8\rho^2 ry + 4(\rho^2 + z_2^2 - z_1^2 + r^2)ry \\ & + 4\rho^2 r^2 + 4\rho^2 x^2 + 4\rho^2 z_2^2 \\ & = (\rho^2 + z_2^2 - z_1^2 + r^2)^2. \end{aligned} \quad (\text{I. 6})$$

Clearly, this is the equation of an ellipse. Completing the square, we can obtain

$$\begin{aligned} & 4(\rho^2 - r^2) \left(y + \frac{(-4\rho^2 r + 2r(\rho^2 + z_1^2 - z_1^2 + r^2))}{4(\rho^2 - r^2)} \right)^2 \\ & + 4\rho^2 x^2 = \left[(\rho^2 + z_2^2 - z_1^2 + r^2)^2 \right. \\ & \quad \left. - 4\rho^2 r^2 - 4\rho^2 z_2^2 \right. \\ & \quad \left. + \frac{(-4\rho^2 r + 2\rho(\rho^2 + z_2^2 - z_1^2 + r^2))^2}{4(\rho^2 - r^2)} \right] \end{aligned} \quad (\text{I. 7})$$

Now the term on the right in the above equality can be simplified by writing it as

$$\begin{aligned}
 & \left[(\rho^2 + z_2^2 - z_1^2 + r^2)^2 4(\rho^2 - r^2) \right. \\
 & \quad - 4(\rho^2 r^2 + \rho^2 z_2^2) 4(\rho^2 - r^2) \\
 & \quad + (4\rho^2 r)^2 - 2(4\rho^2 r) (2r(\rho^2 + z_2^2 - z_1^2 + r^2)) \\
 & \quad \left. + 4r^2(\rho^2 + z_2^2 - z_1^2 + r^2)^2 \right] / (4(\rho^2 - r^2)) \\
 & = \left[4\rho^2(\rho^2 + z_2^2 - z_1^2 + r^2)^2 - 16\rho^2 r^2(\rho^2 + z_2^2 - z_1^2 + r^2) \right. \\
 & \quad \left. - 16\rho^2(z_2^2 \rho^2 - z_2^2 r^2 - r^4) \right] / (4(\rho^2 - r^2)) \\
 & = \left[4\rho^2[(\rho^2 + z_2^2 - z_1^2 + r^2)^2 - 2(2r^2)(\rho^2 + z_2^2 - z_1^2 + r^2) \right. \\
 & \quad \left. + 4r^4] - 16\rho^2 r^4 - 16\rho^2(z_2^2 \rho^2 - z_2^2 r^2 - r^4) \right] / (4(\rho^2 - r^2)) \\
 & = \frac{4\rho^2[\rho^2 - r^2 + z_2^2 - z_1^2]^2 - 16\rho^2 z_2^2(\rho^2 - r^2)}{4(\rho^2 - r^2)} \tag{I. 8}
 \end{aligned}$$

which is the desired result.

Now we can ask the question, where is the point at which the minimum time ray touches the surface? That is for a given ρ , the time from source to receiver is $(R_1 - R_2)/c$. We first want to find the value of x which minimizes this expression. By standard differentiation techniques we obtain

$$x_{\min} = \frac{r z_1}{z_1 + z_2} \quad (I.9)$$

Note that if $z_1 = z_2$, then $x_{\min} = d/2$. Now the time it takes to cover this minimum distance is t_0 , where

$$t_0 = \frac{\sqrt{r^2 + (z_1 + z_2)^2}}{c} \quad (I.10)$$

Compare this to the time between receiver and transmitter, t_r ,

$$t_r = \frac{\sqrt{d^2 + (z_2 - z_1)^2}}{c} \quad (I.11)$$

Now at $t = t_0$, ρ equals $c t_0$.

Then substitution into r_0 yields r_0 equal to zero and x_0 equal to x_{\min} .

Thus as t increases beyond t_0 , the ellipse forms and grows.

GLOSSARY OF TERMS

A	-	antenna area
A_F	-	area of first Fresnel zone
A_i	-	area of i th reflector
$A(t)$	-	irradiated area
$\tilde{b}(\theta, \phi)$	-	complex envelope of time invariant portion of diffuse field
$\tilde{b}(\theta, \phi, t)$	-	complex envelope of diffuse field
c	-	velocity of propagation
d_i	-	distance to i th dipole
d_o	-	interdipole spacing
D	-	divergence factor
$E[\]$	-	expectation
$\text{erf} (\)$	-	error function
E_s	-	energy of transmitted signal
$\frac{E}{-sc}$	-	scattered field
f_k	-	frequency of multipath interference
$\tilde{f}(t)$	-	complex envelope of transmitted signal
$f(x_k, y_k, z_k)$	-	displacement of k th multipath plane
$G(\theta, \psi)$	-	antenna gain
$G_{\Delta}(\theta, \phi)$	-	difference antenna gain
$G_{\Sigma}(\theta, \phi)$	-	sum antenna gain
$I_n(\)$	-	Bessel function

$\underline{J}(\underline{\quad})$	-	current density
k	-	monopulse slope
\underline{k}	-	plane wave vector
$\left. \begin{array}{l} k_x \\ k_y \\ k_z \end{array} \right\}$	-	components of propagation vector
$K(\theta)$	-	channel spread function; azimuth only
$K(\theta, \phi)$	-	channel spread function
$K_s(\underline{r}, \underline{r}')$	-	covariance of diffuse signal
$\underline{\tilde{m}}(\mu)$	-	array delay vector
MID	-	multipath-interference detector
N	-	number of array elements
N	-	number of specular reflectors
\underline{n}	-	normal vector
$\underline{\tilde{n}}(t)$	-	complex envelope of receiver noise
n_A	-	average number of scatterers
$\frac{N_o}{Z}$	-	noise spectral density
P_o	-	power of transmitter
P_i	-	scattering plane septuple
R	-	ground range
$R(\xi)$	-	reflection coefficient
R_e	-	radius of earth
R_h	-	range to horizon
R_i	-	range to i th signal

R_T	-	range from aircraft to antenna
R_{1i}	-	distance from receiver to ith scattering point
R_{2i}	-	distance from transmitter to ith scattering point
r	-	range
\underline{r}	-	point in space
$\tilde{r}(t)$	-	complex envelope of received signal
\underline{r}_0	-	scattering plane displacement
\underline{r}_1	-	location of receiver
\underline{r}_2	-	location of transmitter
\underline{r}_{0i}	-	offset displacement of ith plane
S	-	scattering surface
$S(\phi_1, \phi_2)$	-	shadowing functions
$S(t)$	-	power density at receiver
s	-	magnitude of power received
$s(t)$	-	transmitted signal
$\tilde{s}(t)$	-	complex envelope of transmitted signal
$\tilde{s}(\underline{r})$	-	complex envelope of time invariant diffuse signal
$\tilde{s}(\underline{r}, t)$	-	complex envelope of time variance diffuse signal
SNR	-	signal-to-noise ratio
t	-	time
t_0	-	signal emission time of source
t_1	-	transmission time from transmitter to receiver
t_s	-	transit time of scattered path

\underline{v}_1	-	vector to image antenna
\underline{v}_2	-	vector to transmitter
\underline{v}_3	-	vector to receiver
$\text{var} (\)$	-	variance
x_1	-	half width of first Fresnel zone
$\left. \begin{array}{l} x_1 \\ y_1 \end{array} \right\}$	-	antenna phase center location
z_1	-	antenna height
$\left. \begin{array}{l} x_2 \\ y_2 \\ z_2 \end{array} \right\}$	-	location of aircraft
y_{01}	-	center of first Fresnel zone on y axis
$z(X, Y)$	-	random surface
α	-	cross-range tilt
β	-	range tilt
$\underline{\Gamma}(\underline{r}, \underline{r}')$	-	Greens function
γ	-	noise-to-signal ratio
$\tilde{\Delta}$	-	difference signal
Δ_1	-	deviation of first Fresnel zone from y_0
∇	-	del operator (gradient or divergence)
$\delta(\underline{k} - \underline{k}')$	-	delta function
ϵ_i	-	dielectric constant of ith scattering plane
η	-	diffuse multipath to free space signal ratio
η_{A_i}	-	aperture reflection factor

η_{D_i}	-	diffuse reflection factor
η_{F_i}	-	Fresnel reflection factor
$\hat{\theta}$	-	azimuth estimate
θ_B	-	beamwidth
ϕ_i	-	azimuth of ith signal
λ_0	-	free space wavelength
μ	-	direction cosine
μ_B	-	beamwidth
ξ	-	interference-to-signal ratio
ρ_i	-	ith reflection coefficient
$\tilde{\Sigma}$	-	sum signal
$\tilde{\sigma}(t)$	-	magnitude of time variation of power received
σ_b	-	channel attenuation coefficient
σ_h	-	standard deviation of surface height
σ_I^2	-	diffuse signal energy
σ_i^2	-	power in diffuse field
σ_i	-	scattering cross-section
σ_i	-	conductivity of ith scattering plane
σ_l	-	correlation length of surface
σ_n^2	-	noise covariance
σ_s^2	-	signal energy
$\sigma(\theta_s, \phi_s; \phi_i)$	-	scattering cross sections

σ_{θ}^2	-	variance of azimuth estimate
σ_{μ}^2	-	variance of μ
τ	-	multipath-interference statistic
ϕ_i	-	elevation (incident or ith signal)
ϕ_s	-	elevation of scattered signal
ψ_{F_i}	-	phase due to Fresnel reflection
ψ_i	-	phase difference
$\tilde{\psi}_k$	-	multipath phase
ψ_{R_i}	-	phase due to range
ω_c	-	carrier frequency
$\mathcal{B}(\mu)$	-	array ambiguity function
\mathcal{R}_i	-	transformation matrix

REFERENCES

Ament, W.S.

- [1] "Toward a Theory of Reflection by a Rough Surface," Proc. IRE, 41, (1953) pp. 142-146.
- [2] "Forward and Back-Scattering From Certain Rough Surfaces," IRE, AP-4, (1965) pp. 369-373.

Barrick, D. E.

- [1] "Rough Surface Scattering Based on the Specular Point Theory," IEEE, AP-16, No. 4, (July 1968) pp. 449-454.
- [2] "Unacceptable Weight Correlation Coefficients and the Quasi-Specular Component in Rough Surface Scattering," Radio Science Vol. 5, No. 4, (April 1970) pp. 647-654.
- [3] "Theory of HF and UHF Propagation Across the Rough Sea," Radio Science, Vol. 6, No. 5, (May 1971).

Barrick D. E., Peake, W.H.

- [1] "A Review of Scattering From Surfaces with Different Roughness Scales," Radio Science, Vol. 3, No. 8, (August 1968) pp. 865-868.

Barton, D.K., Ward, H.R.

- [1] Handbook of Radar Measurement, (Prentice-Hall, Englewood Cliffs, N.J., 1969).

Bass, F.G., et al.

- [1] "Very High Frequency Radio Wave Scattering by a Distributed Sea Surface Pt. I," IEEE, Vol. AP-16, No. 5, (Sept. 1968) pp. 554-559.
- [2] "Very High Frequency Radio Wave Scattering by a Distributed Sea Surface Pt. II," IEEE, Vol. AP-16, No. 5 pp. 560-588.

Beard, C.I.

- [1] "Coherent and Incoherent Scattering of Microwaves from the Ocean IEEE, Vol. AP-9, No. 5, (Sept. 1961) pp. 470-483.
- [2] "Behavior of Non-Rayleigh Statistics of Microwave Forward Scatter from a Random Water Surface," IEEE, Vol. AP-15, No. 5 (Sept. 1967) pp. 649-657.

Beard, C.I., et al.

- [1] "Phenomenological Vector Model of Microwave Reflection from the Ocean," IRE, Vol. AP-4, (1956) pp. 162-167.

Beckmann, P.

- [1] "Scattering by Composite Rough Surfaces," Proc. IEEE, (Aug. 1965) pp. 1012-1015.
- [2] "Scattering of Light by Rough Surfaces," Progress in Optics, IV, (E. Wolf, Ed., J. Wiley, N. Y., 1967) pp. 55-70.
- [3] "Shadowing of Random Rough Surfaces," IEEE, AP-14, (1965) pp. 384-388.

Beckmann, P., Spizzichino, A.

- [1] The Scattering of Electromagnetic Waves from Rough Surfaces, (Permagon, N. Y., 1963).

Brockelmann, R. A., Hagfors, J.

- [1] "Note on the Effect of Shadowing on the Backscattering of Waves from a Random Rough Surface," IEEE, Vol. AP-14, No. 5, (Sept. 1966) pp. 621-629.

Clarke, R. H., Hendry, G. O.

- [1] "Prediction and Measurement of the Coherent and Incoherent Power Reflected from a Rough Surface," IEEE, Vol. AP-13, No. 3, (1964) pp. 353-363.

DeLorenzo, J. D., Cassedy, E. S.

- [1] "A Study of the Mechanism of Sea Surface Scattering," IEEE, Vol. AP-14, No. 15, (Sept. 1966) pp. 611-620.

Eckart, C.

- [1] "The Scattering of Sound from the Sea Surface," J. A. S. A., Vol. 25, No. 3 (May 1953) pp. 566-570.

Fung, A. K., Moore, R. K.

- [1] "The Correlation Function in Kirchoff's Method of Solution of Scattering of Waves from Statistically Rough Surfaces," J. Geo. Res., Vol. 71, No. 12, (June 1966) pp. 2939-2943.

Furutsu, K.

- [1] "A Statistical Theory of Ridge Diffraction," Radio Sci., Vol. 1, No. 1, (Jan. 1966) pp. 79-98.

Hagfors, T.

- [1] "Backscattering from an Undulating Surface with Applications to Radar Return from the Moon," J. Geo. Res., Vol. 69, No. 18, (Sept. 1964) pp. 3779-3784.

Hayre, H. S., Moore, R. K.

- [1] "Theoretical Scattering Coefficient for Near Vertical Incidence from Contour Maps," Jour. Res. Nat. Bur. Sts., Series D, Vol. 65D, No. 5, (Sept. -Oct. 1961) pp. 427-432.

Hoffman, W. C.

- [1] "Scattering of Electromagnetic Waves from a Random Surface," Quant. Appl. Math., 13, (1955) pp. 291-304.

Jordan, E. C., Balmain, K. G.

- [1] Electromagnetic Waves and Radiating Systems, (Prentice Hall, Englewood Cliffs, N. J., 1968).

Kerr, D. E.

- [1] Propagation of Short Radio Waves, (Dover, N. Y., 1965).

Kodis, R. D.

- [1] "A Note on the Theory of Scattering from an Irregular Surface," IEEE, Vol. AP-14, No. 1, (Jan. 1966) pp. 77-82.

Lonquet-Higgins, M. S.

- [1] "Reflection and Refraction at a Random Moving Surface, Pt. I," J. O. S. A., Vol. 50., No. 9, (Sept. 1960) pp. 838-844.
- [2] "Reflection and Refraction at a Random Moving Surface, Pt. II," J. O. S. A., Vol. 5, No. 9, (Sept. 1960) pp. 845-850.

Maltz, F. H., Meecham, W. C.

- [1] "The Effect of Curvature Variations on the Scattering from Rough Surfaces," J. Stat. Phy., Vol. 3, No. 4, (1971) pp. 385-394.

McAulay, R. J.

- [1] "The Effects of Interference on Monopulse Performance" Lincoln Laboratory, M. I. T., Technical Note, TN-1973-30, (1 Aug. 1973) ESD-TA-73-176.

McAulay, R. J., McGarty, T. P.

- [1] "An Optimum Interference Detector for DABS Monopulse Data Editing," Lincoln Laboratory M. I. T. Technical Note, TN-1973-48 (26 Sept. 1973) ESD-TR-73-253.

McGarty, T. P.

- [1] "Azimuth-Elevation Estimation Performance of A Spatially Dispersive Channel," IEEE Vol. AES-10, No. 1 (January 1974) pp. 58-69.

Mitzner, K. M

- [1] "Change in Polarization on Reflection from a Tilted Plane," Rad. Sci. Vol. 1, No. 1, (Jan. 1966) pp. 27-29.

Rice, S. O.

- [1] "Reflection of Electromagnetic Waves from Slightly Rough Surfaces," Comm. Pure & Appl. Math, 4, (1951) pp. 351-378.

Silver, S.

- [1] Microwave Antenna Theory and Design, (Dover, N. Y., 1965).

Smith, B. G.

- [1] "Geometrical Shadowing of a Random Rough Surface," IEEE, Vol. AP-15, No. 3, (Sept. 1967) pp. 668-671.

Spingler, G. F.

- [1] "Analysis of Side-Lobe Suppression Capabilities at Joint-Use Radar Beacon Sites," FAA Report No. RD-67-59.

Stratton, J. A.

- [1] Electromagnetic Theory, (McGraw Hill, N. Y., 1941).

Twersky, V.

- [1] "Reflection Coefficients for Certain Rough Surfaces," J. App. Phys., 24, (1953) pp. 659-660.
- [2] "Certain Transmission and Reflection Theorems," J. App. Phys., Vol. 25, No. 7, (July 1954) pp. 859-862.
- [3] "On the Scattering and Reflection of Sound by Rough Surfaces," J. A. S. A. Vol. 29, No. 2, (Feb. 1957) pp. 209-225.
- [4] "On Scattering and Reflection of Electromagnetic Waves from Rough Surfaces," IRE, AP-5, (1957) pp. 81-90.

Van Trees, H. L.

- [1] Detection Estimation and Modulation Theory, Pt. III, (J. Wiley, N. Y. 1971).

Venetsanopoulos, A. N., Tuteur, F. B.

- [1] "Stochastic-Filter Modeling for the Sea-Surface Scattering Channel," J. A. S. A., 49, (1971) pp. 1100-11007.

Wagner, R.J.

- [1] "Shadowing of Randomly Rough Surfaces," J. A.S.A., Vol. 41, No. 1, (1967) pp. 138-147.

Yaglom, A.M.

- [1] "Second-order Homogeneous Random Fields," Proc. 4th Berkeley Symp. Math. Stat. and Prob. 2, pp. 593-620.